Measurement of B^0 Meson Properties Via Partial Reconstruction of the Decay $\bar{B}^0 \to D^{*+}\ell^-\bar{\nu}$

I Chung Lai

Dissertation submitted to the Faculty of the

Virginia Polytechnic Insitute and State University

in Partial Fullfilment of the Requirements for the degree of

Doctor of Philosophy

in

Physics

Kay Kinoshita (Co-Chair), Leo Piilonen (Co-Chair)

Laynam Chang, Randy Heflin

Mark Pitt

June 1999

Blacksburg, Virginia

Keywords: B Meson, Semileptonic Decay, Mixing

Measurement of B^0 Meson Properties

Via Partial Reconstruction of the Decay $\bar{B}^0 \to D^{*+}\ell^-\bar{\nu}$

I Chung Lai

ABSTRACT

Using data recorded by the CLEO II detector operating at the $\Upsilon(4S)$ resonance at the Cornell Electron Storage Ring, several properties of B meson are measured using a partially reconstructed tag of the decay mode $\bar{B}^0 \to D^{*+}\ell^-\bar{\nu}$. Using 2.38 fb^{-1} of on-resonance data and the averaged B meson semileptonic branching fraction through inclusive lepton momentum spectrum obtained by previous CLEO analysis, we measure the B^0 and B^- semileptonic branching fraction to be $(10.78 \pm 0.60 \pm 0.69)\%$ and $(10.25 \pm 0.57 \pm 0.65)\%$ respectively, which yields the lifetime ratio $\tau_+/\tau_0 = 0.950^{+0.117+0.091}_{-0.080-0.068}$, assuming the equality of semileptonic partial branching width for $\bar{B}^0$ and B^-. With a larger dataset of 3.1 fb^{-1}, we measured the $B^0 - \bar{B}^0$ mixing parameter χ_d to be $0.189 \pm 0.019 \pm 0.006$.

Acknowledgment

It has been a very challenging journey.

The author of this thesis is a member of CLEO colloraboration. The results presented here are the fruits of the labors of many, not simply his own. I like to thank the staff who has created this facility that I have been benefited tremendously.

I particularly like to give my thanks to Prof. Kay Kinoshita, who introduced me into the world of experimental high energy physics. Her patience and guidence has enlightened me to get through various difficulties in both as a professional physicist and as a person.

Romulus Godang and Dr.Paula Pomianowski has been my constant source of help. Many thanks to them for their company during the years. Romulus will remain the lone VPI dude in CLEO and Dr. Paula has departed. I wish them the best.

My residency in Ithaca these years happened to be those of the most turbulent years in my beloved homeland, Taiwan. The sense of duty to my country has constantly demanded my concentration away from Physics. As a result, it has been a never-ending tug of war between my daily physics research and the activities that concerned my homeland, whose very existence becomes the pressing question that commands people to respond. It is a stressful and mentally challenging "tour of duty". What a miracle that I am able to make it through. For this part, I have to thank Dr. Joseph Chen at Cornell nutrition department and his wife Meisi Chen. They are like my second parents whose kindness and generousity has made their home to become my constant refugee, and a place to recharge myself.

Finally, the author wishes to thank his parents and his sister for their unconditional support over the years.

Contents

List of Figures

List of Tables

Chapter 1

Particle Physics

1.1 Fundamental Particles

Current knowledge tells us that matters are made of fundamental particles called *fermion*, which is a spin $\frac{1}{2}$ particle. Our world are composed of two kinds of fermions: leptons and quarks. Both of them can be grouped into three families. For leptons, electron and the electron neutrino ν_e make up the first family, μ, τ and their associated neutrino, ν_μ, ν_τ composed the second and third family respectively. Each family is the identical copy of each other, except with different masses.

$$\begin{pmatrix} \nu_e \\ e \end{pmatrix} \begin{pmatrix} \nu_\mu \\ \mu \end{pmatrix} \begin{pmatrix} \nu_\tau \\ \tau \end{pmatrix}$$

We have six kinds of quarks, as the case for leptons, those six quarks are also put into three families.

Table 1.1: charge, mass and isospin of the six leptons

Lepton	Symbol	Charge	Mass (Mev/c^2)	weak isospin
electron	e^-	-1	0.511	1/2
muon	μ^-	-1	105.7	1/2
tau	τ^-	-1	1777	1/2
electron neutrino	ν_e	0	$< 7.0 \times 10^{-6}$	-1/2
muon neutrino	ν_μ	0	< 0.27	-1/2
tau neutrino	ν_τ	0	< 31	-1/2

Table 1.2: charge, mass and isospin of the six quarks

Quark	Symbol	Charge	Mass (Gev/c^2)
Up	u	2/3	0.004
Down	d	-1/3	0.007
Charm	c	2/3	0.3
Strange	s	-1/3	1.3
Beauty	b	2/3	4.8
Top	t	-1/3	174

$$\begin{pmatrix} u \\ d \end{pmatrix} \begin{pmatrix} c \\ s \end{pmatrix} \begin{pmatrix} t \\ b \end{pmatrix}$$

The masses and charges of the fermions can be summarized in Table 1.1 for leptons and in Table 1.2 for quarks.

99% of our world are made of by leptons and quarks in the first family. leptons and quarks in second and third families are largely produced at machine built for high energy experiments.

Table 1.3: table of the four fundamental forces

Force	Boson	Symbol	Charge	Mass (Gev/c^2)	Spin-Parity
Gravitation	graviton	g	0	0	2^+
Electromagnetic	photon	γ	0	0	1^-
Weak	W	$W^\pm$	± 1	80.3	± 1
	Z	Z^0	0	91.2	± 1
Strong	Gluon	g	0	0	1^-

Table 1.4: theory corresponds to the four fundamental forces

Force	theory	source	typical lifetime
Gravitation	general relativity	Masses	
Electro-magnetic	Quantum Electrodynamics	electric charge	10^{-26}
Weak	Quantum Flavor-dynamics	"Weak charge"	10^{-8}
Strong	Quantum Chromodynamics	"color charge"	10^{-23}

1.2 Fundamental Forces

Those fundamental particles interact with each other through exchanging *intermediate vector bosons*, a field quanta with integral spin. Such process gives rise to the fundamental forces. Our understanding is that we have four kinds of fundamental forces: two long range interactions: gravitational and electromagnetic forces, and two forces with short range: weak and strong interactions.

There is a physical theory to each of those forces. The theory describing gravitation is Einstein's general theory of relativity. A completely satisfactory quantum theory of gravity has not yet been worked out, and it is too weak to account for any important effects in particle physics.

The electromagnetic, weak and strong forces accounts for the interactions in particle physics. The character of the field quanta in the four forces is summarized in Table 1.3. In Table 1.4 we listed the corresponding theory to describe them.

Those fundamental particles described in previous section experience different forces according to what kind of "charges" they carry. The quarks are subject to electro-magnetic, weak, and strong interactions. The $e-$, $\mu-$, and $\tau-$ leptons are involved in both the electromagnetic and weak interactions, while the neutrinos, $(\nu_e, \nu_\mu, \nu_\tau)$, interact only through the weak interaction. As previously noted, the gravitional interaction in particle physics is generally ignored.

1.3 Standard Model

Standard Model (SM) provides a general description of fundamental particles and forces in a way that is accessible with modern high energy physics experiment. The theory is based on gauge group $SU(3)_{color} \times (SU(2)_L \times U(1)_Y)_{electroweak}$. The quarks and leptons are grouped into left-handed weak isospin doublets and right-handed singlets.

$$\begin{pmatrix} \nu_e \\ e \end{pmatrix}_L, \begin{pmatrix} \nu_\mu \\ \mu \end{pmatrix}_L, \begin{pmatrix} \nu_\tau \\ \tau \end{pmatrix}_L, e_R, \mu_R, \tau_R$$

$$\begin{pmatrix} u \\ d^{'} \end{pmatrix}_L, \begin{pmatrix} c \\ s^{'} \end{pmatrix}_L, \begin{pmatrix} t \\ b^{'} \end{pmatrix}_L, u_R, c_R, t_R, d^{'}_R, s^{'}_R, b^{'}_R$$

Each of the $d^{'}$, $s^{'}$ and $b^{'}$ is the combination of d, s, b quark state and will be explained in the next section. The $SU(2)_L \times U(1)_Y$ portion of the gauge group introduced four massless gauge bosons: $W^1_\mu, W^2_\mu, W^3_\mu$ for $SU(2)_L$, B_μ for $U(1)_Y$. The four gauge bosons coupled with a scalar Higgs field through a *spontaneous symmetry breaking* mechanism to become the massive W^+, W^-, Z^0 bosons and a massless γ.

The relationship between the four massless field quanta and the intermediate vector bosons are:

$$W_\mu^\pm = \frac{1}{\sqrt{2}}(W_\mu^1 \pm iW_\mu^2)$$

$$Z_\mu = W_\mu^3 cos\theta_w - B_\mu sin\theta_W$$

$$A_\mu = W_\mu^3 sin\theta_w + B_\mu cos\theta_W$$

The θ_W is the *Weinberg Angle* in electroweak theory, which relates electro-magnetic coupling and weak coupling strength. θ_W is about $28.7°$.

The dynamics of the interacting particles can be described in the Standard Model Lagrangian:

$$L^{total} = L_d^f + L_d^b + L_{cp}^{f,h} + L_{cp}^{b,h} + L_{int}^f$$

Where:

- L_d^f is the dynamic term of fermion. For example: $\bar{f}\gamma^\mu \partial_\mu f_L$
- L_d^b is the dynamic term of gauge vector bosons: $W_\mu^\pm, Z_0, \gamma$. For example: $(-\frac{1}{4}W_{\mu\nu} \cdot W^{\mu\nu} - \frac{1}{4}B_{\mu\nu}B^{\mu\nu}$
- $L_{cp}^{f,h}$ is the fermion coupling with higgs to give fermion mass. For example: $(G_1\bar{L}\phi R + G_2\bar{L}\phi_c R + h.c)$
- $L_{cp}^{b,h}$ is the vector boson-higgs coupling term which gives gauge boson mass. exp: $|(\imath\partial_\mu - g\frac{1}{2}\tau \cdot W_\mu - g'\frac{Y}{2}B_\mu)\phi|^2 - V(\phi)$
- L_{int}^f is the interaction term for fermion coupled with intermediate vector boson and/or the colored gluon. For example, $\bar{f}_L\gamma^\mu(\imath\partial_\mu - g\frac{1}{2}\tau \cdot W_\mu - g'\frac{Y}{2}B_\mu)f_L$

We are interested in the interaction term, L^f_{int}, which gives the strong and electroweak interactions:

$$
\begin{aligned}
L^f_{int} = L^{ew}_{int} \quad &+ \quad L^{strong}_{int} \\
L^{ew}_{int} \quad &= \quad L^{ec}_{int} + L^{cc}_{int} + L^{nc}_{int}
\end{aligned}
$$

Where,

- L^{ew}_{int} is the Lagrangian for electroweak interaction
  - L^{em}_{int} is the *electromagnetic current* Lagrangian
  - L^{cc}_{int} is the *charge current* interacting Lagrangian
  - L^{nc}_{int} is the *neutral current* interacting Lagrangian
- L^{strong}_{int} is the strong color force Lagrangian

The individual form of those interacting Lagrangian can be written as follows:

$$
\begin{aligned}
L^{em}_{int} &= \sum_{f=\ell,q} eQ_f(\bar{f}\gamma^\mu f)A^\mu \\
L^{cc}_{int} &= \frac{e}{sin\theta_w\sqrt{2}}[\sum_{f=\ell,q}(\bar{L}\gamma^\mu L)W^+_\mu + (Hermition.Conjugate)] \\
L^{nc}_{int} &= \frac{e}{sin\theta_w cos\theta_w}\sum_{f=\ell,q}[\bar{f}_L\gamma^\mu f_L(T^3_f - Q_f sin^2\theta_w) + \bar{f}_R\gamma^\mu f_R(-Q_f sin^2\theta_w)]Z_\mu \\
L^{st}_{int} &= \frac{g_3}{2}\sum_{f=q}\bar{f}_\alpha\gamma^\mu\lambda^a_{\alpha\beta}f_\beta G^a_\mu
\end{aligned}
$$

1.4 Weak Interaction

Weak Interaction is the primary reason why we divide those fundamental particle species into three families for lepton and quarks. The letpon generation was grouped in the way that it is diagonalized in weak eigenspace. There is no weak interaction involving leptons from different families under current experimental limit. However, weak eigenspace and strong eigenspace doesn't coincide with each other. For quark, which not only interacts weakly but also experiences strong interaction, such effect leads to the phenomenon that quark could decay into another quark, including quarks in different family, through weak interaction. This is not seen in leptons. This "cross-family" decay is because quark was grouped as a eigenvector in strong Hamiltonian H_{strong} but not the weak Hamiltonian H_{weak} where $[H_{strong}, H_{weak}]$ does not commute. For this purpose, a matrix materializing the cross family quark decays called the **Cabibbo-Kobayashi-Maskawa** (CKM) matrix is devised. The $d^{'}$, $s^{'}$,$b^{'}$ in our previous section can be written:

$$\begin{pmatrix} d^{'} \\ s^{'} \\ b^{'} \end{pmatrix} = V_{CKM} \times \begin{pmatrix} d \\ s \\ b \end{pmatrix}$$

The V_{CKM} is:

$$V_{CKM} = \begin{pmatrix} V_{ud} & V_{us} & V_{ub} \\ V_{cd} & V_{cs} & V_{cb} \\ V_{td} & V_{ts} & V_{tb} \end{pmatrix}$$

The CKM matrix can be parameterized in terms of the four rotation angle θ_1,θ_2,θ_3 and δ as:

$$V_{CKM} = \begin{pmatrix} c_1 & c_3 s_1 & s_1 s_3 \\ -s_1 c_2 & c_1 c_2 c_3 - s_2 s_3 e^{i\delta} & c_1 c_2 s_3 + c_3 s_2 e^{i\delta} \\ s_1 s_2 & -c_1 c_3 s_2 - c_2 s_3 e^{-i\delta} & -c_1 s_2 s_3 + c_2 c_3 e^{i\delta} \end{pmatrix}$$

where $c_i = cos\theta_i$, $s_i = sin\theta_i$ [1] and the phase, δ, is within the range 0-2π. A popular approximation to the CKM matrix is given by Wolfenstein[2] in the following:

$$V_{CKM} = \begin{pmatrix} 1-\frac{\lambda^2}{2} & \lambda & A\lambda^3(\rho - i\eta) \\ -\lambda & 1-\frac{\lambda^2}{2} & A\lambda^2 \\ A\lambda^3(1-\rho-i\eta) & -A\lambda^2 & 1 \end{pmatrix}$$

The strength of the quark coupling between generations can be understood in terms of power of $\lambda \simeq 0.22$. As can be seen from above, the suppression for quark mixing in $1^{st} - 2^{nd}$, $2^{nd} - 3^{rd}$ and $1^{st} - 3^{rd}$ family is given by $\lambda, \lambda^2, \lambda^3$ respectively.

Assuming the unitarity of CKM matrix, the measured values of the element within CKM matrix up to date are: [3]

$$V_{CKM} = \begin{pmatrix} 0.9745 - 0.9760 & 0.217 - 0.224 & 0.0018 - 0.0045 \\ 0.217 - 0.224 & 0.9737 - 0.9753 & 0.036 - 0.042 \\ 0.004 - 0.013 & 0.035 - 0.042 & 0.9991 - 0.9994 \end{pmatrix}$$

The electroweak interaction Hamiltonian H_{int} from their interaction Lagrangian, L^{cc}_{int} and L^{nc}_{int} can be obtained as follows:

$$H^W_{int} = \frac{\partial L^W_{int}}{\partial(\partial_0\phi)}\partial^0\phi - L^W_{int}$$

$H^W_{int} = H^{cc}_{int} + H^{nc}_{int}$. where,

- $H^{cc}_{int} = -i\frac{g}{\sqrt{2}}(J^\mu W^+_\mu + J^{\mu\dagger}W^-_\mu)$
- $H^{nc}_{int} = -i\frac{g}{\cos\theta_w}\bar{\phi}_f\gamma^\mu[\frac{1}{2}(1-\gamma^5)T^3 - \sin^2\theta_w Q]\phi_f Z_\mu$

For lepton sector, its charged current J^μ_{lepton} can be written as:

$$\begin{pmatrix} \bar{\nu_e} & \bar{\nu_\mu} & \bar{\nu_\tau} \end{pmatrix} \frac{1}{2}\gamma^\mu(1-\gamma^5) \begin{pmatrix} e \\ \mu \\ \tau \end{pmatrix}$$

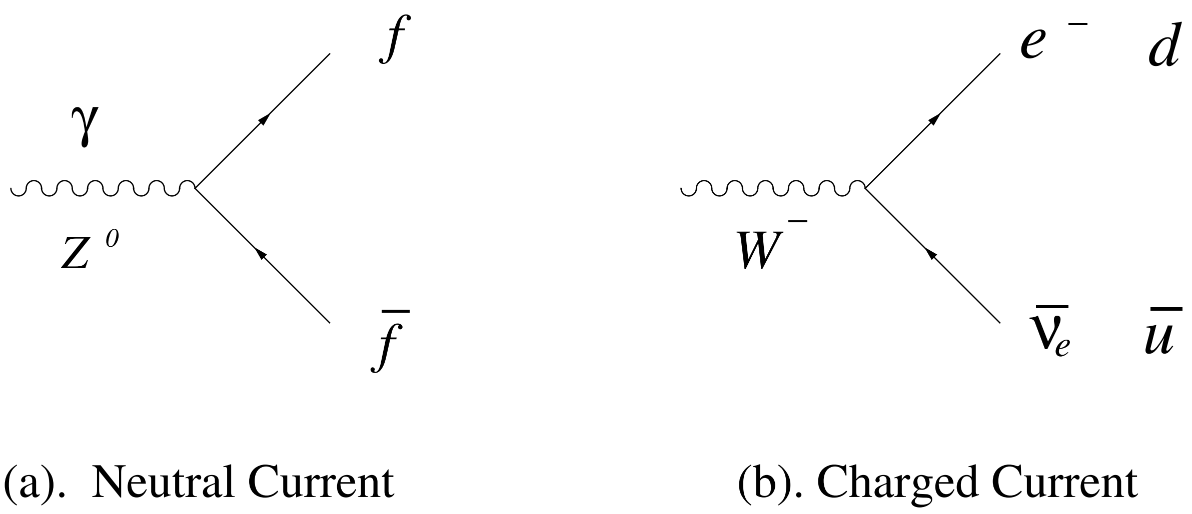

Figure 1.1: The Electroweak currents

charged current for quark is similar except for the additional factor of V_{CKM}. J^{μ}_{quark} is:

$$\begin{pmatrix} \bar{u} & \bar{c} & \bar{t} \end{pmatrix} \frac{1}{2}\gamma^{\mu}(1-\gamma^{5})V_{CKM}\begin{pmatrix} d \\ s \\ b \end{pmatrix}$$

Figure 1.1 shows the electroweak currents. In Figure 1.1(a) shows the photon and Z boson carries the neutral current between a fermion and its anti-fermion. Figure 1.1(b) demonstrates the W boson as the charged current carrier. We are studying the charged weak current in this analysis.

1.5 B Meson

b quark was discovered in 1977 where the narrow $\Upsilon(1S)$ resonance, a $b\bar{b}$ state, was detected [6], [7] at Fermilab by the Columbia-Fermilab-Stony Brook collaboration. The B meson discovery through the establishment of $\Upsilon(4S)$ resonance $J^{pc} = 1^{--}$ in CLEO[8] and CUSB[9]

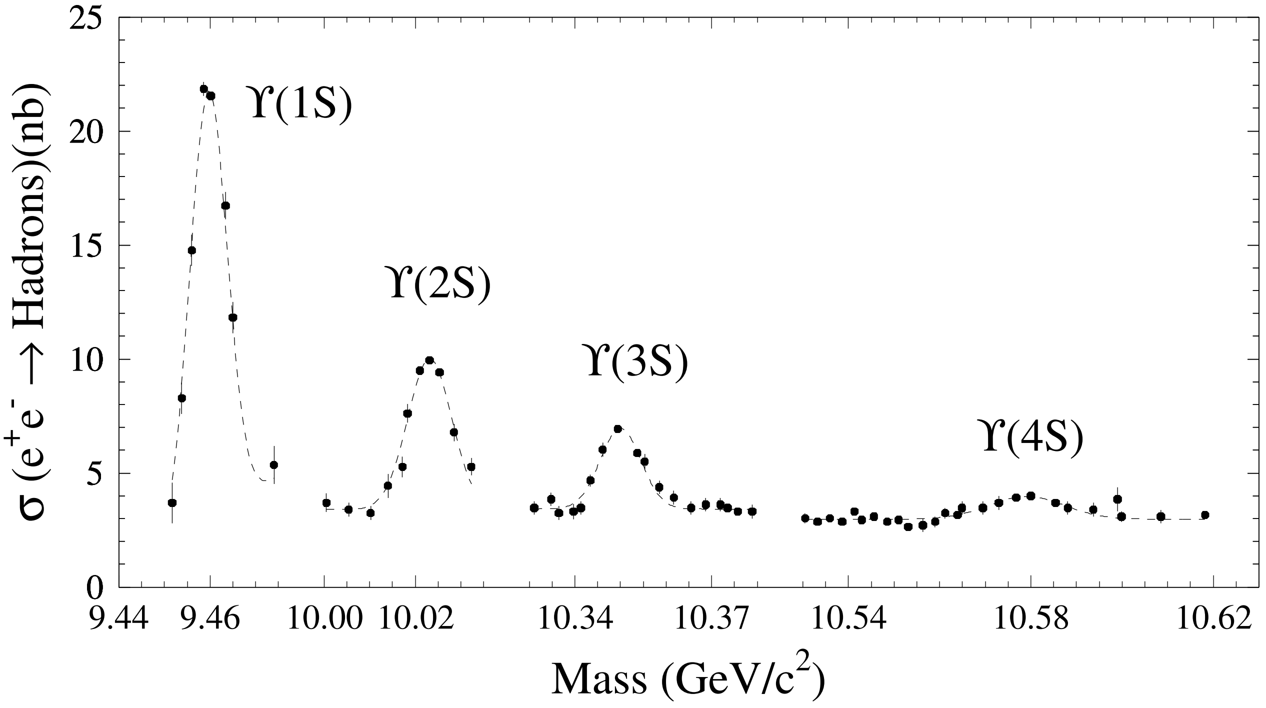

Figure 1.2: The cross section of Υ(1S) to Υ(4S) state

collaboration at CESR storage ring. Its charge assignment favored $-1/3$. With the discovery of τ lepton in 1975[10], [11], the quark content within Υ resonance was assigned as the bottom quark.

The $\Upsilon(4S)$ sits right above the mass threshold of the two lightest B meson: $\bar{B}^0(b\bar{d})$ and $B^-(b\bar{u})$. In addition to $\Upsilon(4S)$, there are other $b\bar{b}$ resonance (bottomonion) from e^+e^- collision at lower energy region: $\Upsilon(1S)$, $\Upsilon(2S)$ and $\Upsilon(3S)$. In Figure 1.2 we can see the cross section of the different $\Upsilon(1S)$ to $\Upsilon(4S)$ states.

$\Upsilon(4S)$ has a broader resonance compared with other lower Υ resonant state. This is a sign of B mesons production that is not existent from $\Upsilon(1S)$ to $\Upsilon(3S)$. B meson is produced in pair in $\Upsilon(4S)$ decay. The mass spectrum of B meson can be seen at Figure 1.3

Besides B_d^0 and B_u^+ meson, b-quark can combine with a heavier anti-quark (or vice versa) to form other kinds of B meson. $\bar{B}_s$ meson, a b$\bar{s}$ quark-anti-quark pair, has been discovered

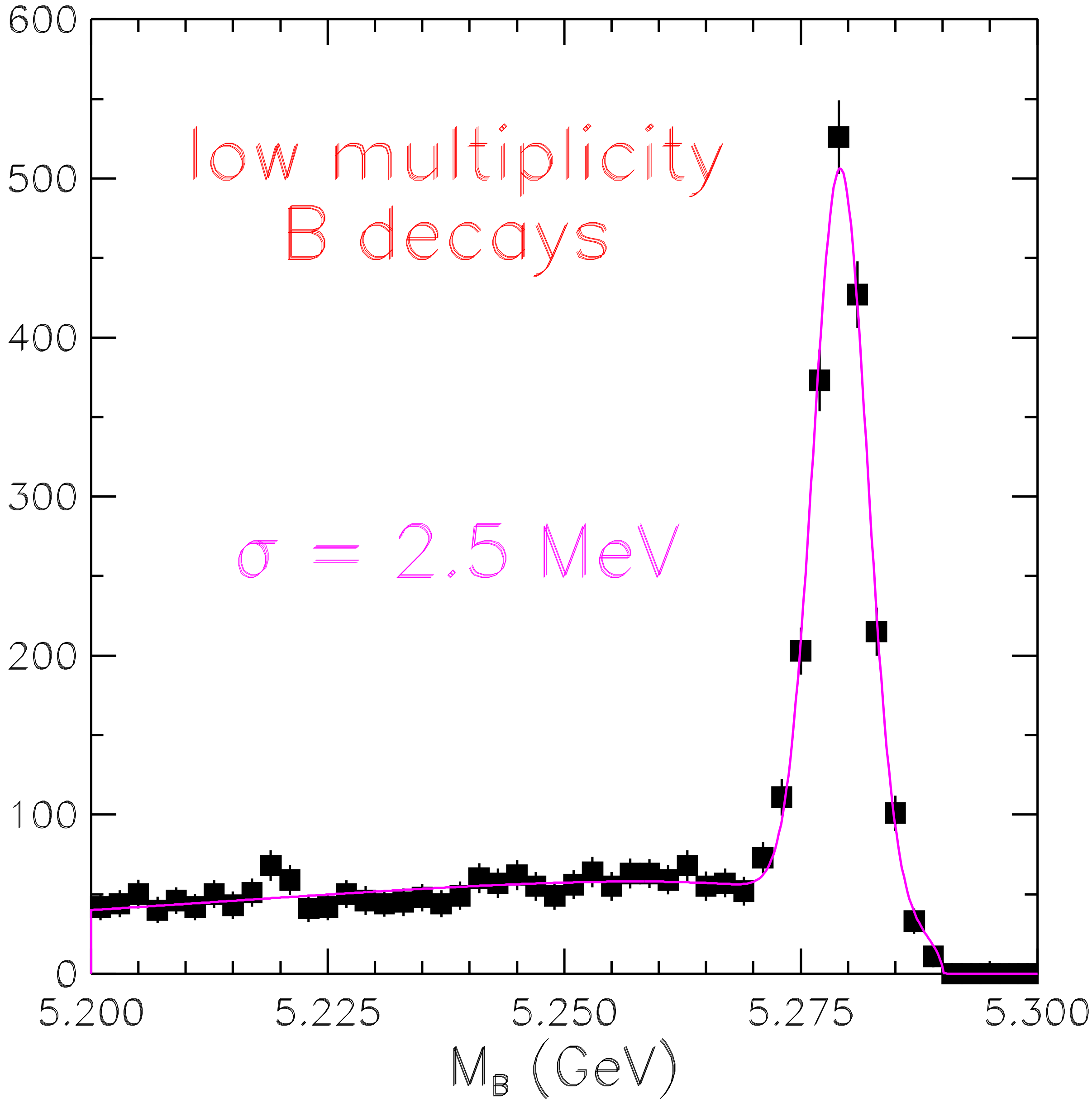

Figure 1.3: The B meson mass spectrum

at higher energy experiment at LEP [4]. Up to now, B_c meson, a b$\bar{c}$ quark pair, has not yet been seen. The following discussion will focus on $\bar{B}^0$ and B^- produced at CLEO experiment.

In CLEO, B meson pair is produced at $\Upsilon(4S)$ state from the collision of e^+, e^- at center of mass energy 10.58 GeV/c.

$$e^+e^- \rightarrow \gamma^* \rightarrow \bar{B}^0 B^0, B^- B^+$$

Under the $\Upsilon(4S)$ energy region, there are other processes in addition to the B meson production. The $\Upsilon(4S)$ can also decay into other lighter quark-antiquark pair:

$$e^+e^- \rightarrow \gamma^* \rightarrow c\bar{c}, s\bar{s}, d\bar{d}, u\bar{u}$$

The above production is referred as *continuum*. Since in $\Upsilon(4S)$ the cross section ratio of $b\bar{b}$ to *continuum* is about 1 : 3, the *continuum* needs to be estimated in care. For this reason, CLEO runs the experiment approximately 2/3 of its time at $\Upsilon(4S)$ energy region (*On* resonance data) and 1/3 of its time at energy about 60 Mev lower (*Off* resonance data) in order to simulate the *continuum* production. After we scaled the *Off* data by a factor corrected for the energy and luminosity difference to obtain the *continuum* portion in $\Upsilon(4S)$ production, then the *On* data will subtract the *continuum* to obtain the data predominantly enriched in B mesons for our analysis.

B meson can decay through the weak interaction of b quark: $b \rightarrow cW^-$ or a more suppressed $b \rightarrow uW^-$ channel. We will discuss some of its findings in the next chapter.

Chapter 2

B Meson Physics

2.1 Introduction

The first impression of B meson by looking at the PDG table is that B meson has two distinct properties: (1) longer lifetime compared with the other heavy flavor meson D for example, and (2) it has lots of decay modes with small branching fraction.

The long lifetime of B meson is the result of the CKM matrix suppression in B meson decay. Because t-quark is much heavier than b quark, b quark has to decay into a different generation, most likely to charm quark. The current measured V_{cb} value is a small number about 0.04. If we compare this number with charm meson decay, then the allowed in-generation decay of charm to strange quark makes the charm meson have a shorter lifetime than a B meson because V_{cs} is much bigger than V_{cb}..

The heaviness of the b quark reserves a large room of phase space for b quark to decay to. Unlike π, ρ, ω and strange flavored meson which were saturated by a few decay modes, B meson has enormous amounts of decay channels.

Figure 2.1 shows some feynman diagrams of B meson decays. The B semileptonic decay studied in this dissertation goes through the external spectator diagram, where the virtual W boson materializes into a lepton and neutrino pair.

2.2 CKM Matrix and B Physics

In standard Model, B meson physics plays a key role to probe the CKM matrix, the matrix that couples weak and strong eigenstate. CKM matrix is also the source of CP violation in standard model. The CKM matrix can be parameterized by Wolfenstein parameterization [2]:

$$V_{CKM} = \begin{pmatrix} 1-\frac{\lambda^2}{2} & \lambda & A\lambda^3(\rho - i\eta) \\ -\lambda & 1-\frac{\lambda^2}{2} & A\lambda^2 \\ A\lambda^3(1-\rho-i\eta) & -A\lambda^2 & 1 \end{pmatrix}$$

Among the four independent parameters, λ has been well measured from nuclear beta decay and the measurement of semileptonic decay of strange meson. The remaining A, ρ and η can be seen closely associated with the third generation. There are four CKM elements can be obtained from B physics measurement: V_{ub}, V_{cb}, V_{td} and V_{ts}. By looking at the CKM matrix and with the knowledge that V_{us} in Wolfenstein parameterization $\lambda = sin\theta_c = 0.22$ from measurement of strange particle decay, we can obtain:

$$|V_{cb}/V_{us}^2| = A \quad and \quad |V_{ub}^*/V_{cd}V_{cb}| = \sqrt{\rho^2 + \eta^2} \tag{2.1}$$

The measurement of $|V_{cb}|$ essentially determine A. The constraint from $|V_{ub}|$ defines a circle in the (ρ, η) plane. $|V_{cb}|$ and $|V_{ub}|$ can be directly measured by the semileptonic B meson decay. $|V_{td}|$ and $|V_{ts}|$ can be indirectly inferred by the $B - \bar{B}$ mixing measurement.

Direct t decay measurement of CKM Matrix element $|V_{tb}|$, $|V_{ts}|$ and $|V_{td}|$ is not yet feasible.

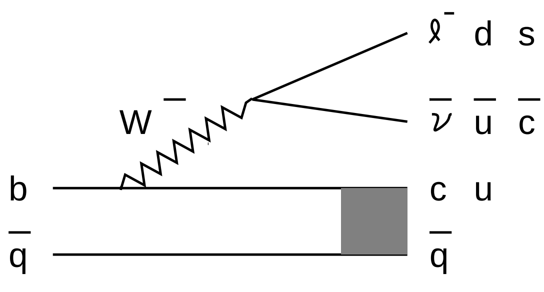

(a) Spectator

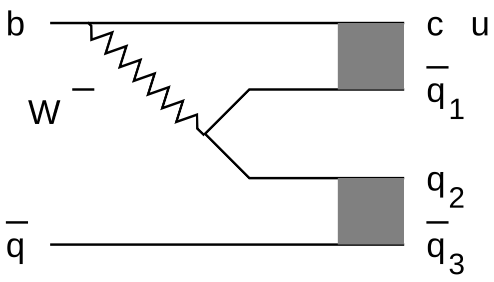

(b) Color Suppressed

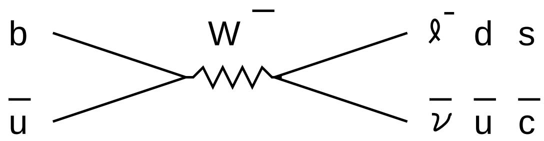

(c) Annihilation

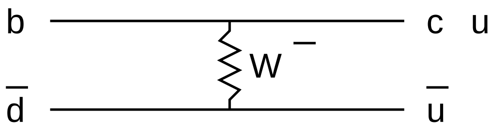

(d) Exchange

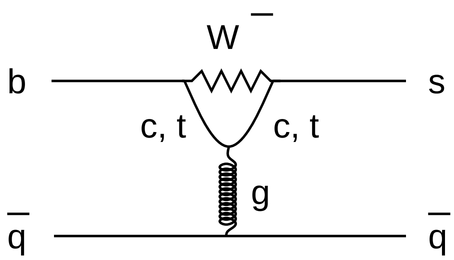

(e) Penguin

Figure 2.1: The feynman diagrams of B decay. Shown in the plot is the external spectator decay, internal spectator decay 9color suppressed), annihilation of B meson, the exchange of W boson between the two B meson quarks and the penguin decay.

Table 2.1: Source and Relative Strength of Weak Transition

Relative amplitude	$\lvert V_{ij}\rvert$	Source of information	example
≈ 1	$\lvert V_{ud}\rvert$	Nuclear β decay	$n \to pe^-\bar{\nu}_e$
≈ 1	$\lvert V_{cs}\rvert$	Charmed particle decay	$D^0 \to K^-e^+\nu_e$
≈ 0.22	$\lvert V_{us}\rvert$	Strange particle decay	$K \to \pi\ell\nu$
≈ 0.22	$\lvert V_{cd}\rvert$	neutrino production of charm	$\nu_\mu d \to \mu^- c$
≈ 0.04	$\lvert V_{cb}\rvert$	B decay to Charm	$\bar{B}^0 \to D^{*+}\ell^-\bar{\nu}_\ell$
≈ 0.003	$\lvert V_{ub}\rvert$	Charmless B decay	$B \to \pi(\rho)\ell\bar{\nu}_\ell$

For other elements like $|V_{ud}|$, $|V_{cs}|$, $|V_{us}|$, $|V_{cd}|$, $|V_{cb}|$ and $|V_{ub}|$, we list its relative amplitude and source of information in Table 2.1 [33]

2.3 Semileptonic B Decay

Semileptonic B decays proceeds when a b quark decays to a c or u quark and a virtual W^- boson, then this virtual W^- boson decays to a $(\ell^-, \bar{\nu}_\ell)$ pair subsequently. The accompanying light quark u, or d does not involve in this process is known as the spectator quark. The feynman diagram of B semileptonic is shown in Figure 2.1.(a).

The partial width for the weak decay of the free quark Q to fermions of non-zero masses was calculated by Corthes [22]. The calculation for $Q \to qW^*$, $W^* \to f_1\bar{f}_2$, where f_1, f_2 are fermions and $m_Q \ll m_W$, is

$$\Gamma(Q \to qf_1\bar{f}_2) = \Gamma_0 N_c \mid V_{qQ} \mid^2 \mid V_{f_2f_1} \mid^2 I(\frac{m_q}{m_Q}, \frac{m_{f_1}}{m_Q}, \frac{m_{f_2}}{m_Q}) \tag{2.2}$$

where,

$$\Gamma_0 = G_F^2 m_Q^5 / 192\pi^3 \tag{2.3}$$

$$I(x, y, z) \quad = \quad 12\int_{(x+y)^2}^{(1-z)^2} \frac{ds}{s}(s - x^2 - y^2)(1 + z^2 - s)$$

$$\times([s-(x-y)^2][s-(x+y)^2][(1+z)^2-s][(1-z)^2-s])^{1/2}$$

and,

- N_c, 3 for hadronic decay, 1 for semileptonic decay
- $V_{f_2 f_1}$ is the CKM element for $W \to \bar{f}_2 f_1$

The function I has a familiar form as μ decay when only one final state particle has non-zero mass:

$$I(x,0,0) = I(0,x,0) = I(0,0,x) = 1 - 8x^2 + 8x^6 - x^8 - 24x^4 lnx$$

The B semileptonic branching fraction is given by:

$$Br(B \to X\ell\bar{\nu}_\ell) = \frac{\Gamma(B \to X\ell\bar{\nu}_\ell)}{\Gamma(B \to All)}$$

where,

$$\begin{aligned}
\Gamma(b \to X\ell\bar{\nu}_\ell) &\approx \Gamma(b \to ce^-\bar{\nu}) = \Gamma(b \to c\mu^-\bar{\nu}) \\
\Gamma(B \to All) &\approx \Gamma(b \to ce^-\nu) + \Gamma(b \to c\mu^-\nu) + \Gamma(b \to c\tau^-\nu) + \\
&\quad \Gamma(b \to c\bar{u}d) + \Gamma(b \to c\bar{c}s) + \Gamma(b \to c\bar{u}s) + \\
&\quad \Gamma(b \to c\bar{c}d)
\end{aligned}$$

We have ignored the small contribution from $b \to u$, as well as the rare decay and penguin process in our B meson total decay width approximation. This will lead us to a crude estimation of B semileptonic branching fraction as:

$$Br(B \to X\ell\bar{\nu}_\ell) \approx \frac{r_\ell}{r_\ell + r_\tau + 3\eta_{\bar{u}d}r_{\bar{u}d} + 3\eta_{\bar{c}s}r_{\bar{c}s} + 3\eta_{\bar{u}s}r_{\bar{u}s} + 3\eta_{\bar{c}d}r_{\bar{c}d}} \tag{2.4}$$

Where,

- η accounts for the QCD factor for each channel
- r accounts for the available phase space
- the number 3 accounts for the 3 colors of quark

Ignoring the small contribution from $b \to c\bar{u}s$ and $b \to c\bar{c}d$ because of its small CKM strength, and the QCD correction for each channel, we can calculate the branching fraction with the assigned value of mass for leptons and quarks. Since the masses of lepton are well measured, and the masses of neutrino are very small, we have $r_\ell = 0.45$ and $r_\tau = 0.12$. The quark masses bears some uncertainty, we assign the value of our best knowledge $m_u \approx m_d \approx 0$ and $m_s = 0.5$ GeV/c^2, $m_c = 1.4$ GeV/c^2, we obtain $r_{\bar{u}d} \approx r_\ell \approx 0.45$, $r_{c\bar{s}} \approx r_\tau \approx 0.12$ [14] then we have $Br(\bar{B} \to X\ell\bar{\nu}_\ell)$:

$$Br(\bar{B} \to X\ell\bar{\nu}_\ell) = \frac{\Gamma_\ell}{\Gamma_B} = \frac{r_\ell}{2r_\ell + r_\tau + 3r_{\bar{u}d} + 3r_{c\bar{s}}} = 16.5\% \qquad (2.5)$$

This simplified picture needs some corrections. We need to add the gluon radiation and gluon exchange process [15] [16] to the calculation, as illustrated in feynman diagram at Figure 2.2. The new result is to enhance the hadronic width in spectator decay process. Gluon exchange can modify the hadronic event examplified as follows. From equation 2.2 the decay width of $b \to c\bar{u}d$ can be written as:

$$\Gamma(b \to c\bar{u}d) = 3\Gamma_0 I(\frac{m_c}{m_b}, 0, 0)\eta J \qquad (2.6)$$

where:

- $\eta = \frac{c_-^2 + 2c_+^2}{3}$ for hard gluon exchange with
    - $c_\pm$ is the Wilson Coefficient. $c_+ = [\frac{\alpha_s(\mu)}{\alpha_s(M_W)}]^{-6/23}$. $c_- = [\frac{\alpha_s(\mu)}{\alpha_s(M_W)}]^{12/23}$

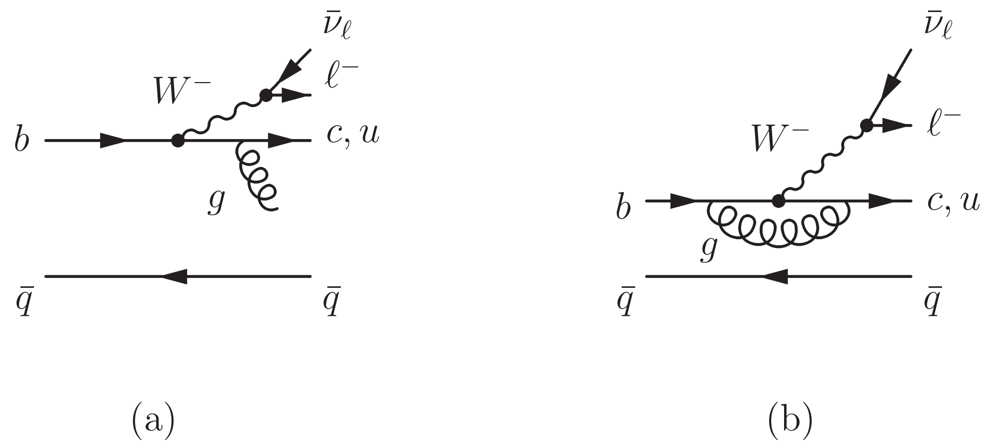

Figure 2.2: First order gluon correction in B semileptonic decay. (a) is for the gluon radiation and (b) illustrates the gluon exchange between initial and final quark

- V_{ud} is approximated as 1
- μ is the renormalization scale. This is a non-physical artifact of the calculation, which only includes the effects of virtual gluons in the momentum range from μ to M_W.
- J: for softer gluon momentum below the cutoff μ.
- $\Gamma_0 = \frac{G_F^2 M_Q^5}{192\pi^3}$

For $\mu = m_b$, the value is $\eta \approx 1.$ and J ≈ 1.15. This results the enhancement of hadronic width by a factor of 1.27 to be inserted into calculation. If we calculate the decay width using mass value: $m_b = 4.6(5.0)$, $m_c = 1.2$ (1.7), $m_s = 0.15(0.3)$, $m_u = m_d = 0(0.16)$, we have the following result:

$$B_{sl} = (12.2 \pm 0.45(scale) \pm 0.8(\alpha_s))\% \tag{2.7}$$

for light masses calculation and

$$B_{sl} = (14.4 \pm 0.45(scale) \pm 0.8(\alpha_s))\% \tag{2.8}$$

for heavy masses calculation. The error on scale comes from the uncertainty of μ when we varied μ between $1/2m_b$ and m_b.

One of the mystery in B meson semileptonic decay is the large discrepancy between model prediction and experimental measured value. The experimental value of the inclusive semileptonic branching fraction is well below 12.5%, the lower bound of the theoretical model prediction[57]. This discrepancy is about at least 4 σ away. It needs the 10-11% reduction of theoretical prediction in semileptonic decay width to match with experimental value, which requires 20% enhancement of hadronic decay width to make it work.

Our lack of knowledge of the non-perturbative QCD process prohibits us from calculating hadronic current in B meson semileptonic decay width. Various phenomenological model has emerged to simulate the dynamic system for calculation. Those models can be characterized into two categories: inclusive and exclusive models. The inclusive model works on quark level. The exclusive model assumes that B semileptonic decays are saturated by a few resonant final states and calculate them correspondingly. In our measurement, we don't intend to examine the validity of those models, but through the lepton spectrum those models provided to obtain the B meson semileptonic branching fraction, the $\Upsilon(4S)$ $B^0 - \bar{B}^0$ mixing parameter χ_d and the lifetime ratio of charged verse neutral B meson, τ_+/τ_0.

2.3.1 Inclusive Model (ACCMM)

In the pioneering work by Altarelli Cabibbo, Corbo Maiani and Martinelli (ACCMM) [17], the momentum of the spectator quark in B meson semileptonic decay is described by a Gaussian distribution $f(p)$:

$$f(p) = \frac{4}{\sqrt{\pi}p_f^3} exp(-p^2/p_f^2) \tag{2.9}$$

The mass of b quark is assigned by an off-shell mass squared:

$$m_b^2 = m_B^2 + m_{sp}^2 - 2m_B\sqrt{p^2 + m_{sp}^2} \tag{2.10}$$

where, p_f is the Fermi momentum parameter determining the width of $f(p)$, m_B, the mass of B meson and m_{sp}, the mass of spectator quark.

We then obtain at the following semileptonic partial width to get leptonic momentum spectrum:

$$\frac{d\Gamma_{sl}}{dx} = \frac{G_F^2 V_{cb}^2 m_b^5}{96\pi^3}\Phi(x,\epsilon)[1 - \frac{2\alpha_s}{3\pi}G(x,\epsilon)] \tag{2.11}$$

The free quark distribution term, $\Phi(x,\epsilon)$ and the gluon radiation term, $G(x,\epsilon)$, can be described in the following:

$$\Phi(x,\epsilon) = \frac{x^2(1-\epsilon^2-x)^2}{(1-x)^3}[(1-x)(3-2x)+(3-x)\epsilon^2] \tag{2.12}$$

$$\begin{aligned} G(x,\epsilon) &\approx \frac{1}{x_M}2ln(x_M - x)[2x_M + (2-x_M)ln(1-x_M)] \\ x &\rightarrow x_M \end{aligned}$$

where x= $2E_\ell/m_b$, $\epsilon = m_c/m_b$ and $x_M = 1-(m_c/m_b)^2$. $\Phi(x,\epsilon)$ is the free quark decay distribution [19].

The ACCMM model prediction for $b \to c\ell^-\bar{\nu}_\ell$ inclusive lepton spectrum has given a nice fit to the experimental measurement[46]. Its reliability for $b \to u\ell^-\bar{\nu}_\ell$ lepton spectrum at endpoint region is controversial. For our measurement, since $b \to u\ell^-\bar{\nu}_\ell$ only makes very small contribution and can be safely neglected, the consideration of $b \to u\ell^-\bar{\nu}_\ell$ is managed by estimating their systematic error.

2.3.2 Exclusive Model prediction

General Form

The hadronic current can be constructed from the available four-vectors that are momentum and spin polarization vectors: $H^\mu = V^\mu - A^\mu$, where V^μ and A^μ corresponds to vector and axial vector current respectively. The matrix of hadronic current in B decay can categorized as the following:

- $P(Q\bar{q}) \rightarrow P^{'}(q^{'}\bar{q})\ell\nu$: pseudo-scalar to pseudo-scalar decay, such as $B^0 \rightarrow D^-\ell^+\nu_\ell$
- $P(Q\bar{q}) \rightarrow V(q^{'}\bar{q})\ell\nu$: pseudo-scalar to vector decay, like $\bar{B}^0 \rightarrow D^{*+}\ell^-\bar{\nu}_\ell$ for example.

$P \rightarrow P^{'}\ell\nu$:

The $P(Q\bar{q}) \rightarrow P^{'}(q^{'}\bar{q})\ell\nu$ type of decay can be written as the following. Since axial vector current disappear in this type of decay [24],[60]:

$$< P^{'}(p^{'})|V^\mu - A^\mu|P(p) >=< P^{'}(p^{'})|V^\mu|P(p) > \tag{2.13}$$

we have:

$$< P^{'}(p^{'})|V^\mu|P(p) >= f_+(q^2)(p+p^{'})^\mu + f_-(q^2)(p-p^{'})^\mu \tag{2.14}$$

If we only refer lepton as e, μ in B meson semileptonic decay, then in the limit of $m_\ell \rightarrow 0$, term proportional to $(p-p^{'})$ are negligible because $(p-p^{'})^\mu L_\mu = 0$ at small lepton mass. Thus for $\ell = e$ or μ, the hadronic current can be written in terms of single form factor $f_+(q^2)$:

$$< P^{'}(p^{'})|V^\mu|P(p) >= f_+(q^2)(p+p^{'})^\mu \tag{2.15}$$

$P \to V\ell\nu$:

For $P(Q\bar{q}) \to V(q^{'}\bar{q})\ell\nu$ type of decay, the hadronic current is written as the following:

$$\begin{aligned} < V^{'}(p^{'},\varepsilon)|V^{\mu} - A^{\mu}|P(p) > &= \frac{2i\epsilon^{\mu\nu\alpha\beta}}{M + m_V}\varepsilon^{*}_{\nu}p^{'}_{\alpha}p_{\beta}V(q^2) \\ &- (M + m_V)\varepsilon^{*\mu}A_1(q^2) \\ &+ \frac{\varepsilon^{*}q}{M + m_V}(p + p^{'})^{\mu}A_2(q^2) \\ &+ 2m_V\frac{\varepsilon^{*}q}{q^2}q^{\mu}A_3(q^2) \\ &- 2m_V\frac{\varepsilon^{*}q}{q^2}q^{\mu}A_0(q^2) \end{aligned}$$

where,

- $V^{\mu} = \bar{q}^{'}\gamma^{\mu}Q$
- $A^{\mu} = \bar{q}^{'}\gamma^{\mu}\gamma_5 Q$
- $A_3(q^2) = \frac{M+m_V}{2m_V}A_1(q^2) - \frac{M-m_V}{2m_V}A_2(q^2)$
- $A_0(0) = A_3(0)$.

If we neglect the τ lepton in B meson semileptonic decay, with the same reason when we simplified the $P(Q\bar{q}) \to P^{'}(q^{'}\bar{q})\ell\nu$, we can obtain the following simplified form:

$$\begin{aligned} < V^{'}(p^{'},\varepsilon)|V^{\mu} - A^{\mu}|P(p) > &= \frac{2i\epsilon^{\mu\nu\alpha\beta}}{M + m_V}\varepsilon^{*}_{\nu}p^{'}_{\alpha}p_{\beta}V(q^2) \\ &- (M + m_V)\varepsilon^{*\mu}A_1(q^2) \\ &+ \frac{\varepsilon^{*}q}{M + m_V}(p + p^{'})^{\mu}A_2(q^2) \end{aligned}$$

There are several models devised to predict the exclusive decay. We will discuss the one used in this analysis, ISGW model.

ISGW model

The model developed by Isgur, Scora, Grinstein and Wise[18], called ISGW model, assumes the B semileptonic decays are saturated by a few resonant final states: $D(1^1S_0)$, $D^*(1^3S_1)$ and the higher resonance states called D^{**} when the c quark, decayed from b quark, combined with the spectator quark to form hadron(s).

The hadronic current of those resonant final states are expressed by form factors. The ISGW model input of the hadronic current of decay mode of $B \to D\ell\nu$ and $B \to D^*\ell\nu$ is expressed below:

$$\begin{aligned}
< D|A_\mu|\bar{B} > &= 0 \\
< D|V_\mu|\bar{B} > &= f_+(p_B + p_D)_\mu + f_-(p_B - p_D)_\mu \\
< D^*|A_\mu|\bar{B} > &= f\epsilon^*_\mu + a_+(\epsilon^* * p_B)(p_B + p_{D^*})_\mu + a_-(\epsilon^* * p_B)(p_B - p_{D^*})_\mu \\
< D^*|V_\mu|\bar{B} > &= ig\epsilon_{\mu\nu\rho\sigma}\epsilon^{*\nu}(p_B + p_{D^*})^\rho(p_B + p_{D^*})^\sigma
\end{aligned}$$

The f, a and g are the form factors varied from model to model. The form factors are functions of q^2, the mass of the *virtual* W boson.

ISGW[18] argues the heaviness of b quark makes it possible to use non-relativistic approximation to model B meson decay. The form factor are obtained by solving the shrödinger equation with a coulomb plus linear potential for the bound state of B meson:

$$V(r) = -\frac{4\alpha_s}{3r} + c + br \tag{2.16}$$

where $\alpha_s = 0.5$, c= -0.84 Gev and b = 0.18 GeV/c^2. We can have the q^2 dependence on the form factor $F(q^2)$ as:

$$F(q^2) \propto F(q^2_{max}) exp(\frac{q^2 - q^2_{max}}{\kappa Q^2}) \tag{2.17}$$

where κ is a parameter introduced to account for the relativistic effect.

ISGW model calculates the form factor value of the minimum recoil of the final state meson, where the q^2 is maximum, then extrapolate to other q^2 region to obtain the lepton momentum spectrum distribution.

2.3.3 The Lepton Spectrum of B Semileptonic Decay

In our analysis, the lepton spectrum of B semileptonic decay plays a key role to access the measurement of semileptonic branching fraction of neutral B, the $B^0 - \bar{B}^0$ mixing parameter χ_d and the lifetime ratio of B^+ vs. B^0. We spend sometime here to have a more qualitative picture of inclusive lepton spectrum of B semileptonic decay.

The lepton spectrum is strongly affected by the following three factors: (1) the V-A coupling, (2) the quantum number of the daughter hadron from B semileptonic decay and (3) the distribution of q^2, which is the square of the W boson four momentum.

V-A coupling

If we first neglect the quantum number of the daughter meson and focus on the quark level, then the $b \to c\ell^-\bar{\nu}$ and $b \to u\ell^-\bar{\nu}$ produces the c- and u-quarks that are predominately helicity $\lambda = -1/2$ in association with charged lepton that is almost purely helicity $\lambda = -1/2$. This allows the collinear configuration where the charged lepton recoils against the neutrino and the daughter quark, leading to a higher possible lepton energy.

For semileptonic charm decay, since $c \to s\ell^+\nu$ produced helicity $\lambda = -1/2$ s-quark and a helicity $\lambda = +1/2$ lepton in the decay. The collinear configuration of a lepton recoiling against the daughter quark and the neutrino is forbiddened, thus leading to a softer lepton spectrum.

Angular Momentum of the Daughter Meson

The above discussion ignores the daughter meson's quantum number. The quantum number of daughter meson affects the lepton spectrum through the cosine angle distribution, $cos\theta_\ell$, where the θ_ℓ is the angle between lepton and the daughter meson in the rest frame of B meson. If a spin-0 daughter meson (like $\bar{B} \to D\ell^- \bar{\nu}_\ell$ or $\bar{B} \to \pi\ell^- \bar{\nu}_\ell$) is produced from a B semileptonic decay, then the virtual W^- must have helicity 0 in order to conserve both momentum and spin in B meson rest frame. The $cos\theta_\ell$ distribution of the lepton will be proportional to $sin^2\theta_\ell$, a situation not really favoring higher lepton momentum.

If this B decays semileptonically to a spin-1 daughter meson, like $\bar{B} \to D^*\ell^- \bar{\nu}_\ell$ or $\bar{B} \to \rho\ell^- \bar{\nu}_\ell$, then the helicity information of daughter c- or u-quarks is preserved since this quark needs to combine with the spectator quark to form a spin-1 meson, which tends to have helicity $\lambda = -1$ rather than $\lambda = +1$. This forces the predominance of $\lambda_{W^-} = -1$ over $\lambda_{W^-} = +1$, and consequently, the $cos\theta_\ell$ distribution of lepton will be dominated by $(1 + cos\theta_\ell)^2$, the cosine angle distribution of lepton from a helicity $\lambda = -1$ W^- meson.

This quantum number effect gives us the softer lepton spectrum for pseudoscalar to pseudoscalar decay, $P \to P^{'}\ell^- \bar{\nu}_\ell$, than the pseudoscalar to vector decay, $P \to V\ell^- \bar{\nu}_\ell$ in B meson.

For charm meson decay, because of the predominance of helicity $\lambda = +1/2$ in charm semileptonic decay, it is just the reverse: the $P \to V\ell^+\nu_\ell$ has a harder lepton spectrum than the $P \to P^{'}\ell^+\nu_\ell$.

q^2 distribution

Finally, if we are able to have higher q^2 for B semileptonic decay, then the phase space tends to allow higher lepton energy. However, the q^2 distribution in B decay also depends on the quantum number of the daughter meson. First take a look from the $P \to P^{'}\ell^{-}\bar{\nu}_{\ell}$ decay rate:

$$\frac{d\Gamma}{dq^2} = \frac{G^2}{24\pi^3}|V_{pp'}|P^3_{p'}f^2_+(q^2) \tag{2.18}$$

We immediately see that the high q^2 is suppressed by the low momentum value of $P^3_{p'}$ for that q^2.

For $P \to V\ell^{-}\bar{\nu}_{\ell}$, the maximum q^2 corresponds to the total overlap of the initial and final meson wave function, the form factor will have biggest value there.

2.4 $B - \bar{B}$ mixing

Oscillation between particle and anti-particle was predicted in 1955 [26] and was observed in 1956 in the $K^0 - \bar{K}^0$ [27] and again in 1987 in the $B^0 - \bar{B}^0$ system [28]. These oscillation was described in Standard Model by second order weak transition, as demonstrated in the known feynman *box diagram* in Figure 2.3

An arbitrary neutral B meson state $\psi(t) = a(t)|B^0> +b(t)|\bar{B}^0>$, is governed by the time dependent shrondinger equation,

$$H\begin{pmatrix} B^0 \\ \bar{B}^0 \end{pmatrix} = \begin{pmatrix} M - i\frac{1}{2}\Gamma & M_{12} - \frac{1}{2}i\Gamma_{12} \\ M^*_{12} - \frac{1}{2}i\Gamma^*_{12} & M - i\frac{1}{2}\Gamma \end{pmatrix}\begin{pmatrix} B^0 \\ \bar{B}^0 \end{pmatrix}$$

Diagonalization of Hamiltonian Matrix leads to CP eigenstates B_L and B_H which are

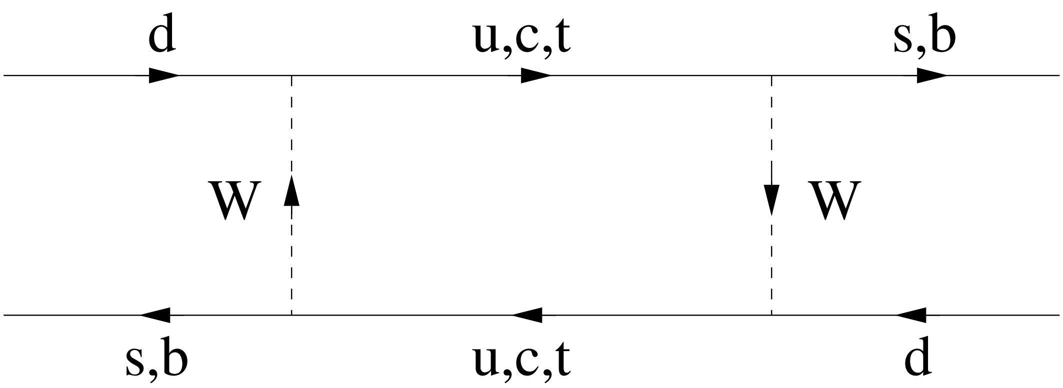

Figure 2.3: One example of feynman "box" diagrams for $B^0 - \bar{B}^0$ mixing

linear combination of flavor eigenstates. we obtain,

$$|B_L >= p|B^0 > +q|\bar{B}^0 >) \tag{2.19}$$

$$|B_H >= p|B^0 > -q|\bar{B}^0 >) \tag{2.20}$$

The eigenvalue of the two new diagonalization B_H, B_L are:

$$m_{H,L} = M \pm Re[(M_{12} - \frac{i}{2}\Gamma_{12})(M^*_{12} - \frac{i}{2}\Gamma^*_{12})] \tag{2.21}$$

$$\Gamma_{H,L} = \Gamma \mp 2Im[(M_{12} - \frac{i}{2}\Gamma_{12})(M^*_{12} - \frac{i}{2}\Gamma^*_{12})] \tag{2.22}$$

respectively.

The proper time evolution of an initially $(t = 0)$ pure B^0 or $\bar{B}^0$ is given by:

$$\begin{aligned} |B^0_{phys}(t) > &= e^{(-\Gamma t/2)} e^{(-iMt)} \\ &\times (cos(\Delta M t/2)|B^0 > +i(q/p)sin(\Delta M t/2)|\bar{B}^0 >) \end{aligned}$$

$$\begin{aligned} |\bar{B}^0{}_{phys}(t) > &= e^{(-\Gamma t/2})e^{(-iMt)} \\ &\times (i(p/q)sin(\Delta M t/2)|B^0 > +cos(\Delta M t/2)|\bar{B}^0 >) \end{aligned}$$

where $\Delta M = M_H - M_L$ and $\Gamma \approx \Gamma_L = \Gamma_H$. The quantity of M_H, M_L and $\Gamma_{L,H}$ are the masses and decay width of the two heavy and light B CP eigenstates. p,q are related with the CP violation parameter ϵ, as we saw in theoretical calculation [29]:

$$|\frac{q}{p}| = \frac{1-\epsilon}{1+\epsilon} = [\frac{M_{12}^* - \frac{i}{2}\Gamma_{12}^*}{M_{12} - \frac{i}{2}\Gamma_{12}}]^{1/2} \tag{2.23}$$

The decay width and mass difference are:

$$\Delta\Gamma = \Gamma_H - \Gamma_L = -4Im[(M_{12} - \frac{i}{2}\Gamma_{12})(M_{12}^* - \frac{i}{2}\Gamma_{12}^*)]^{1/2} \tag{2.24}$$

$$\Delta M = M_H - M_L = 2Re[(M_{12} - \frac{i}{2}\Gamma_{12})(M_{12}^* - \frac{i}{2}\Gamma_{12}^*)]^{1/2} \tag{2.25}$$

For a particle created at time t=0 as a B^0, the probability to find a $B^0(\bar{B}^0)$ at a time t is given by $P_{B^0}(t)(P_{\bar{B}^0}(t))$ is:

$$P_{B^0}(t) = \frac{1}{2}e^{-\Gamma t}(1 + cos(\Delta M t)) \tag{2.26}$$

$$P_{\bar{B}^0}(t) = \frac{1}{2}e^{-\Gamma t}|\frac{q}{p}|^2(1 - cos(\Delta M t)) \tag{2.27}$$

In B meson system, $|\Delta\Gamma| \ll \Delta m$, we have $\epsilon \ll 1$, then $q \approx p$ [30], we have the following:

$$\Delta\Gamma \approx 2Re\Gamma_{12}, \quad \Delta M \approx 2ReM_{12} \tag{2.28}$$

The frequency of $B^0 - \bar{B}^0$ oscillation is driven by the mass difference between two CP eigenstate of neutral B meson ΔM:

$$\Delta M = 2Re\sqrt{(M_{12} - \frac{i\Gamma_{12}}{2})(M_{12}^* - \frac{i\Gamma_{12}^*}{2})} \tag{2.29}$$

This ΔM is evaluated from box diagram calculation. With the above approximation, we can calculate ΔM through matrix element M_{12} as the following: [30]

$$\Delta M \approx 2ReM_{12} = \frac{G_F^2 M_W^2}{8\pi^2} < \bar{B}^0 | j_\mu^{V-A} j^{V-A,\mu} | B^0 > \sum_{u,c,t} \lambda_i \lambda_j A_{ij} \eta_{QCD} \quad (2.30)$$

The λ_i is the CKM matrix element, $V_{ib}^* V_{id}$, and the η_{QCD} is the QCD correction factor, which is calculated to lie in the range 0.78-0.85.[31]

The unitarity of CKM matrix requires:

$$\sum_{u,c,t} \lambda_i = 0 \quad (2.31)$$

Thus we can remove the u quark dependency:

$$\sum_{u,c,t} \lambda_i \lambda_j A_{ij} = (\lambda_c^2 U_{cc} + \lambda_t^2 U_{tt} + 2\lambda_c \lambda_t U_{ct}) \quad (2.32)$$

where

$$U_{ij} = A_{uu} - A_{ij} - A_{ui} - A_{uj} \quad (2.33)$$

A_{ij} is evaluated by loop integral and found out that $U_{cc}, U_{ct} \ll U_{tt}$. On the other hand, $|\lambda_c| \approx |\lambda_t|$. So the contribution from the t quark dominates $\bar{b}d - b\bar{d}$ process.

$$U_{tt} \approx \frac{m_t^2}{M_W^2} F(\frac{m_t^2}{M_W^2}) \quad (2.34)$$

with:

$$F(z) = \frac{1}{4} + \frac{9}{4(1-z)} - \frac{3}{2(1-z)^2} - \frac{3z^2 lnz}{2(1-z)^3} \quad (2.35)$$

The matrix element of $< \bar{B}^0 | j_\mu^{V-A} j^{V-A,\mu} | B^0 >$ can be written as:

$$\begin{aligned} < \bar{B}^0 | j_\mu^{V-A} j^{V-A,\mu} | B^0 > &= < \bar{B}^0 | [\bar{b}\gamma_\mu (1-\gamma_5) d][\bar{b}\gamma_\mu (1-\gamma_5) d | B^0 > \\ &= \boxed{B_B \tfrac{4}{3} f_B^2 M_B} \end{aligned}$$

where :

- B_B is the bag parameter
- f_B is the decay constant
- M_B is the mass of the B meson

Putting all things together, we have the expression for Δm:

$$\Delta m = \frac{G_F^2}{6\pi^2} B_B f_B^2 M_b |V_{tb}^* V_{td}|^2 m_t^2 F(\frac{m_t^2}{M_W^2}) \eta_{QCD} \tag{2.36}$$

From time integrated rates $N(B^0)$ and $N(\bar{B}^0)$, with the approximation $|q| \approx |p|$:

$$N(B^0) = \int_0^\infty P_{B^0}(t) = \frac{1}{2}[\frac{1}{\Gamma} + \frac{\Gamma}{\Gamma^2 + (\Delta M)^2}] \tag{2.37}$$

$$N(\bar{B}^0) = \int_0^\infty P_{\bar{B}^0}(t) = \frac{1}{2}[\frac{1}{\Gamma} - \frac{\Gamma}{\Gamma^2 + (\Delta M)^2}] \tag{2.38}$$

one can determine the parameter $r \equiv \frac{N(\bar{B}^0)}{N(B^0)}$:

$$r = \frac{(\Delta M/\Gamma)^2}{2 + (\Delta M/\Gamma)^2} \tag{2.39}$$

This value x_d is:

$$x_d = \frac{\Delta M}{\Gamma} \tag{2.40}$$

Through this expression and the evaluation of the loop diagram mentioned earlier, we can relate x_d through our information of ΔM:

$$x_d = \tau_{B^0} \frac{G_F^2}{6\pi^2} B_B f_B^2 m_b |V_{tb}^* V_{td}|^2 m_t^2 F(\frac{m_t^2}{M_W^2}) \eta_{QCD} \tag{2.41}$$

where $F(\frac{m_t^2}{m_W^2})$ is a function that derceases slowly with the t-quark mass. The dominant uncertainty is the decay constant f_B, which hasn't been measured with statistical significance through B^- leptonic decay.

The mixing parameter χ_d is the probability of a $B^0/(\bar{B}^0)$ decays into its anti-particle $\bar{B}^0/(B^0)$. It is equal to:

$$\begin{aligned} \chi_d &= \frac{N(\bar{B}^0)}{N(\bar{B}^0) + N(B^0)} \\ &= \frac{r}{1+r} \end{aligned}$$

By looking at the formula on χ_d in equation 2.41, we immediately expect a bigger $B-\bar{B}$ mixing rate than $D-\bar{D}$ mixing. The $D-\bar{D}$ mixing diagram is similar to B-mixing by replacing t- and b-quark with b- and c-quark and substitute CKM element $|V_{tb}^* V_{td}|^2$ by $|V_{cb}^* V_{ub}|^2$. The discovery of t-quark by Fermilab has t-quark mass 38 times heavier than b-quark mass. The CKM element in $D-\bar{D}$ mixing, compared with the rate of $B-\bar{B}$ mixing is also suppressed by the factor of $(|V_{cb}|/|V_{tb}|)^2$. Another factor at work here, though not as significant, is that B^0 has longer lifetime than D^0, $\tau(B^0) = 1.56$ ps and $\tau(D^0) = 0.42$ ps. Putting these all together, the rate of $D-\bar{D}$ mixing is much smaller than the rate of $B-\bar{B}$ mixing.

The $\Upsilon(4S)$ provides a special environment for $B-\bar{B}$ mixing measurement. The B meson pair produced in $\Upsilon(4S)$ is at a coherent state 1^- which forbids the co-existence of $(B-B)$ or $(\bar{B}-\bar{B})$ meson pair at the same time. For B to decay into $\bar{B}$ or vice versa, it can happen only when the other $\bar{B}$ (or B) has decayed away. This means if we are able to tag the flavor of a b quark, and supposing the other b quark through decay reconstruction carries the same flavor as the tagged b quark, then we know this is a mixed event.

The $B-\bar{B}$ mixing measurement in the 80's has contributed to set the limit of t-quark mass before its discovery in 1994. The big mixing rate measured at that time surprised a lot of people, and the indication of large t-quark mass was recognized.

$B-\bar{B}$ mixing also provides another channel to measure the CP- violation in B meson decay. The *indirect CP violation* is caused by the interference between B and $\bar{B}$ to a CP eigenstate both states can decay to. Since this analysis does not focus on the discovery of CP violation in B meson decay, It will not be elaborated here.

2.5 Lifetime Ratio of B^+/B^0

The lifetime is proportional to the inverse of decay rate. The measurement of B meson semileptonic branching fraction combined with lifetime measurement of B meson could let us access the total B meson hadronic decay width information because:

$$B_{sl} \equiv \frac{\Gamma(B \to X\ell\nu)}{\Gamma(B \to all)} = \Gamma(B \to X\ell\nu)\tau_B \tag{2.42}$$

In the $\Upsilon(4S)$ experiment, we can not directly measure the lifetime of B meson because of B meson pair was produced at near rest and will decay immediately without traveling further before CLEO detector can catch its trace. What we do in $\Upsilon(4S)$ experiment is to measure the ratio of the semileptonic branching ratio of charged and neutral B meson, then through isospin symmetry of B^- and $\bar{B}^0$ in the decay, we can obtain the lifetime ratio of charged vs. neutral B meson: $\tau_{B^-}/\tau_{\bar{B}^0}$ as follows:

$$\begin{aligned}
\frac{Br(B^+ \to X\ell\bar{\nu_\ell})}{Br(B^0 \to X\ell\bar{\nu_\ell})} &= (\frac{\Gamma(B^+ \to X\ell\bar{\nu_\ell})}{\Gamma(B^+)})/(\frac{\Gamma(B^0 \to X\ell\bar{\nu_\ell})}{\Gamma(B^0)}) \\
&= \frac{\tau_{B^+}}{\tau_{B^0}}
\end{aligned}$$

Since the B meson lifetime is inversely proportional to B decay width and we know the heaviness of b-quark makes the spectator diagram the pre-dominant mechanism of B meson decay, we can argue that $\bar{B}^0$ and B^- has similar lifetime via $\bar{B}^0, B^-$ isospin symmetry.

The theoretical prediction of B meson lifetime ratio varied, but all not too far from 1. For example, Neubert [70] gives the estimate of lifetime ratio:

$$\frac{\tau_{B^-}}{\tau_{\bar{B}^0}} = 1 + O(1/m_b^3) \tag{2.43}$$

where O is the $1/m_b^3$ correction. In another literature, Bigi concludes [34]:

$$\frac{\tau_{B^-}}{\tau_{B^0}} = 1 + 0.05[\frac{f_B^2}{(200MeV)^2}] \tag{2.44}$$

Chapter 3

Apparatus

3.1 CESR Storage Ring

CESR, the Cornell Electron Storage Ring, was built from 1977 to 1979. It is located in a tunnel 768 meters in circumference under an athletic field on the Cornell University campus, Ithaca, New York. Its main objective is to accelerate particles to the desired energy, to store them for collisions, and to focus these tiny beams to produce as high a luminosity as possible. The CESR ring is shown in Fig 3.1.

CESR operation contains three parts:

- electron and positron beam production from Linac
- synchrotron acceleration
- CESR storage ring

CESR is processed as follows: injected electron and positron beams produced in LINAC will be directed to synchrotron to be accelerated to the desired energy, then guided into the

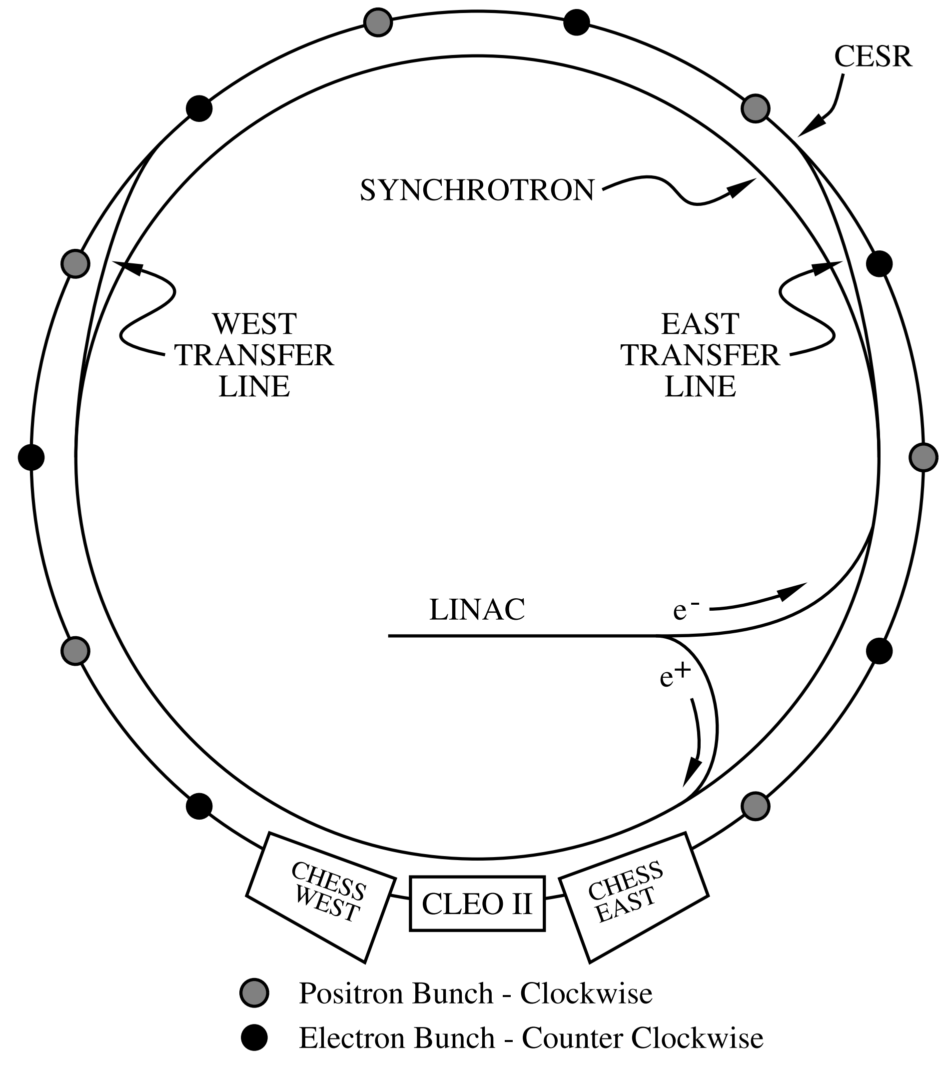

Figure 3.1: The CESR Accelerator

CESR storage ring to acculumate electrons and positrons in opposing directions. The two beams collide at the center of CLEO detector.

3.1.1 Production of Electron and Positron Beam

The electron beam is produced by applying high voltage at the back end of heated Linac to create the electron beam. The electrons gain energy to about 200 MeV while accelerating in the 30 meter long vacuum tube before being projected into synchrotron ring.

Some of the electrons in the Linac will be directed to bombard a tungsten target to produce electron-positron pairs. The positrons will be accelerated and then injected into synchrotron ring.

3.1.2 Beam in Synchrotron

There are magnets in the synchrotron ring. Because electrons and positrons have the same mass with opposite charge, they will travel in opposite direction when they are accelerated in the synchrotron until they reach an energy of about 5 GeV, about 4000 turns in the synchrotron. This energy for electron and positron corresponds to 99.9999995% of the light speed

While electrons and positrons circulate, they lose on average about 1 MeV per turn by emitting x-ray radiation. The radiofrequency cavities, RF, add this energy back on every loop.

3.1.3 CESR for Collision at CLEO

When electrons and positrons reach the desired energy, they will experience a "kick" to push them into the CESR ring for collision at the center of CLEO detector. Those electrons and positrons in the synchrotron do not come continuously but travel in bunches. Each bunch has as many as 1.5×10^{11} particles in it and its size is about 1.1 mm wide, 0.1 mm high and about 1.0 cm long. The bunches circulate at about 396 kHz in the ring.

Accelerator performance is measured by luminosity. The formula to calculate luminosity is the following:

$$L = fn\frac{N_{e^+}N_{e^-}}{A} \tag{3.1}$$

where,

- f: revolution frequency
- n: number of bunches of each particle type
- N_{e^-}: number of electrons in each bunch
- N_{e^+}: number of positrons in each bunch
- A: cross-section area of the beam.

The luminosity of CESR has achieved world record $4.0 \times 10^{32} cm^{-2} s^{-1}$. The CESR luminosity history can be seen in Figure 3.2

3.2 CLEO II Detector

The data for this dissertation is collected at CLEO-II detector located at Cornell University, Ithaca, New York. CLEO II detector was installed in 1989-1990. Figure 3.3 and in Figure 3.4

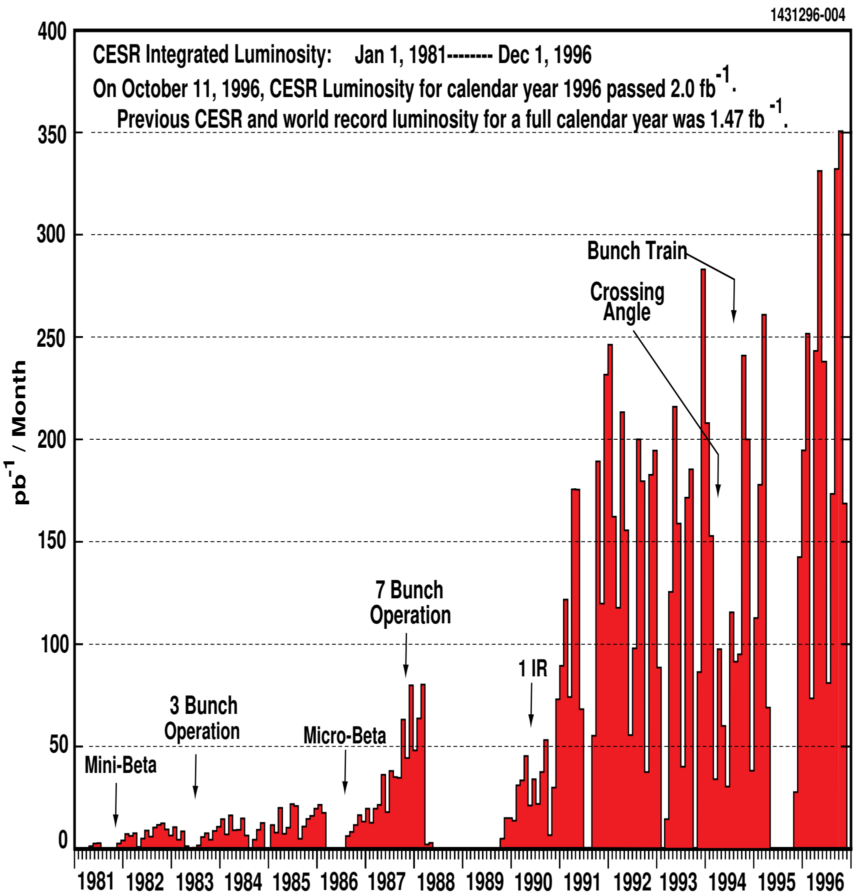

Figure 3.2: The CESR Luminosity history from 1981-1996. Originally, CESR was running on one bunch of each species. It then increased to three bunches, seven bunches, nine bunches and finally to nine trains with two bunches in each train. A major shut down was taken place in 1988-1989 to install CLEO II detector. After that shutdown, CESR also only collide on one detector instead of two (CLEO and CUSB)

shows the cross section of side and end view of CLEO-II detector.

CLEO-II detector is a 4π detector, which means it covers almost all the solid angles. The entire detector is about 6.5 m tall, 6.5 m wide, and 5.8 m long and weighs about 1000 tons. Its major upgrades in 1989 included a smaller radius beam pipe, a straw tube tracking chamber inside the vertex detector, a time of flight system, a large radius of superconducting solenoid and a cesium iodide (CsI) crystal calorimeter. The detailed description of CLEO II detector can be found at [32]

The CLEO-II detector is composed of several components. For a particle produced at the center of detector, where the electron-positron beam collision takes place, the particle will first pass through beam pipe (BP), then the central detector region (CD) which is composed of several different parts of drift chamber. Outside the central detector is the Time of Flight detector (TF).

Both neutral and charged particles that pass through the Time of Flight detector enter the calorimeter (CC). The calorimeter gives a very accurate measurement of the energy and position through the "shower" that particle left behind. Electrons and photons lose almost all of their energy in these showers. Some other particles like muon lose very little. The comparison between energy of the shower and the momentum of the particle allow one to identify the electron candidates.

Outside the calorimeter sits the Superconducting Solenoid Coil that generates a uniform magnetic field of 1.5 Telsa pointing along the beam axis. A charge particle with momentum component perpendicular to the beam will be bent by the magnetic field. The curvature of the track can also provide information of the momentum of the charged particle.

The muon chamber is sitting outside Superconducting Solenoid. The muon itself interacts rather weakly with the various detectors inside muon chamber. Muon candidates are identified as any track that makes it through to hit the muon chamber. Some charged hadronic

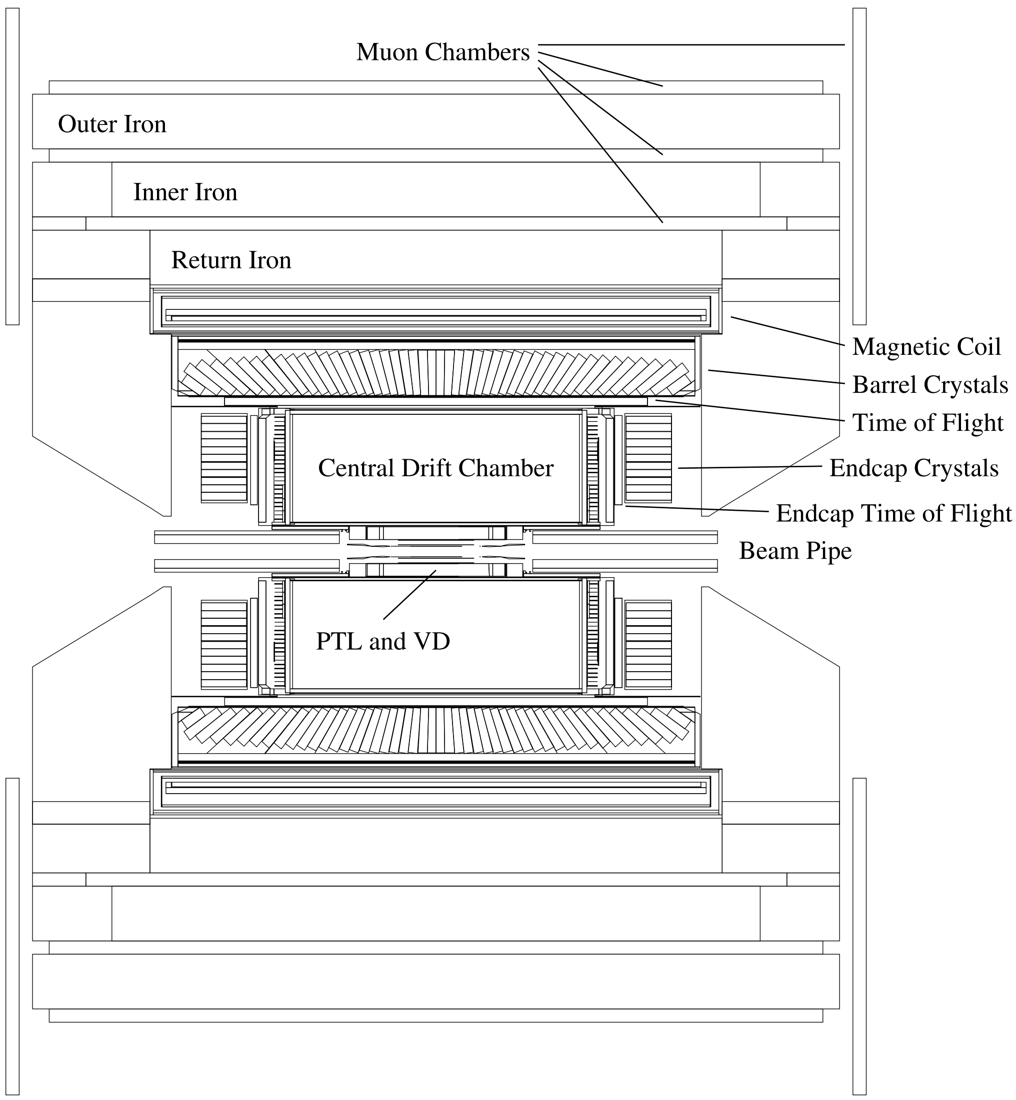

Figure 3.3: The CLEO II Detector Side-View

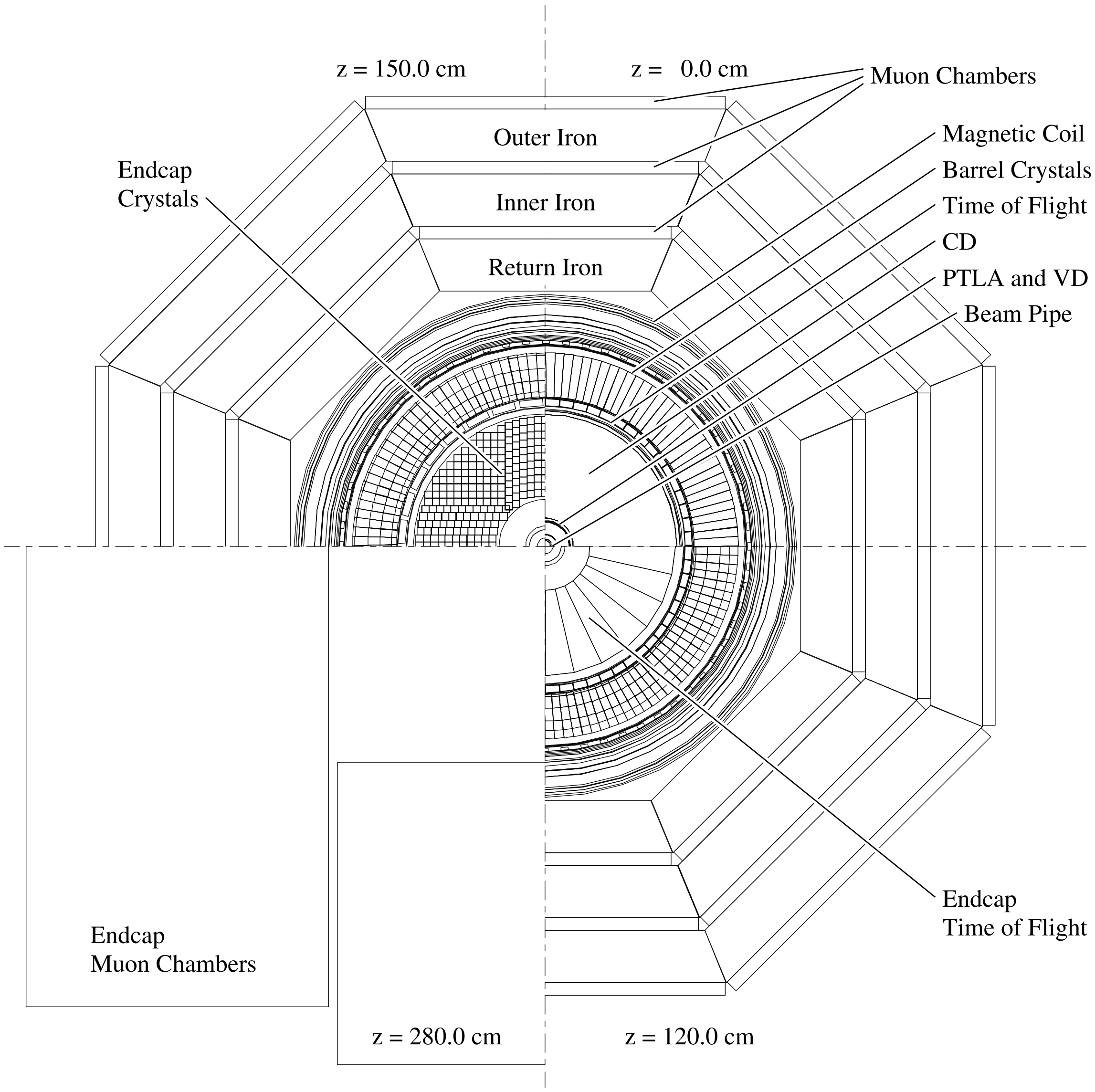

Figure 3.4: The CLEO II end view, four quarters at different z

particles will interact with the irons to produce secondary charged particles which then leave traces in the muon chamber, thus creating "fake" muon candidates. The iron placed before the muon chamber allows only muons with momentum greater than 0.8 GeV/c to leave its trace in the superlayor in muon chamber.

We use cylindrical coordinate system for describing the CLEO-II detector where the z axis is parallel to the beam pipe. The $r - \phi$ plane is the plane transverse to the beam axis.

3.2.1 Beam Pipe

The beam pipe is a thin walled beryllium pipe that separates the vacuum of the storage ring from the detector. This beryllium pipe is of thickness of 0.5 mm with length of 33 cm and radius of 3.5 cm. A silver layer of 20 microns and a nickel layer less than 1 microns are plated inside the beam pipe to reduce the unwanted background from synchrotron radiation.

3.2.2 Central Detector

Precision tracking layer (PT), vertex detector (VD) and main drift chamber (DR) constitute our central detector. The central detector is basically a big drift chamber which is composed of many sense and field wires to attract electron and positive ions respectively. When a charged particle pass through gas, it leaves a trace of ionized gas through ionization energy loss. Those ionized particle induced by this process will be collected at the adjacent sense or field wire to enable us to register the location of the charged particles. These three concentric chambers (PT, VD and DR) runs parallel, or nearly parallel, to the beam pipe, allowing excellent tracking reconstruction in $r - \phi$ plane.

Precision Tracking Layer(PT)

The PT extends from -22.5 cm to 22.5 cm in the z direction, 4.7 cm to 7.2 cm in the radial direction. It consists of six concentric rings of 64 aluminized mylar tubes in each layer. Each tube serves as a cathode with a wire strung down the middle as an anode. The tubes have diameter between 2.2 and 3.5 mm. The PT chamber is operated at a high voltage of about 1500 V for each tube.

There were different gases used in PT. Originally an equal mixture of Argon-Ethane was used as the gas, which results the position resolution approximately 100 μm. In 1992, a new gas DME (Dimethyl Ether) was used to substitute the Argon-Ethane gas, improving the position resolution to 60 μm.

Vertex Detector(VD)

VD extends from -35 cm to 35 cm in z direction and 8.4 cm to 16.0 cm in radial direction. The inner five layers consists of 64 cells and the outer five layers of 96 cells. Gas in VD is an equal mixture of Argon -Ethane with a higher pressure (20 psi), compared with PT, to reduce the diffusion.

There are about 800 sense wires for these 10 layers, with field wires forming hexagonal cells about them. Cathode strips were place inside of both the inner and outer radius walls of VD. These strips are composed of 8 μm of aluminum deposited on 75 μm thick mylar and serves to measure the z-position. Since anode wires are read out at both ends, a z position measurement can be achieved through the "charge division" method: the ratio of charge measured at the two ends of the highly resistive sense wire gives a measure of the z position of the track: the closer the track to one end the more of the charge collected at that end.

The figure of Precision Tracking Chamber (PT) along with Vertex Detector (VD) is shown in Fig 3.5

Main Drift Chamber(DR)

The DR is located outside the VD, and extends from 17.5 cm to 95.0 cm in radius and -94.5 cm to 94.5 cm in length. It consists of 51 layers in 12240 sense wires and 36270 field wires. DR covers 94% of 4π at the inner surface and 71% of 4 π at the outer surface. Figure 3.6 shows the picture of CLEO-II Drift Chamber (DR)

Among the 51 layers, 40 of them are the axial layers whose sense wire is pointing parallel to the beam. Those 40 axial layers provide position measurements in the azimuthal direction.

Groups of three or five axial layers alternate with a "stereo layer" whose sense wires are about 5 degree to the beam axis. These "stereo layers" and the cathode strips in the inner and outer surfaces of the chamber provide measurements in z direction. There are a total of 11 stereo layers in the main drift chamber.

Each cell is about 14 mm by 14 mm in size, with eight field wires surrounding a gold plated 20 μm diameter tungsten sense wire. In the first 40 layers, we use aluminum for field wires. For the remaining 11 layers, copper-beryllium is used.

The resolution of tracking system is measured to be

$$(\delta p_t/p_t)^2 = (0.0011p_t)^2 + (0.0067)^2 \tag{3.2}$$

where p_t is the transverse momentum perdendicular in beam direction in GeV/c. For $p_t = 5.280$ GeV/c, the resolution, δp_t is about 47 MeV/c. The angular resolution in $e^+e^- \to \mu^+\mu^-$ in ϕ is about 1 mrad and about 4 mrad in θ.

The particle identification in this main drift chamber is realized by picking up the ionization energy collected at the sense wire. Particles with velocity, $\beta = \frac{v}{c}$ are characterized

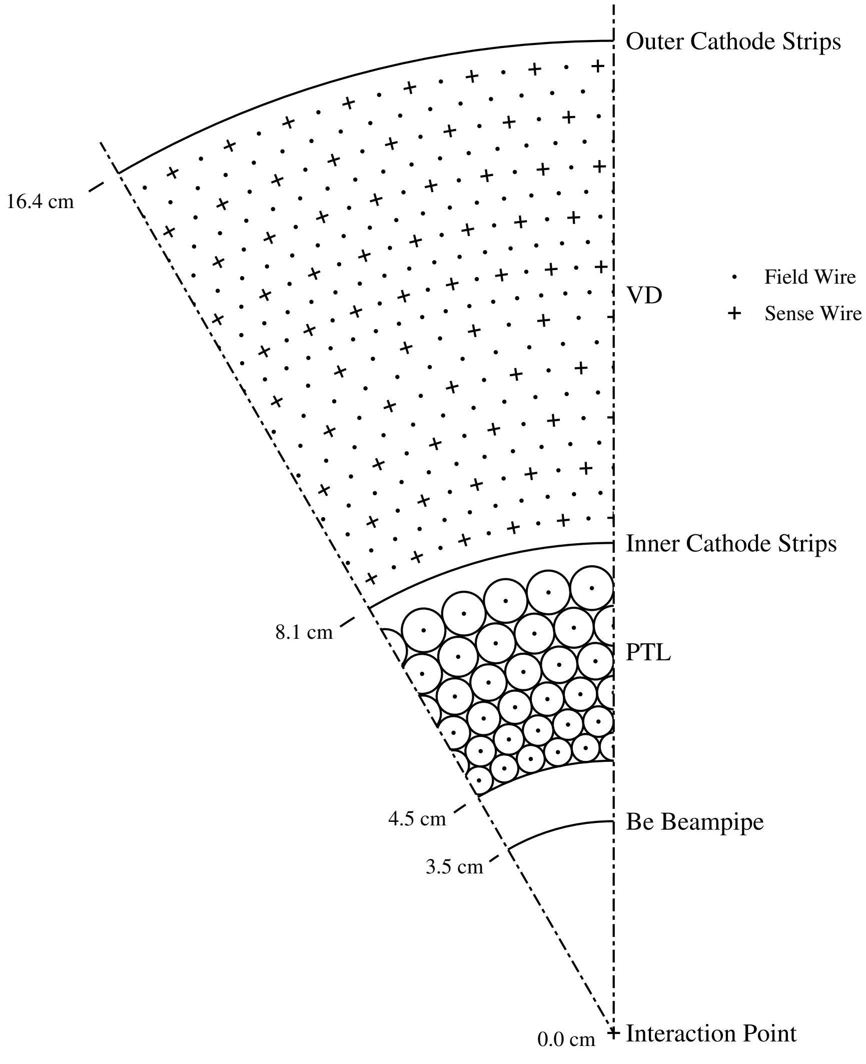

Figure 3.5: The CLEO II Precision Tracking Chamber and Vertex Detector

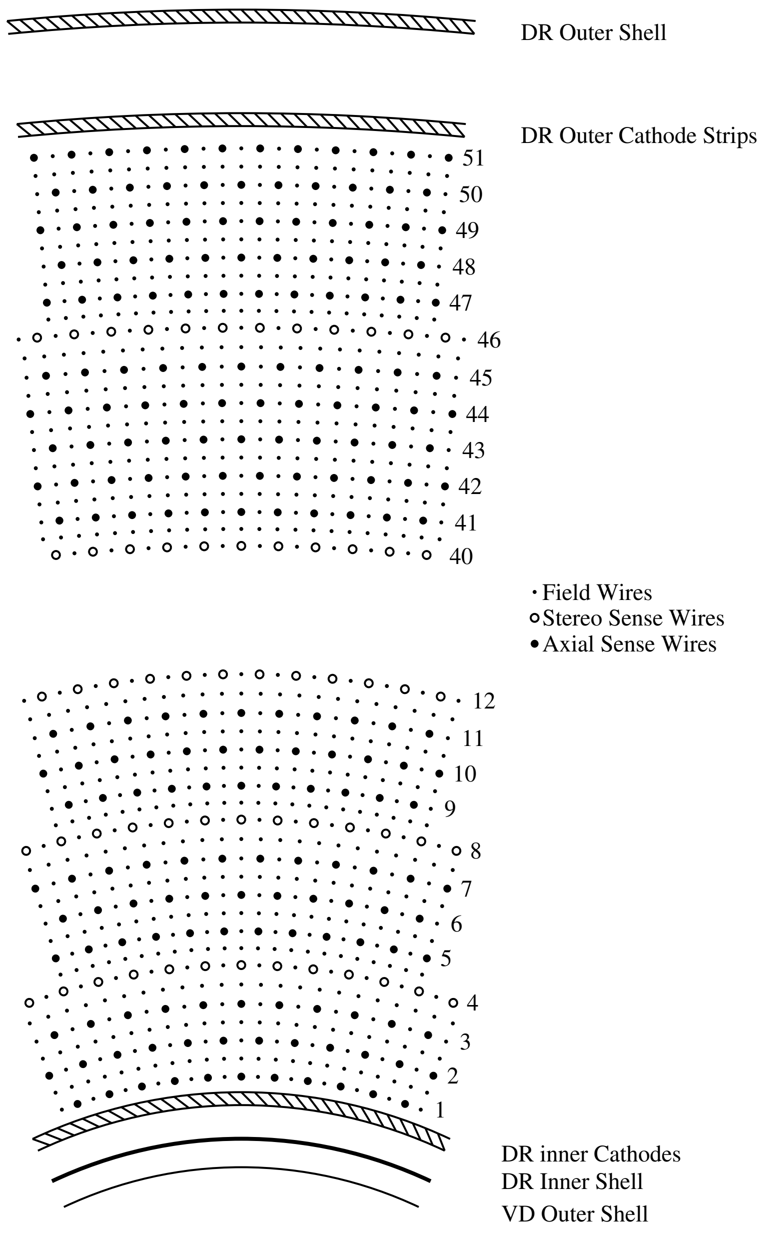

Figure 3.6: The CLEO II Drift Chamber

by their ionization energy loss per distance according to the following ionization energy loss formula:

$$\frac{dE}{dX} = K\frac{Z}{A\beta^2}[\frac{1}{2} - ln\frac{2m_e\beta^2\gamma^2T_{max}}{I^2} - \beta^2 - \frac{\delta}{2}] \tag{3.3}$$

Fig 3.7 is the diagram of ionization energy loss for different particle species as the function of momentum.

3.2.3 Time of Flight Counter(TF)

Outside DR is the TF counter, which covers 97% of 4π region by "barrel TF" counter and "endcap TF" counter at both ends. Barrel TF covers $35^0 - 145^0$ and endcap TF covers $15^0 - 35^0$ and $145^0 - 165^0$ to cover both end.

The barrel TF module is made of a scintillator, lightguide and photomultiplier tube. A charged particle passing through the plastic excites the organic molecules, which then emit ultraviolet light when they decay back to the ground state. Photons will bounce through internal reflection down the length of the scintillator into a plastic light guide that directs light into a photomultiplier glued at the end. There are 64 scintillators for barrel TF and 279.4 cm long and about 10 cm wide. The CLEO-II TF barrel system is shown at picture Figure 3.8.

For endcap TF, we have 28 scintillators that are trapezoidal in shape. The photomultiplier is directly attached at the end of the scintillator. The endcap TF scintillator is about 4.8 cm thick. The endcap TF counter is shown at Figure 3.10

The time of flight system determines the species of the charged particle by measuring particle's velocity, once the momentum is known from the curvature of the track within the tracking chambers. Figure 3.9 shows the TF $1/\beta$ diagram for different particle species as the

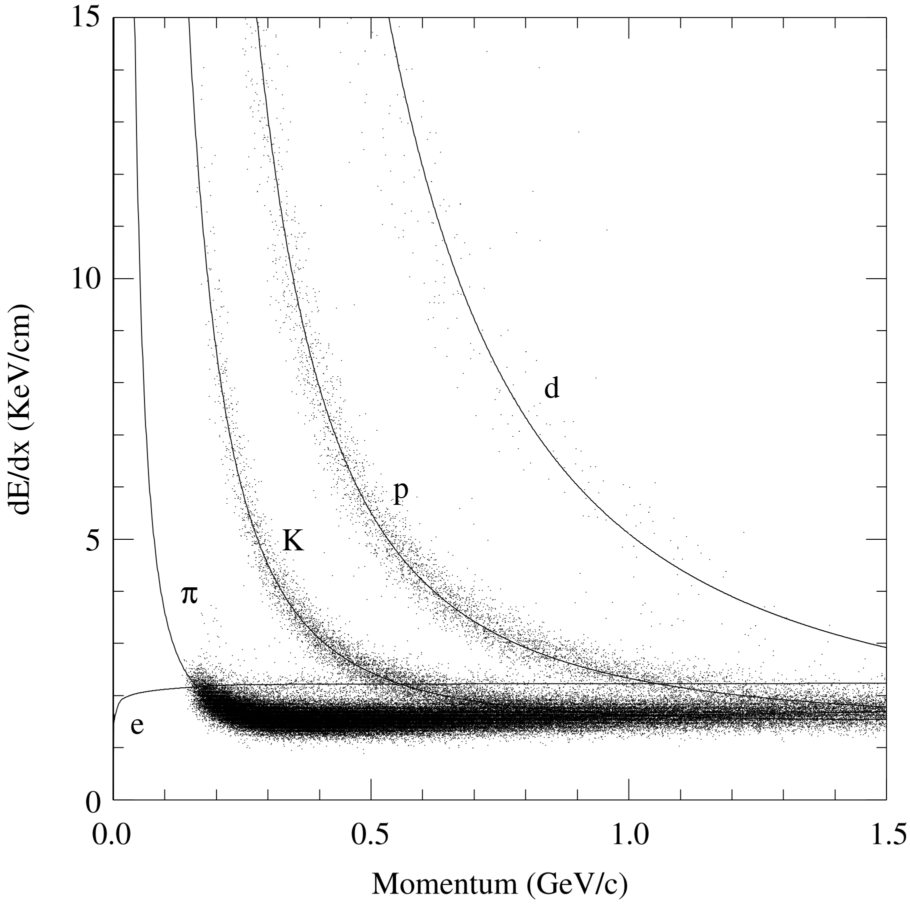

Figure 3.7: The Particle ionization energy loss with momentum

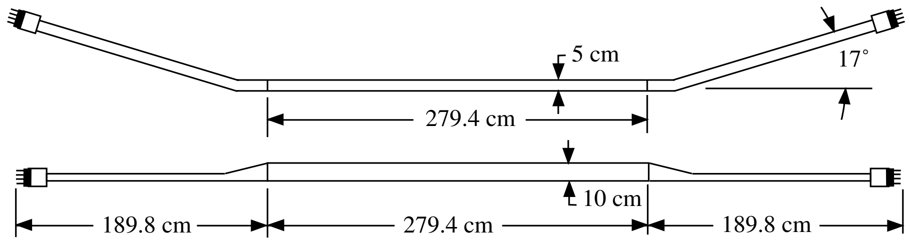

Figure 3.8: The CLEO II Barrel TF Counter

function of momentum, where $\beta = v/c$.

3.2.4 Electromagnetic Calorimeter

Outside the TF counter is Electromagnetic Calorimeter (CC). Like TF, it also consists of barrel and endcap. CC is made of 7800 scintillating cesium iodide crystal block doped with thallium. Each crystal is about 5 cm in square and 30 cm in length. The crystal end is pointed a few centimeter away from interaction point to avoid showering photons slipping back through a crack. The 30 cm length of crystal is about 16 radiation length, to assure very little energy leak out the back of crystal. Through pulse height of the readout, we can get information of energy deposited in the crystal. The barrel contains 6144 crystals for barrel region and 828 crystals at endcap.

Electrons and photons lose nearly all of their energy in CC, and the shower shape is very localized. Muons lose very little of their energy. Hadrons don't lose all of their energy either. And because secondary hadron can be produced through nuclear interaction at CC, we will have second hadron shower, which makes the shower shape non-localized.

This Calorimeter has achieved very good resolution for photon. The energy resolution of photon is about 1.5%(2.6%) for photon with momentum of 5 GeV/c and 3.8%(5%) for photon with 100 Mev/c in momentum for barrel (endcap). The spatial resolution of photon with momentum 5 GeV/c is about 3 mrad (9 mrad) and 11 mrad (19 mrad) of photon with momentum 100 MeV/c for barrel(endcap) region. The excellent performance of CLEO Crystal Calorimeter gives CLEO great advantage in detecting neutral particles. For neutral pion decays to 2 photons, the energy resolution of π^0 is about 5 Mev.

In this thesis, the usefulness of the calorimeter lies in its ability to help to identify electrons. The ratio E/p of the energy measured in the calorimeter and momentum measured in

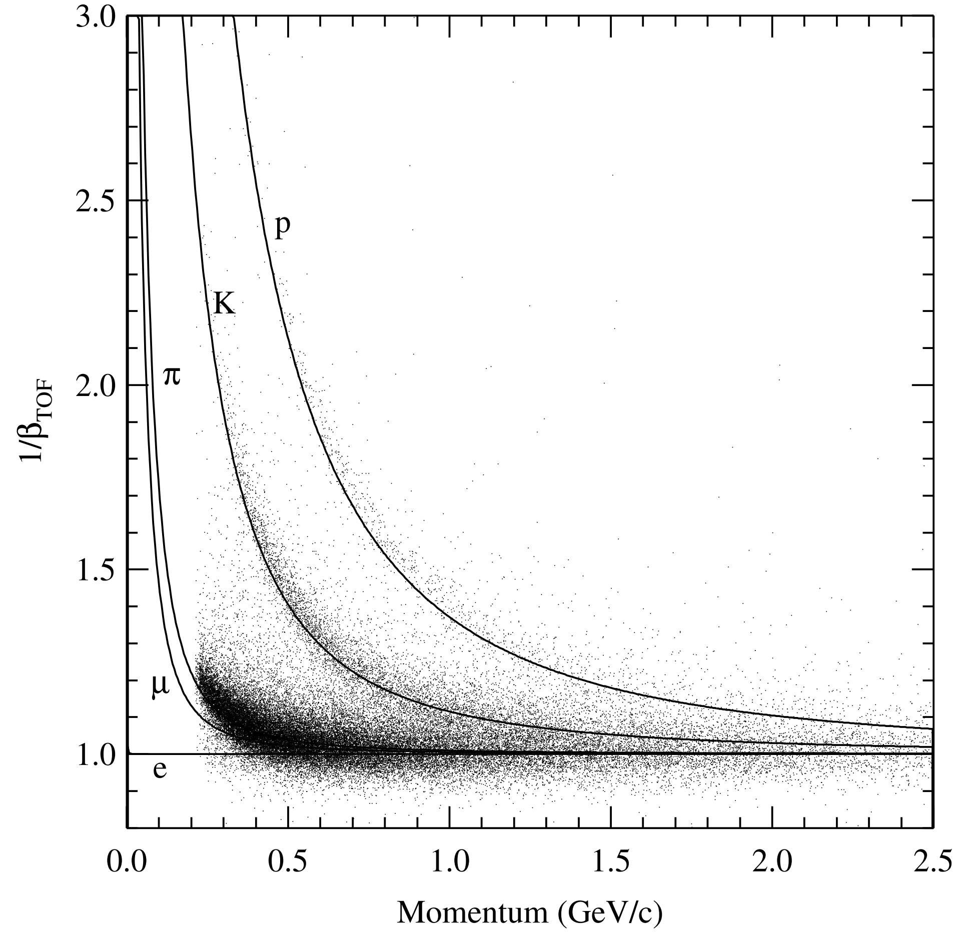

Figure 3.9: The CLEO II Time of Flight particle velocity with momentum

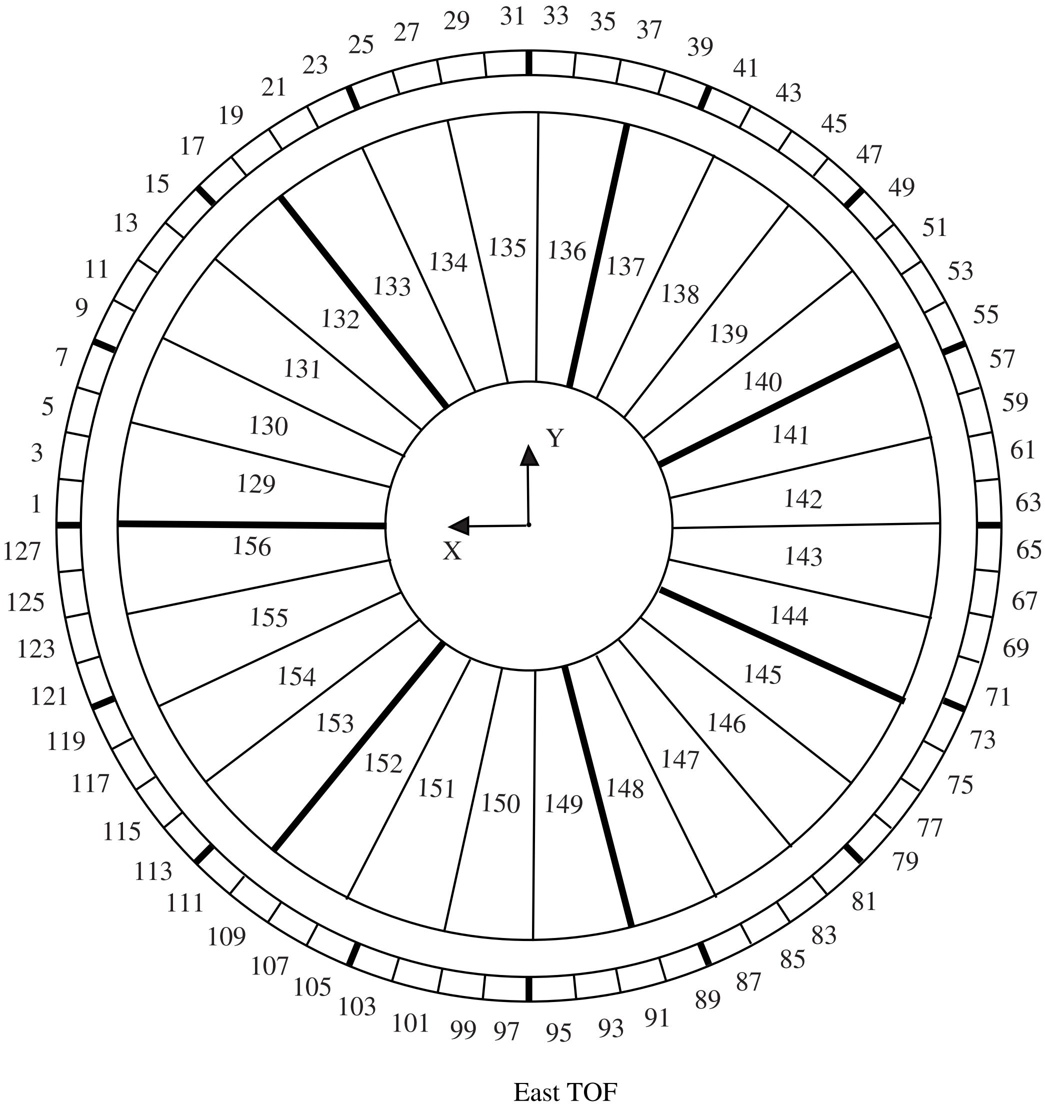

Figure 3.10: The CLEO II Endcap TOF Counter

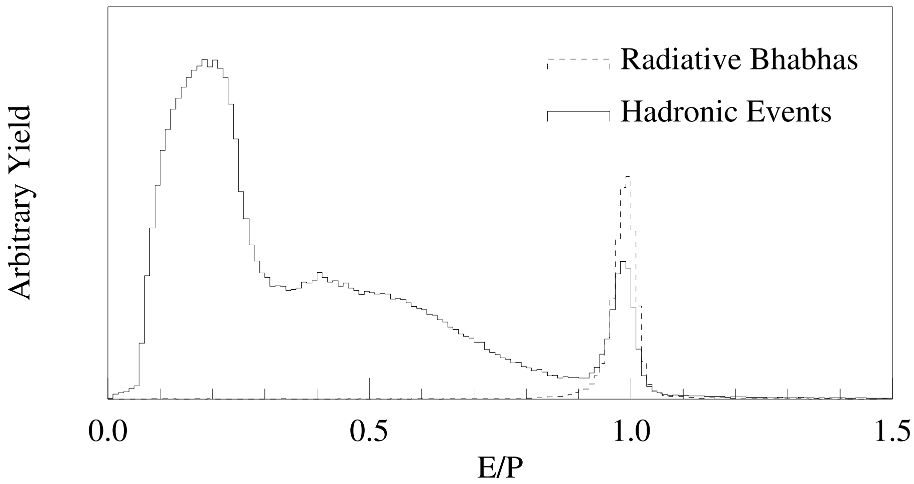

Figure 3.11: E/P yield for electrons from radiative Bhabha events compared to charged tracks in hadronic events in the momentum range 0.8-3.0 GeV/c at barrel region.

central detector tracking chambers is a very powerful figure of merit for electron identification. An E/p close to 1 is consistent with an electron hypothesis since all of the electron;'s energy should be deposited in the calorimeter. Hadrons and muons have smaller E/p. An example of E/p can be seen in Figure 3.11. This can be combined with other information from the calorimeter, and from the dE/dX measurement in the drift chamber to calculate the sum of log likelihood ratio L_e for the track to be an electron. We define it to be:

$$L_e = \sum_i ln(P_{ei}/P_{\neq ei}) \tag{3.4}$$

where P_{ei} is the probability that a track is an electron according to the i^{th} estimator, and $P_{\neq ei}$ is the probability that the track to be identified as μ, K, p, π acordingly.

3.2.5 Superconducting Solenoid

The Superconducting Coil weighs about 30 tons and sits outside CC. It produces 1.5 Telsa field in the z direction. The coil consists of two layers, each with 650 turns of a superconducting cable made by Cu-Nb-Ti. The liquid helium is used to maintain the coil at temperature at 4 Kelvin. The 800000 kg steel yoke is to use to shield magnetic flux for the outermost muon chamber.

3.2.6 Muon Chamber

The muon chamber is the outermost component of CLEO-II detector. The barrel muon counters cover angular region $45^0 - 90^0$ and $30^0 - 45^0$ for the endcap muon counters. The barrel muon counter is composed of eight octants of three layers of 30 cm thick steel interleaved with "super layers". Those super layers are composed of three single layers of proportional drift cells formed from extruded plastics, 5 m long and 8.3 cm wide. Hit position in ϕ is measured by reading the anode wire, and z direction from external copper strip. The "charge division" method mentioned in vertex detector is used to measure the location. The Argon-Ethane gas recycled from drift chamber flows through the muon counter.

In the barrel region, muons with momentum greater than 0.8 GeV/c can reach the first layer. To reach second and third layer, muons need to have momentum greater than 1.4 GeV/c and 1.8 GeV/c respectively. The resolution of muon hit positions are determined by the error on the propagation of the track to the muon counters, the intrinsic resolution of the muon counters and the multiple scattering in material in front of the counters.

In Fig 3.12 is the cross section of muon proportional chamber. We can see in Fig 3.13 the cross section of the superlayer chamber in the muon detector.

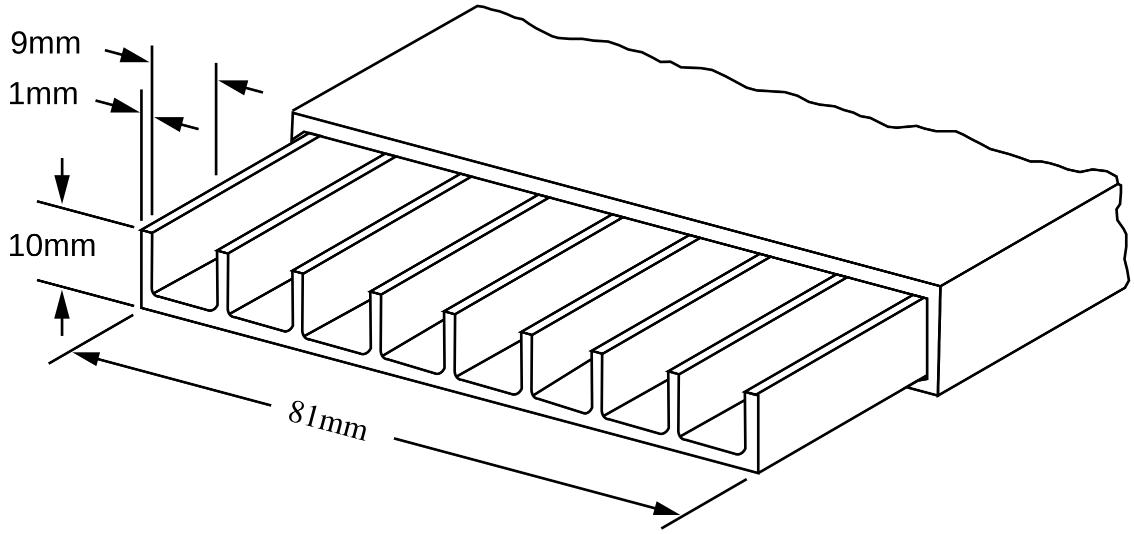

Figure 3.12: Cross Section of Muon Proportional Chamber

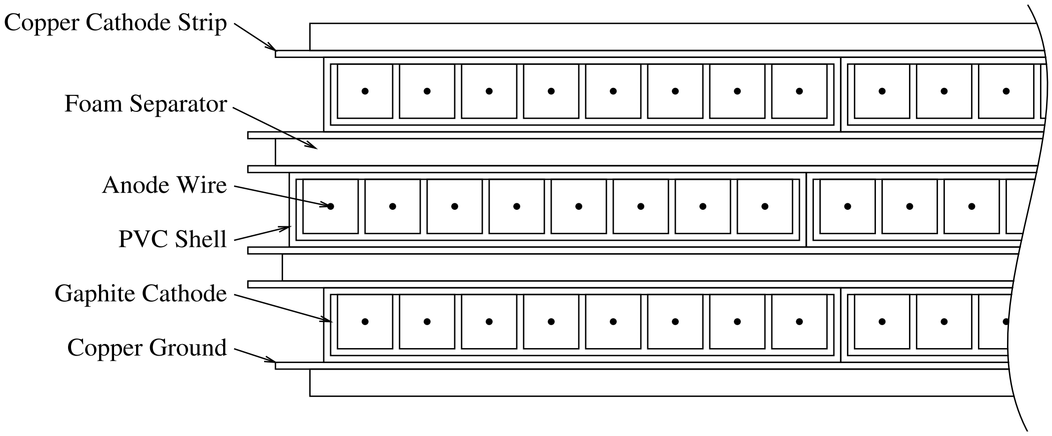

Figure 3.13: Cross Section of Superlayer Chamber in Muon Detector

3.2.7 Trigger System

There are a huge amount of data can be collected at the colliding beam experiment. Some of the e^+e^- collision results in unwanted events. For example, the glancing collision where electron and positron just bunces off each other. There are also other unwanted events like the cosmic ray which is not originated from $\Upsilon(4S)$ but still leave traces in detector anyway. The trigger system is to filter out those events and optimize the acceptance as much as possible.

CLEO-II has 3 level of triggers L0, L1 and L2 to screen out events. Events need to pass all three triggers to be written onto disk. Later, after further filtering in offline software, information at disk will be stored into magnetic tape for later physics analysis.

Different level of trigger uses different criteria. The following is the detector information used by each level of triggers:

1. L0: use TF, VD and CC
2. L1: after L0, use VD, DR, TF, CC
3. L2: after L1, use DR and VD
4. L3: on-line software for disk to tape writing

L0 trigger is the fastest and is the first trigger to select events. L0 trigger accepts information from TF, VD and CC to select events if anyone of them turns on. L0 trigger attempted to reduce 2.7 MHz crossing frequency to a rate on the order of 20 kHz.

After L0 trigger, all detector gating is disabled, and a search is made for a L1 trigger requirement. L1 use information from CD,CC and TF for events passed L0 trigger. It takes about 1.0μ second for event to arrive at L1 circuitry, causing about 2% dead time after L0 trigger got fired. If L1 is not satisisfied, the system is reset and detector gating resumes. The goal of L1 trigger is to reduce the event rate to about 25-50 Hz.

L2 trigger uses information from DR and VD to evaluate incoming events after L1 trigger fired. It takes about 50 times longer than L1 trigger to write an event, 50μ seconds. L2 typically fired about 10-20 Hz, depending on CESR condition. When L2 trigger fired, CLEO-II data acquisition system writes out all the information gathered from various detector components to disk. Further filtering will be employed with software when information are dumping from disk to tape.

L3 is the software to further discard some unwanted events for tape storage. For example, only a pre-determined percentage of bhabha events will be written to magnetic tape. Another job L3 trigger does is to kill the "beam wall" event, which is about 45% of the events passed L2 trigger. A percentage of "random trigger" events is also kept in order to check what trigger has thrown away is really uninteresting.

3.2.8 Monte Carlo

CLEO-II Monte Carlo is the simulation of $\Upsilon(4S)$ event for CLEO-II detector environment. We use Monte Carlo to estimate the background in our analysis of data, and various systematic checking.

CLEO-II Monte Carlo contains two parts:

- QQ: for physics simulation
- CLEOG: for detector simulation

QQ is based on our current understanding of particle physics. The program QQ generates particles produced in e^+e^- annihilation, then decay according to several routines embedded within QQ to subsequent modes. The QQ is constantly tuned to match our current understanding of particle physics.

The decay history of the QQ program is then passed through a program called CLEOG, based on GEANT from CERN. CLEOG simulates the complete detector response to the event. Those particles which are not decayed within QQ are handled here, such as decay in flight of μ and K. All manner of detailed processes are simulated in CLEOG in order to make the simulated data match the true data as accurately as possible. The program simulates the energy loss of the particles while passing through the matter of the detector, the electromagnetic showering within the calorimeter, and the ionization of the drift chamber gas. Random noise hits in the various detectors is modeled by adding hits from random triggered events in data.

Chapter 4

B^0 Meson Semileptonic Branching Fraction

4.1 Introduction

In this chapter, we partially reconstruct a $\bar{B}^0$ through the decay $\bar{B}^0 \to D^{*+}\ell^-\bar{\nu}_\ell$, $D^{*+} \to D^0\pi^+$ to tag neutral B events and reconstruct the B^0 meson inclusive leptonic spectrum.[1] By comparing the leptonic spectrum with an earlier CLEO analysis of the $\Upsilon(4S)$ inclusive leptonic spectrum, we are able to derive the charged and neutral B meson semileptonic branching ratio and the charged to neutral B lifetime ratio, τ_{B^+}/τ_{B^0}, assuming the isospin symmetry of B^- and $\bar{B}^0$ in semileptonic decay.

We will briefly review some previous analyses on B semileptonic decay, and discuss the motivation of B^0 tagging through the method of *partial reconstruction*. We outline the rest of this analysis as follows: The method of *partial reconstruction* will be discussed in section

[1] Charge conjugation is implied throughout this thesis.

4.4. We then lay out our event sample and tabulate our cut in section 4.5. and 4.6. In 4.7 we will focus on the inclusive lepton spectrum from B^0 semileptonic decay. The various systematic errors will be detailed in 4.8. We then proceed to compare the different lepton spectra with an earlier CLEO analysis based on single lepton. The branching ratio, lifetime ratio and other interesting physics quantities will be calculated in 4.10. Our summary and result will be laid out in 4.11

4.2 B Semileptonic Branching Fraction

Over the past decade, there have been intensive research activities on semileptonic decays of B mesons. Despite various experimental and theoretical efforts, the measured semileptonic branching fraction of B meson decay is not in agreement with the theoretical prediction that the branching fraction of Br($B \to X\ell\bar{\nu}_\ell$) should be no less than 12.5%[57]. Most experimental values are found to be lower than that value.

The inclusive B semileptonic decay is denoted as $B \to X\ell\bar{\nu}_\ell$, where X means any hadrons, ℓ means electron or muon only. While the measurement of individual modes, for example $Br(B \to D^*\ell\bar{\nu}_\ell)$ and $Br(B \to D\ell\bar{\nu}_\ell)$ (**exclusive modes**) could probe the dynamics of B meson decay and measure the properties like q^2 distribution and value of V_{cb}, the **inclusive** analysis can give us the total inclusive branching fraction. Since the total B meson decay width are dominated by the width of B semileptonic decay and the width of B hadronic decay, the knowledge of the B semileptonic decay width can effectively probe the hadronic portion of the total B decay width, which must be well measured in oder to evaluate the CKM matrix elements.

There have been several previous measurements of inclusive B semileptonic branching fractions. The methods can be grouped as (1) single lepton analysis and (2) dilepton analysis for $\Upsilon(4S)$, and (3) lepton transverse momentum analysis in $Z \to b\bar{b}$ environment. The analyses in $\sigma(Z \to b\bar{b})$ environment were performed by several LEP experiments (ALEPH, DELPHI, L3 and OPAL) at CERN. The $\Upsilon(4S)$ measurements were done by the CLEO and ARGUS collaborations.

4.2.1 Inclusive Lepton Analysis

In single lepton analysis, [37], [38], [39], [40] all leptons are selected to construct the leptonic momentum spectrum. The lepton spectrum consists of two main sources of leptons with very different shapes. Those shapes were calculated based on some theoretical models and are used to separate the primary leptons, which come directly from B meson decay, from secondary leptons, which are from the decay product of B meson such as D and Ψ mesons and other. The total number of primary leptons estimated from fit then will be normalized to the total number of $B, \bar{B}$ events to give the semileptonic branching fraction averaged over the mixture of neutral and charged B in $\Upsilon(4S)$ event. In Figure 4.1 is the lepton spectrum of previous CLEO B semileptonic decay measurement based on single lepton method. There are two assumptions in this method: (1) there is no non-$B\bar{B}$ decay in $\Upsilon(4S)$ and (2) $\Upsilon(4S)$ resonance decays equally to charged and neutral B mesons, $f_{+-}/f_{00} = 1$, where f_{+-}, f_{00} are the fraction of charged and neutral B production in $\Upsilon(4S)$ decay rspectively. This analysis is rich in statistics and was the first accessible approach during the early period of detector running when limited data were available.

4.2.2 Dilepton Analysis

By looking at the inclusive lepton spectrum at Figure 4.1, we notice that for a lepton with momentum greater than 1.4 GeV/c, that lepton very probably comes from the decay $B \to$

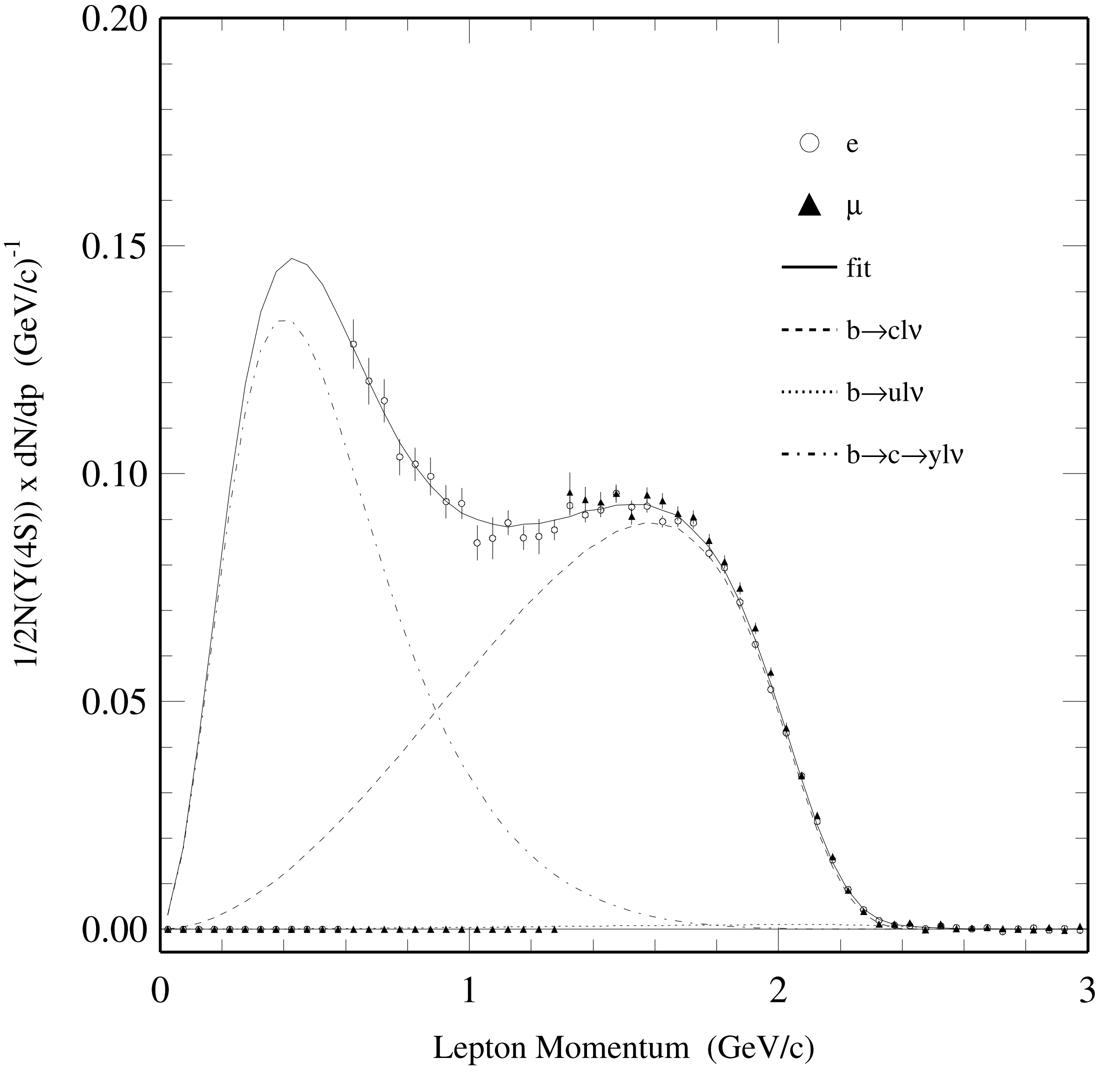

Figure 4.1: CLEO II B semileptonic decay lepton spectrum from single lepton measurement

$X\ell\nu$. The charge of the lepton can also serve as the flavor tag of the b quark. If the lepton carries the negative(positive) charge, it should come from the weak decay of b($\bar{b}$) quark. This feature was used by the dilepton analysis.

In dilepton analysis, leptons with momentum greater than 1.4 GeV/c are used as a tag of the B meson, then a search is made for second leptons in the momentum range between 0.5 GeV/c to 2.5 GeV/c. It then uses the correlation between charge and the angle of the secondary lepton that comes from the same B meson as the tag lepton. The angle θ between the two leptons when the second lepton is from the same B meson as the tag will mostly be in opposite hemisphere, $cos\theta < 0$, as they tend to decay back to back, with opposite charge. Second leptons from the the other B meson won't demonstrate such behavior as the distribution in $cos\theta$ is essentially flat. Through this correlation and the input of $B-\bar{B}$ mixing parameter χ_d, a model independent inclusive primary and secondary lepton spectrum of the averaged neutral and charged B meson is obtained, [44] and [45]. The primary and secondary lepton spectrum from this di-lepton analysis can be seen at Fig 4.2.

This method eliminates the assumption that B($\Upsilon(4S) \rightarrow B\bar{B}$) = 100%. It also does not rely on theoretical model to predict the primary and secondary leptons in the lepton momentum spectrum it produced. But it can not differentiate the neutral from charged B meson.

4.2.3 Lepton Transverse Momentum Measurement

For experiments at energy of Z boson production, the B mesons are produced incoherently. B mesons created here are also boosted to a larger momentum, thus making higher momentum leptons from B meson primary decay. Primary leptons from B meson decay usually can be characterized as having large traverse momentum. By fitting the distribution of both the transverse momentum P_t and P from the theoretical models, a measurement on B

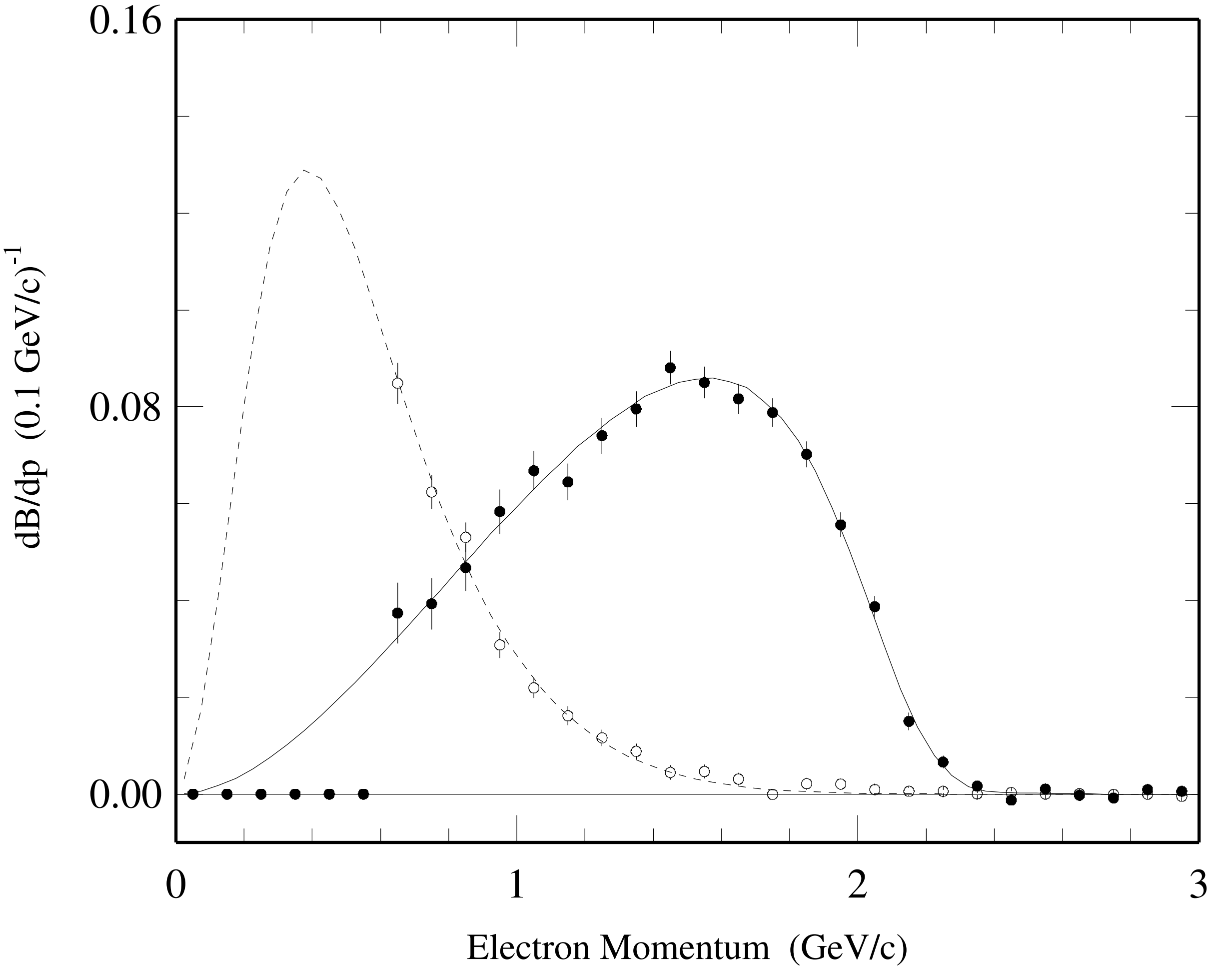

Figure 4.2: CLEO II B semileptonic decay lepton spectrum from dilepton measurement

semileptonic branching fraction is made, see the LEP analysis [41], [42], [43].

4.3 Motivation of Partial Reconstruction

The single and di-lepton analyses both can not differentiate $\bar{B}^0$ from B^-, and since the averaged B semileptonic branching fraction is less than theory has predicted, the natural step is to measure the semileptonic branching fraction of B^0 and B^+ separately. Tagging the charge of B meson can remove such uncertainty. The first method comes to mind is to explicitly reconstruct a $B^0(B^+)$ meson. For example, using the decay chain:

$$
\begin{aligned}
\bar{B}^0 \quad \rightarrow \quad & D^{*+}\ell^-\bar{\nu}_\ell \\
& D^{*+} \rightarrow D^0\pi^+ \\
& \quad\;\; D^0 \rightarrow K^-\pi^+
\end{aligned}
$$

Although the ambiguity of neutral/charged B meson has been eliminated, the statistical power suffers because the $Br(D^0 \rightarrow K^-\pi^+)$ is only 3.8%. Including $D^0 \rightarrow K^-\pi^+\pi^0$, a mode with branching ratio about 13.9%, does not increase the statistical power a lot, because we have large amount of $\pi^0 \rightarrow \gamma\gamma$ combinatorial background. We would like to gain clean signal with good statistical power and to reduce the systematic uncertainty as much as possible.

With this in mind, the method of *Partial Reconstruction* was developed. This method takes advantage of the character of $\Upsilon(4S)$ decay and the strong correlation between the π^+ from D^{*+} decay without explicitly reconstructing the D^0. If we compare this with the B^0 tagging through exclusive D^0 reconstruction, we can immediately know by not reconstructing D^0, the statistics jumps up 25 times!

This method was first suggested by CLEO in 1983, then employed by ARGUS and CLEO as a tag of $\bar{B}^0$ meson. [47], [50],[49]. We will explain the method of *partial reconstruction* later. It also has been explained in detail elsewhere. [48]

4.4 Analysis Overview

The strategy of this analysis is to use **partial reconstruction** method to tag a neutral $\bar{B}^0/B^0$. For each tagged event, we then look for additional charged leptons from semileptonic $B^0/\bar{B}^0$ meson decay, to reconstruct the lepton spectrum of the opposing B. We extract the portion of primary leptons in this reconstructed additional lepton spectrum. The ratio of the number of *additional primary leptons* to the total number of tags will be B^0 semileptonic branching fraction. It can be visualized as follows:

$$X\ell^{\pm}_{\mathbf{add}}\bar{\nu}_\ell \leftarrow \boxed{B^0/\bar{B}^0, \bar{B}^0} \rightarrow D^{*+}\ell^{-}_{\mathbf{tag}}\bar{\nu}_\ell$$

$$D^{*+} \rightarrow D^0\pi^{+}_{\mathbf{tag}}$$

We get N_{tag}, the number of tags, $(\ell^{\pm}_{tag}, \pi^{\mp}_{tag})$, and extract N_ℓ, the number of additional primary leptons in the tagged event, $(\ell_{add}, [\ell^{\pm}_{tag}, \pi^{\mp}_{tag}])$. The ratio of those two number: N_ℓ/N_{tag} is b_{tag}, the semileptonic branching ratio in an event sample highly enriched in B^0. The semileptonic branching fraction measured in inclusive analysis mentioned earlier is obtained in a sample that has roughly equal mixture of B^0 and B^-. By comparing these two number one can obtain the neutral and charged B semileptonic ratio, b_+ and b_0, respectively. Using isospin symmetry in $\bar{B}^0$ and B^- semileptonic decay, we can obtain the lifetime ratio of charged to neutral B, τ_+/τ_0.

As reasons mentioned earlier in inclusive lepton analysis, we require the tag lepton to be within the momentum between 1.4-2.4 GeV/c.

The tagged pion is moving slowly. We require the momentum of the tagged pions to be lower than 190 MeV/c. The tagged lepton and pion pair should carry opposite charges for the signal decay. This opposite charge lepton-pion pair is denoted as the "right sign" combination.

For additional lepton, we require the momentum to be between 0.5 GeV/c and 2.5 GeV/c, and 1.5 - 2.5 GeV/c for electrons and for muons respectively. We reconstruct the additional lepton spectrum for electrons and muons separately.

4.5 Data and Event Cut

We use the CLEO II [32] (4s2 - 4sA) data set which has an integrated luminosity of 2.38 fb^{-1} taken at the $\Upsilon(4S)$ resonance, and 1.13 fb^{-1} taken at off resonance, which is 60 Mev below the $\Upsilon(4S)$. All events considered here are required to pass our standard hadronic criteria, which require at least 3 well-fitted charged tracks, a measured energy at least 0.15 times the center of mass energy and an event vertex consistent with the known interaction point (KLASGL = 10). We select hadronic events with at least 5 charged tracks (NTRKCD $\geq$ 5). To suppress continuum background, we require the ratio of Fox-Wolfram[86] moments to be less than 0.4 (R2GL $<$ 0.4).

Leptons in the tag are required to have momentum between 1.4 GeV/c and 2.5 GeV/c. Electrons are further required to have R2ELEC $\geq$ 3.0, and muons are required to have MUQUAL = 0 and DPTHMU $\geq$ 5. The tagged lepton candidates must come from the fiducial region $|CZCD| < 0.79$ and satisfy the standard CLEO-II tracking cuts. For additional leptons, the momentum must be within 0.5 Gev/c to 2.5 GeV/c for electrons, and 1.5-2.5 GeV/c for muon candidates. All the cuts for leptons are listed as follows:

For tag lepton,

- $KINCD = 0$ (good fitted track)
- $NHITPT + NHITVD > 0$ (must have at least one PT or VD hit)
- $RHITDR > 0.4$ (40% of DR penetration)
- at least any two of the following:
  - $|DBCD| < 5$ mm
  - $|ZOCD| < 5$ cm (within 5 centimeter in z of interaction)
  - $RESICD < 1$ mm (tracking quality fit cut)
- 1.4 GeV/c $< P_\ell <$ 2.5 GeV/c
- for electron
  - R2ELEC ≥ 3.0
- for muon
  - MUQUAL $= 0$
  - DPTHMU ≥ 5.0
  - $|CZCD| \leq 0.79$

Pions in the tag must have a charge opposite to that of the tag lepton and pass the following cuts:

- $P_\pi \leq 0.190$ GeV/c
- $KINCD = 0$ (good track)
- $|SGPIDI| < 2.0$ (within 2 σ of π ID from dE/dX)

- $|DBCD| < 5$ mm
- $|ZOCD| < 5$ cm.

For second lepton, all is same with tagged lepton except:

- second lepton as electron
  - 0.5 GeV/c $< P_\ell <$ 2.5 GeV/c
  - for electron, $|CZCD| < 0.7071$
- for second lepton as muon
  - 1.5 GeV/c $< P_\ell <$ 2.5 GeV/c
  - $|CZCD| < 0.61$

4.5.1 $\pi^\pm$ Identification

The kinematic cut on pion is a little bit tighter than the maximum momentum allowed for pion from $\bar{B}^0 \rightarrow D^{*+}\ell\bar{\nu}_\ell, D^{*+} \rightarrow D^0\pi^+$ decay, which is about 225 MeV/c. The particle identification for pion relies on the dE/dX identification using information from drift chamber. It works very well for such low momentum pion.

Pion momentum smaller than 60 MeV/c can not be detected because the reconstruction efficiency for charged track that slow is very small. Small momentum charged tracks tend to leave few hits in the drift chamber, making it hard to reconstruct the tracks. CLEO has studied the pion tracking reconstruction efficiency and had simulated the data with Monte Carlo[63].

As we have discussed in a previous chapter, the existence of a strong magnetic field will make the low momentum charged tracks highly curved that could have multiple hits in each of several layers. Since the tracking reconstruction takes only one hit per layor, hits in different layer belong to one single track could be reconstructed as two or more tracks. This creates the "ghost tracks" where two or more tracks are reconstructed from a single particle. We use the TRKMAN processor[35] to eliminate the ghost tracks. TRKMAN considered the two tracks as "ghost pair" when there are two tracks in the event with very similar curvature and ϕ value, but there are very few layers where both tracks have a hit. The track in the pair with fewer stereo and cathode hits are rejected, taking the track with better z momentum measurement as the real track.

Monte Carlo study shows CLEO tracking reconstruction routine, DUET processor, makes about 3.5 mistakes per $B\bar{B}$ event. The TRKMAN/TMNG reduced the number of mistakes by a factor of two.[35]

4.5.2 Lepton Identification

Fake Lepton

Some hadronic tracks will be identified as leptons when they leave traces in Crystal Calorimeter and/or in Muon Chamber. The "Fake Lepton" candidates need to be accounted and subtracted as background. CLEO has studied this fake lepton effect and come up with a fake rate as a function of momentum for different hadron species[46].

Fake rate is the probability of misidentifying a hadron as an electron or muon and is momentum dependent. The probabilities of pion, proton and kaon to pass the lepton identification are different from each other. CLEO[46] has studied the fake lepton probability of K, p, π respectively in $\Upsilon(4S)$. CLEO selects charged pions from $K_s \to \pi^+\pi^-$, protons from $\Lambda \to p\pi$, kaons from $D^* \to D^0\pi$, $D^0 \to K\pi$. While we have many pions and an adequate number of protons in our data sample, the amount of $\Upsilon(4S)$ event was not enough to produce kaons through $D^0 \to K\pi$. Due to the lack of statistics for the $\Upsilon(4S)$, especially on kaon sample, to produce the fake rate with the fine momentum distribution this analysis required, we used the fake rates obtained from $\Upsilon(1S)$ sample[46].

Unlike $\Upsilon(4S)$, hadronic decays in $\Upsilon(1S)$ are not expected to produce leptons. Therefore fake rates can be calculated simply by counting $\Upsilon(1S)$ tracks which passed the lepton identification packages. The only sources of real leptons are from the decay $\Upsilon(1S) \to \gamma^* \to q\bar{q}$ which has the same physics as in the continuum. This source of real leptons were removed by appropriately scaling the OFF data sample and subtracting from $\Upsilon(1S)$.

There is good agreement between the two measurements and we have used the difference as an estimate of systematic error in the fake correction. The Figure 4.3 shows the electron and muon fake rate study of $\Upsilon(1S)$ and $\Upsilon(4S)$.

In this analysis, we use hadronic tracks that failed the lepton identification criteria and sort according to their momentum, then multiply the fake rate in that particular momentum range to obtain the number of fake leptons in that momentum bin. This fake lepton components will be subtracted from our lepton samples.

Lepton Identification Efficiency

Muon Identification

MUTR[71] processor is used for muon identification information. Each track is extrapolated into muon chamber and matched to muon hits on the basis of their separation. A track must have two hits in a particular super layer to be considered a muon candidate. If the muon has hits at deeper layer but not so at layer of shallower depth, the track quality MUQUAL is registered as non-zero to flag this muon track candidate as not good. The

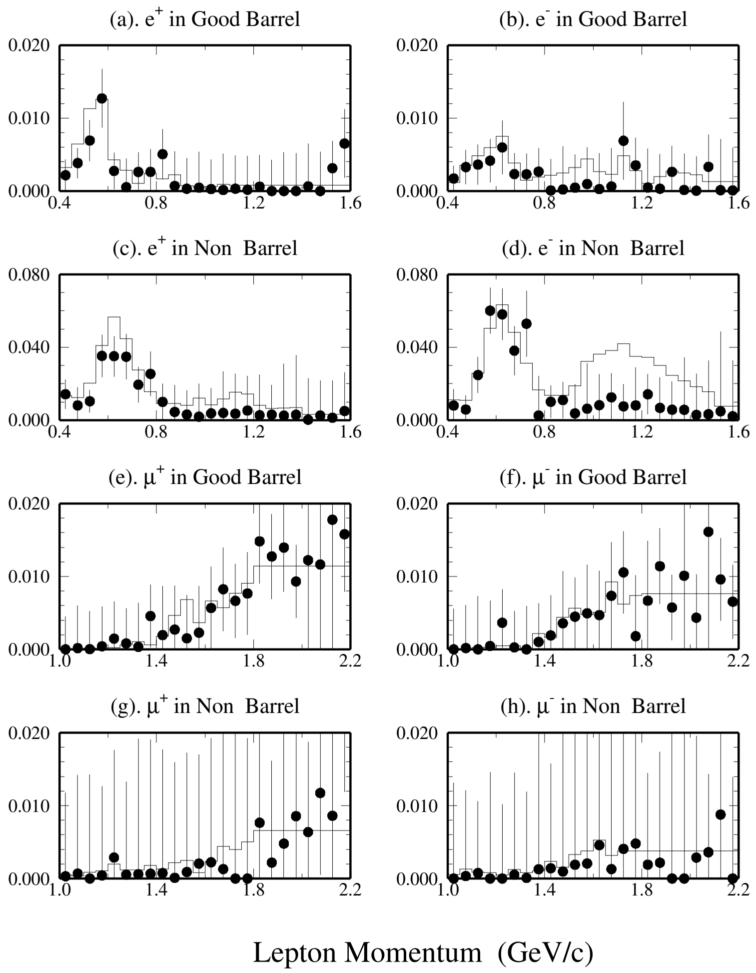

Figure 4.3: electron and muon fake rate: $\Upsilon(1S)$ (histogram) overlay by $\Upsilon(4S)$(dot). Good agreement shown in good barrel region, where the electron and muon candidates are taken. Courtesy of Dr. Roy Wang Ph.D thesis

variable DPTHMU marks the depth of outermost layer with a hit. The deeper the muon hits, the larger muon momentum is. For the case of DPTHMU > 3.0, the muon momentum is greater than 1.4 GeV/c.

The efficiency for muon identification is determined by the chamber efficiencies and the momentum dependent energy loss experienced by muons in the materials in front of each muon chamber. Monte Carlo simulates the efficiency for each layer to be within ±1%[46]. The energy loss in the material is understood at a level of 10 MeV[73].

Electron Identification

CLEO electron identification package CEID combines the available information from several sources to form a probability variable, R2ELEC, for electron ID. Those sources include the ratio of (E/P) which is the energy measured in electromagnetic calorimeter to the momentum of the track, the dE/dX, the track-crystal shower matching, the shower shape in crystal and information from TF. The probability variable, R2ELEC, is written as:

$$R2ELEC = \sum_i ln(\frac{P_e}{P_{\neq e}})_i \tag{4.1}$$

Here P_e and $P_{\neq e}$ are the probabilities that a charged track being identified as an electron or hadron based that source i. P_e were determined by embedding the bhabha electrons into hadronic events. $P_{\neq e}$ is determined by data taking at $\Upsilon(1S)$ events, where very few electrons are produced.

CLEO has studied the electron identification efficiency [46]. The tracks from radiative Bhabha events in data are embeded into hadronic events from data to assess electron identification in the $B\bar{B}$ events and found the efficiency generally above 90%. The uncertainty in electron efficiency has been estimated to be about ±2%. The muon identification effi-

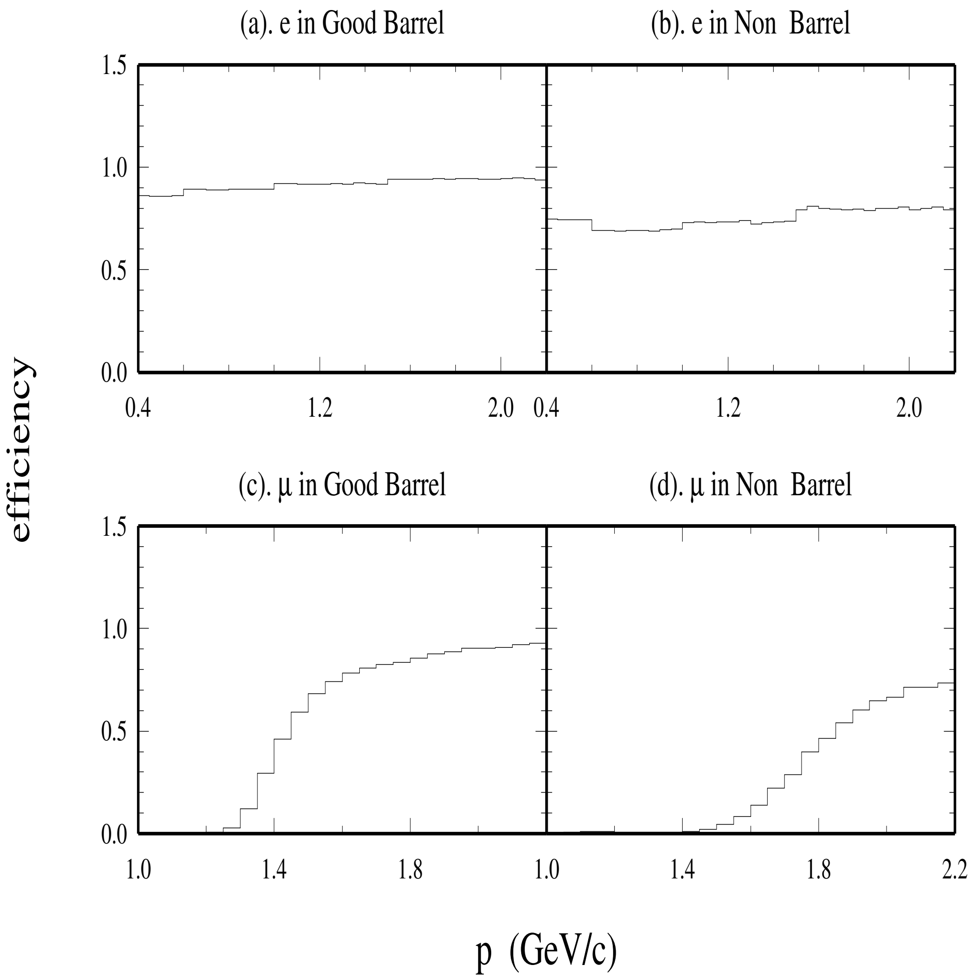

Figure 4.4: The lepton identification efficiency. Electron ID efficiency obtained from track embedding study and muon ID efficiency from Monte Carlo

ciency estimated from Monte Carlo and electron efficiency measured from embedding study is shown in Fig 4.4.

4.6 Partial Reconstruction of B^0

In this section, we will describe the CLEO developed technique of *partial reconstruction* in detail.

B's produced at $\Upsilon(4S)$ are tagged through the partial reconstruction of the semileptonic decay $B \to D^{*+}\ell^-\bar{\nu}_\ell, D^{*+} \to D^0\pi^+$ without explicitly reconstructing the D^0. In brief, we can use the soft pion from D^{*+} decay to approximate the four momentum of D^{*+} by taking advantage of the extremely low phase space available in $D^{*+} \to D^0\pi^+$. Combining with the detected lepton, we can calculate the mass square of the neutrino, which is also called "missing mass square" in other literature and we will use it from now on. For leptons and pions coming from the signal decay, the calculated missing mass square value should be close to zero.

The four momentum of D^{*+} can be approximated by the pion from $D^{*+} \to D^0\pi^+$ as:

$$E_{D^*} \simeq \frac{E_\pi}{E_\pi^{CM}} M_{D^*} \equiv \widetilde{E}_{D^*}, \mathbf{p}_{D^*} \simeq \frac{\mathbf{p}_\pi \times \sqrt{\widetilde{E}^2_{D^*} - M^2_{D^*}}}{|p_\pi|} \equiv \tilde{\mathbf{p}}_{D^*} \tag{4.2}$$

where E_π is the the π^+ energy, $E_{\pi^+}^{CM} \approx 145$ MeV is the energy of the π^+ in the D^{*+} rest frame, and M_{D^*} is the mass of the D^{*+}. Because the B momentum in $\Upsilon(4S)$ is very small, about 300 Mev/c, we can approximate $\mathbf{p_B} \simeq 0$. Since we also have detected the lepton, we can calculate the *missing mass square* through energy-momentum conservation. The square of the neutrino mass is:

$$\widetilde{M^2_\nu} \equiv (E_{\text{beam}} - \widetilde{E}_{D^*} - E_\ell)^2 - (\tilde{\mathbf{p}}_{D^*} + \mathbf{p}_\ell)^2. \tag{4.3}$$

There are several approximations made in this method. The study on those approximations has been documented in great detail in [48]. The discussions follows directly from that pioneer study.

The complete expression of M_ν^2 is:

$$\begin{aligned} M_\nu^2 &= E_\nu^2 - P_\nu^2 = (E_{\text{beam}} - E_l - E_{D^*})^2 - |\vec{P}_B - \vec{P}_l - \vec{P}_{D^*}|^2 \\ &= (E_{\text{beam}} - E_l - E_{D^*})^2 - |\vec{P}_l + \vec{P}_{D^*}|^2 - P_B^2 + 2\vec{P}_B \cdot (\vec{P}_l + \vec{P}_{D^*}). \end{aligned} \tag{4.4}$$

In $\Upsilon(4S)$ resonance, B meson is moving with approximately $|P_B| = 300$ MeV/c and we do not know its direction. The last two terms associated with B meson momentum in the lab frame on average contribute to about 0.002 GeV^2. Approximating $|P_B| = 0$ will widen the resolution to 0.4 GeV^2 at $\widetilde{M_\nu^2}$ and not significantly moving the mean of $\widetilde{M_\nu^2}$ from zero.

Secondly, the energy of D^{*+} is approximated by the slow pion. The energy of charged pion in the lab frame can be calculated as follow:

$$E_\pi = \gamma(E_\pi^{CM} + \beta P_\pi^{CM} cos\theta) \tag{4.5}$$

where the $cos\theta$ is the cosine angle between pion in the D^{*+} frame and the direction of D^{*+} seen in the lab. The γ and β are the lorentz transformation factor to boost π from the center of mass frame of D^* to the lab frame. The term proportional to $cos\theta$ is canceled by taking the average. γ can then be approximated as:

$$\gamma \simeq \frac{E_\pi}{E_\pi^{CM}} \equiv \hat{\gamma} \tag{4.6}$$

This $\hat{\gamma}$ enables us to calculate the average energy of D^{*+}:

$$E_{D^*} \simeq \hat{\gamma} M_{D^*} = \frac{E_\pi}{E_\pi^{CM}} M_{D^*} \equiv \widetilde{E_{D^*}} \tag{4.7}$$

The resolution of γ, then D^{*+} energy, depends on the polarization of D^{*+}. It is estimated to be about 8% [48]. This approximation is better for D^{*+} of helicity $= \pm 1$ than for D^{*+} of helicity $= 0$ since π^+ are preferentially emitted towards $cos\theta = 0$ and consequently experienced the same boost as the D^{*+}. The Fig 4.5 shows the ratio $(\hat{\gamma} - \gamma)/\gamma \equiv \delta\gamma/\gamma$ for unpolarized and polarized D^*.

The third approximation is we assume the direction of the soft π is in the same direction of D^{*+} seen in the lab. It is estimated from Monte Carlo [48] that the direction approximation

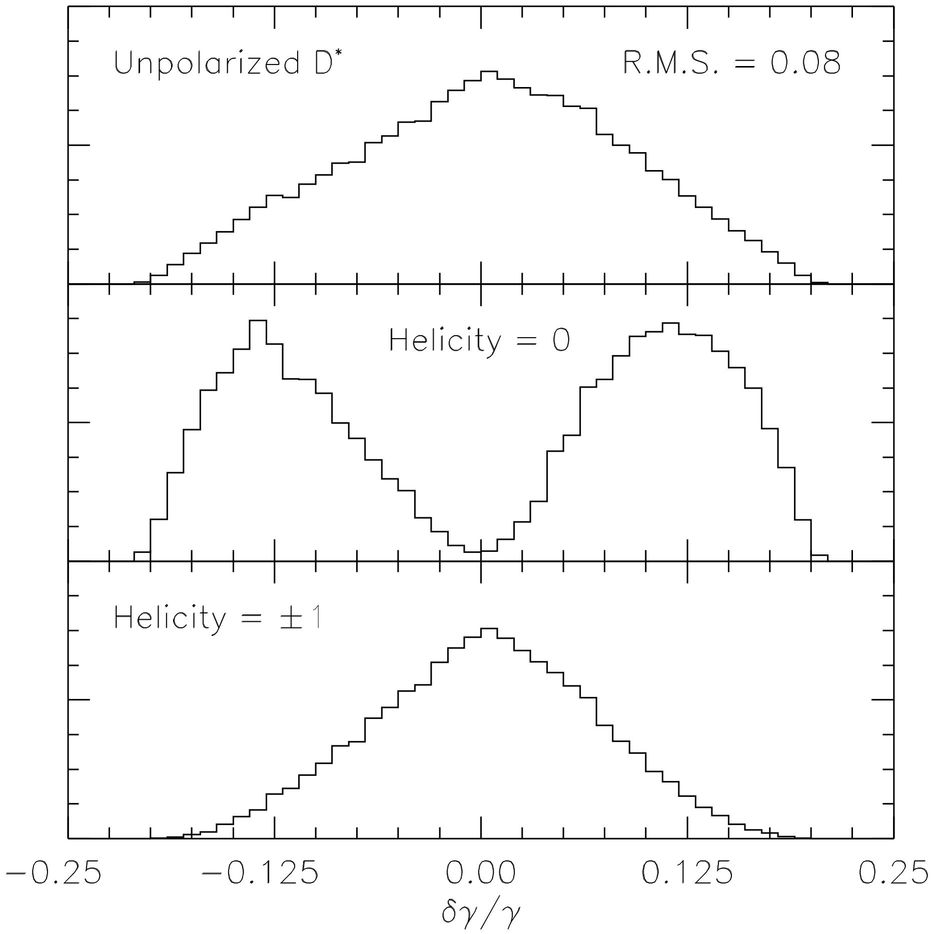

Figure 4.5: Error on Gamma approximation. courtesy of Mike Sauliner Ph.D thesis [48].

also depends on the polarization of D^{*+} meson, but works better for helicity 0 D^{*+} meson than for D^{*+} meson with helicity equals 1. This is just opposite to the energy approximation we mentioned previously.

The combination of the the last two approximations give us about 600 Mev/c uncertainty in D^{*+} momentum. Comparing this with the error of momentum approximation in B meson, $P_B \simeq 300MeV/c$, we expects the width of $\widetilde{M_\nu^2}$ resolution in the *partial reconstruction* won't be much wider than twice of 0.4 GeV^2. The Monte Carlo simulation did find the error to be $\simeq 0.9\ GeV^2$ as can be seen in Fig 4.6 in [48].

4.7 B^0 Tag from Partial Reconstruction

There are two major backgrounds to be subtracted in our tag sample, the continuum and the combinatorial background. The continuum background occurs when the lepton and pion tracks comes not from $\Upsilon(4S)$ event, but from $e^+e^- \to q\bar{q}$, where q means u,d,s,c quark. The combinatoric background from $B\bar{B}$ events are the random combination of the oppositely charged lepton pion pairs which pass our kinematic cut.

4.7.1 Continuum Background Estimation

To estimate the continuum background, we analyze events taken at *Off* resonance energy. The $\widetilde{M_\nu^2}$ was calculated of the oppositely charged lepton-pion pair at events 60 MeV below the $\Upsilon(4S)$. The resulting histogram was scaled for the luminosity and energy difference to normalize to the continuum events in the $\Upsilon(4S)$. We then subtract this scaled continuum from data. The scaling factor is calculated as follows:

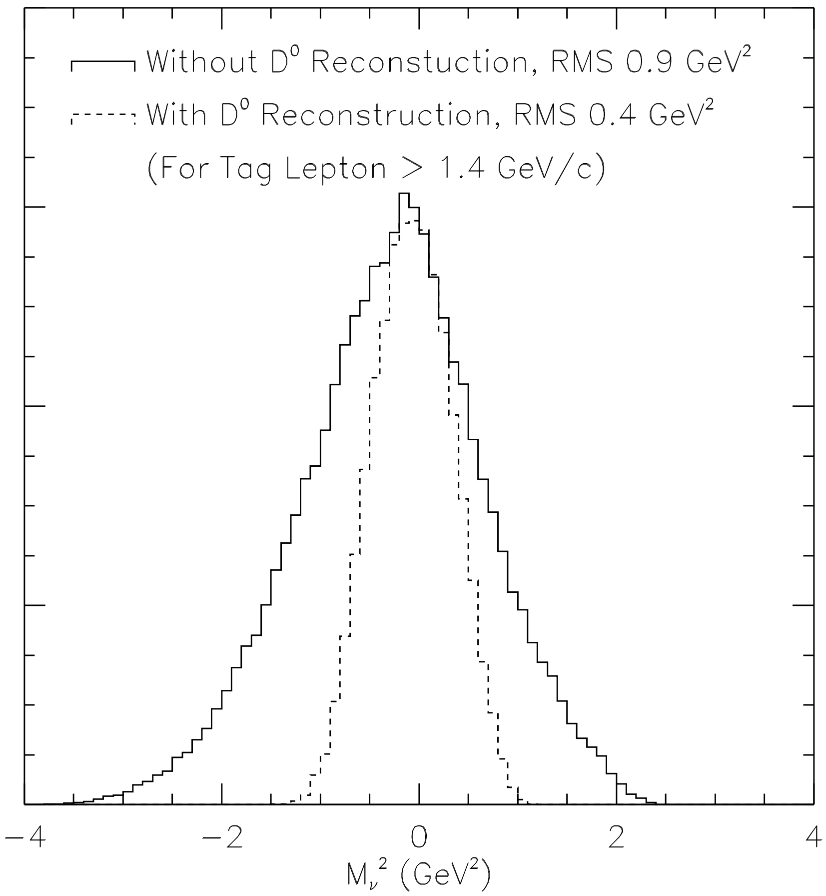

Figure 4.6: The missing square signal for tag lepton $P_\ell > 1.4$ GeV/c with and without D^0 reconstruction. from[48].

$$Scaling\ \ Factor = \frac{L_{on}}{L_{off}} \frac{E^2_{beam}(off)}{E^2_{beam}(on)} = 2.11 \tag{4.8}$$

The L_{on} and $E_{beam}(on)$ corresponds to the luminosity and energy of the beam at $\Upsilon(4S)$. and L_{off}, $E_{beam}(off)$ corresponds to the value in off resonance.

4.7.2 Combinatoric Background Estimation

We use CLEO generic $B\bar{B}$ Monte Carlo to simulate this combinatoric background. The scaling factor for Monte Carlo is obtained by matching the entries of Monte Carlo to Data in the **side-band region**, $-25 \leq \widetilde{M^2_\nu} \leq$ -4 GeV^2. Only the entries in the signal region, $-2 \leq \widetilde{M^2_\nu} \leq 5$ GeV^2 before subtracting from combinatoric background will be collected to account as the tag, N_{tag}. In Fig 4.7 is the $\widetilde{M^2_\nu}$ of data, overlayed by continuum and Monte Carlo estimated combinatoric background. The net signal after the continuum and combinatoric background subtraction can be seen at Fig 4.8

To know if our Monte Carlo simulates the data correctly, we take the wrong sign lepton-pion combination, where the tag leptons and pions have the same charge, and repeat the same procedure as we did for the right sign sample, $(\ell^{\pm}_{tag}, \pi^{\mp}_{tag})$. In Fig 4.9 we can see the result of wrong sign sample $\widetilde{M^2_\nu}$ in signal region is consistent with being zero. This confirms our Monte Carlo has simulated the combinatoric background well in our data.

It is important not to use the wrong sign combination in the data as the combinatoric background in our right sign tag. The wrong sign and right sign combinatoric background have different composition ratio of correlated/uncorrelated background, where lepton and pion are from the same B/different B. Because the correlated and uncorrelated background have different missing mass square shape, thus it results to different $\widetilde{M^2_\nu}$ shape for right sign and wrong sign background.

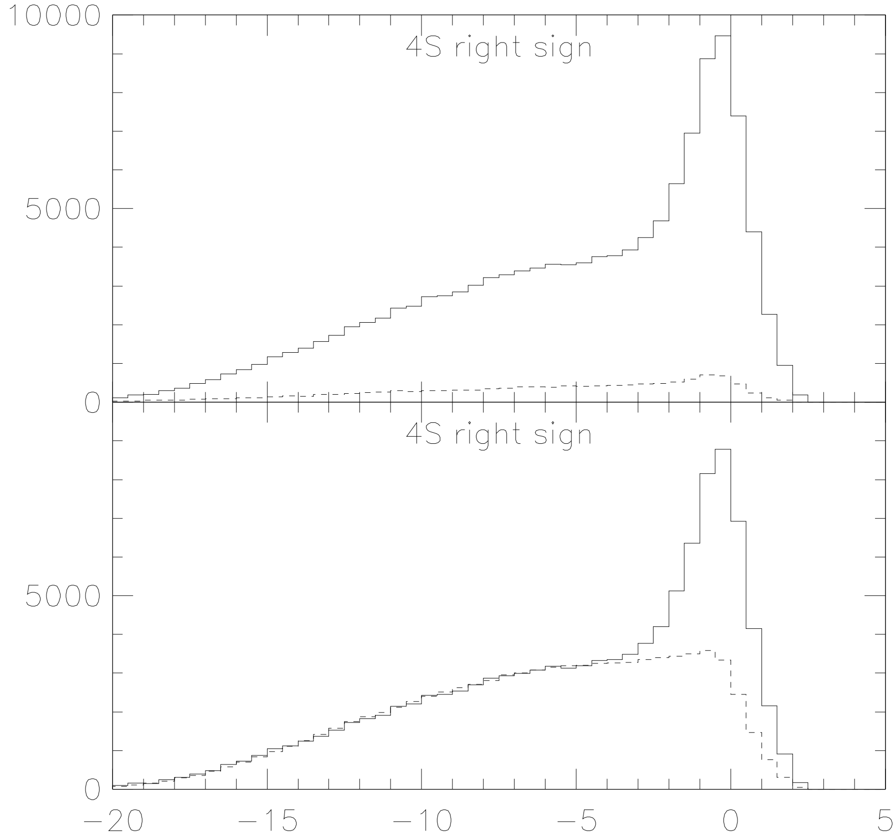

Figure 4.7: right sign missing mass square overlayed by continuum (dash line) for above. The bottom plot is the continuum subtracted plot overlaid with random background (dash line). Only the entries between $-2 \leq \widetilde{M_\nu^2} \leq 5Gev^2$ region is counted as signal tag.

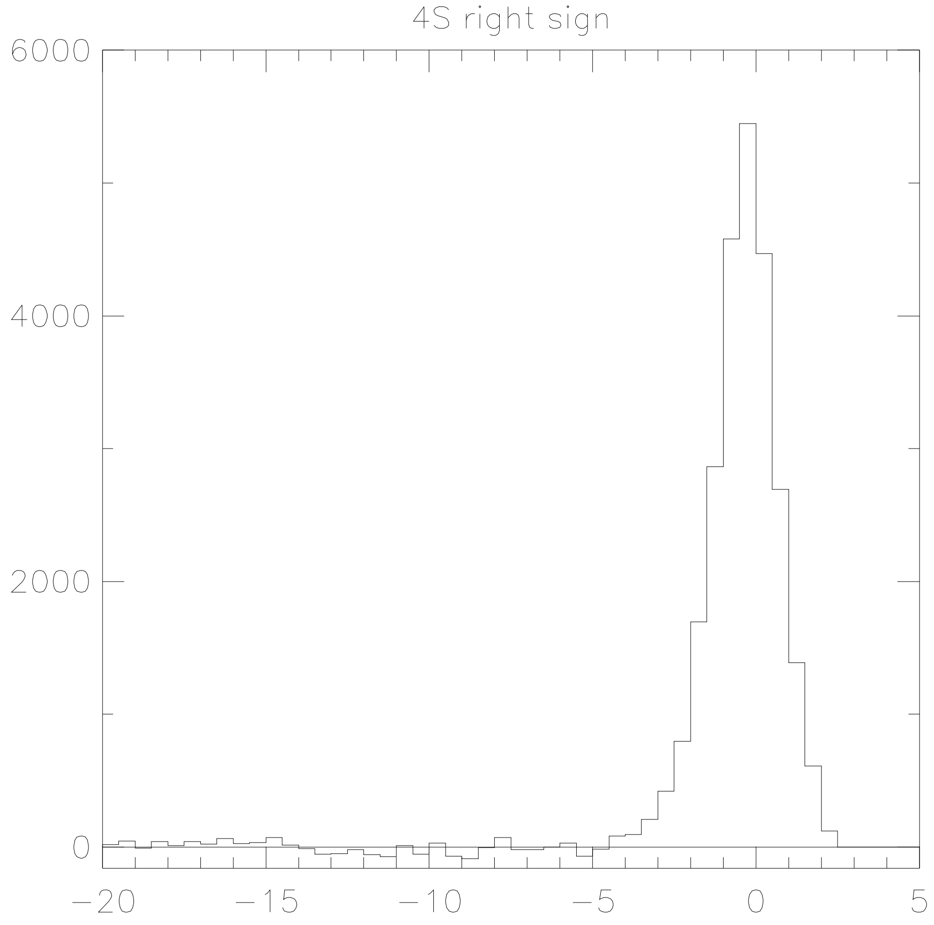

Figure 4.8: The missing mass square plot for tag signal after continuum and combinatoric background subtraction. We see a nice peak at our signal region $-2 \leq \widetilde{M_\nu^2} \leq 5Gev^2$ and there is no tail.

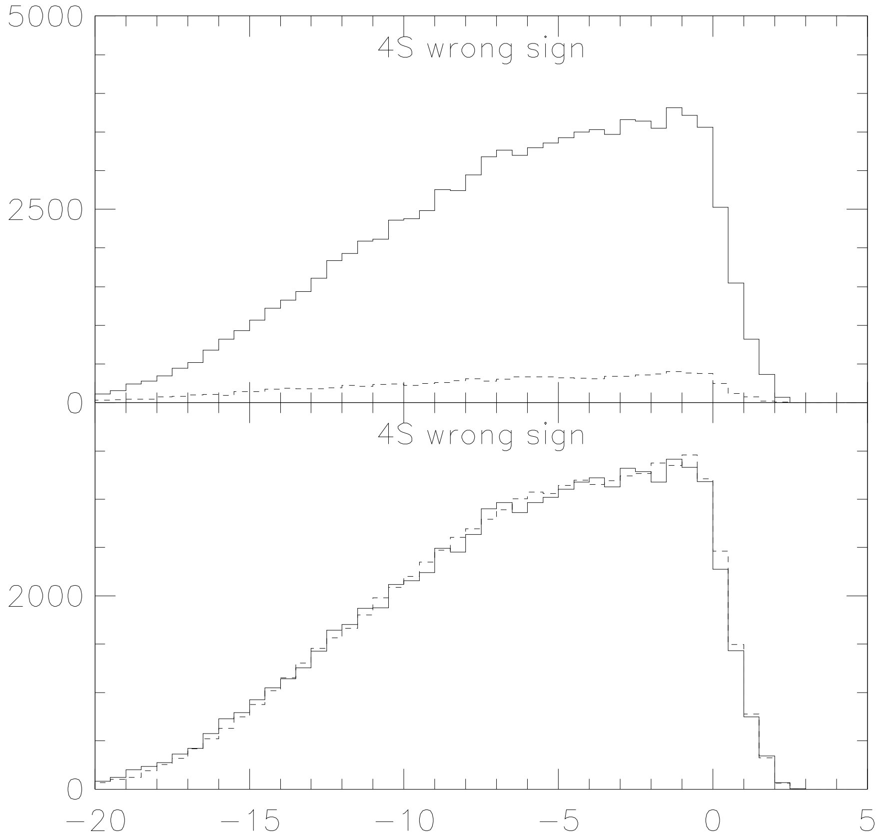

Figure 4.9: wrong sign missing mass square plot. As the case for right sign, the dashed line stands for continuum at top, and the combinatoric background at the bottom. We see the Monte Carlo simulates the wrong sign background very well

Table 4.1: number of tag

Source	right sign	wrong sign
data(signal region)	46118.0 ± 214.8	19970.0 ± 141.3
continuum(signal region)	7043.9 ± 121.1	4164.7 ± 93.15
data-continuum(signal region)	39074 ± 246.58	15805 ± 169.28
data-continuum(side band)	47265.0 ± 306.6	45043.0 ± 293.4
MC background(side band)	211341 ± 459.7	210108 ± 458.4
MC background(signal)	178373 ± 422.35	78379 ± 279.96
scaling factor	0.2236	0.2144
MC scaled bg(signal region)	16194.0 ± 94.5	16803.0 ± 58.7
yield	22880 ± 283.0	-277.27 ± 179.2

For tag in signal region, we have gathered 46118.0 ± 214.8 for event taken at $\Upsilon(4S)$, 7043.9±121.1 for events at continuum and 16194.0±94.5 for events estimated as combinatoric background. The overall number of tagged lepton-pion pair, $N(\ell^{\mp}_{tag}, \pi^{\pm}_{tag})$ after this procedure is:$N_{tag} = 22880 \pm 283(stat)$ We tabulate the number related with tag in Table 4.1.

4.8 Additional Lepton Spectra Reconstruction

After a tag lepton-pion pair has been found, a search for additional leptons in the same event is performed. The $\widetilde{M_\nu^2}$ distribution is calculated as we did for the tag, except we now sort it in 100 Mev/c bin in terms of the additional leptons momentum. We also separate the second lepton according to its particle species. The additional leptons include all leptons except the one being counted as tag in the event.

In each bin of $\widetilde{M_\nu^2}$, we subtract the contributions from continuum, additional leptons that are fake and combinatoric background. After those subtractions, the remaining entries in the signal region will be used to construct our second lepton momentum spectrum. This spectrum will be corrected for lepton identification and reconstruction efficiency. Then the additional leptons from $B \to J/\Psi \to \ell^+\ell^-$ decay are subtracted to obtain the lepton momentum spectrum for fitting.

This reconstructed additional lepton spectrum contain leptons from primary leptons, $b \to \ell$, secondary leptons, $b \to c \to X\ell\nu$ and leptons from "other sources" like D_s, τ, Λ_c, photon conversion and π^0 dalitz decay. The leptons from "other sources" will be denoted as "other leptons". The contribution of these "other leptons" are very small compared with primary and secondary leptons. Their contaminations will be studied in systematic error section.

4.8.1 Continuum, Fake Lepton and Random Background

The continuum background was estimated by taking events at off resonance data and scaled to account for the energy and luminosity difference in $\Upsilon(4S)$. For the fake leptons estimation, we first replace the additional leptons with any charged hadronic tracks that pass all the additional lepton cuts except the lepton ID. We then subtract the hadron-tag sample that are from the continuum. The result then will be multiplied by the corresponding fake rate in that charged hadronic track momentum to obtain the number of fake lepton at that particular momentum bin.

After the continuum and fake additional lepton entries have been subtracted, we then subtract random background in the same way as we do for the tag. The entries collected at signal region ($-2 \leq \widetilde{M_\nu^2} \leq 5$ GeV/c^2) in missing mass square distribution for each bin will be the entries of the additional leptons in that particular momentum bin to construct the inclusive lepton momentum spectrum. Plots in Fig 4.10,Fig 4.11, Fig 4.12 are the bin-by-bin $\widetilde{M_\nu^2}$ plot of tag with second electrons from 0.5-2.5 GeV/c and muon at momentum 1.5-2.5 GeV/c each respectively. Their respective entries bin-by-bin is listed at Table 4.8.1

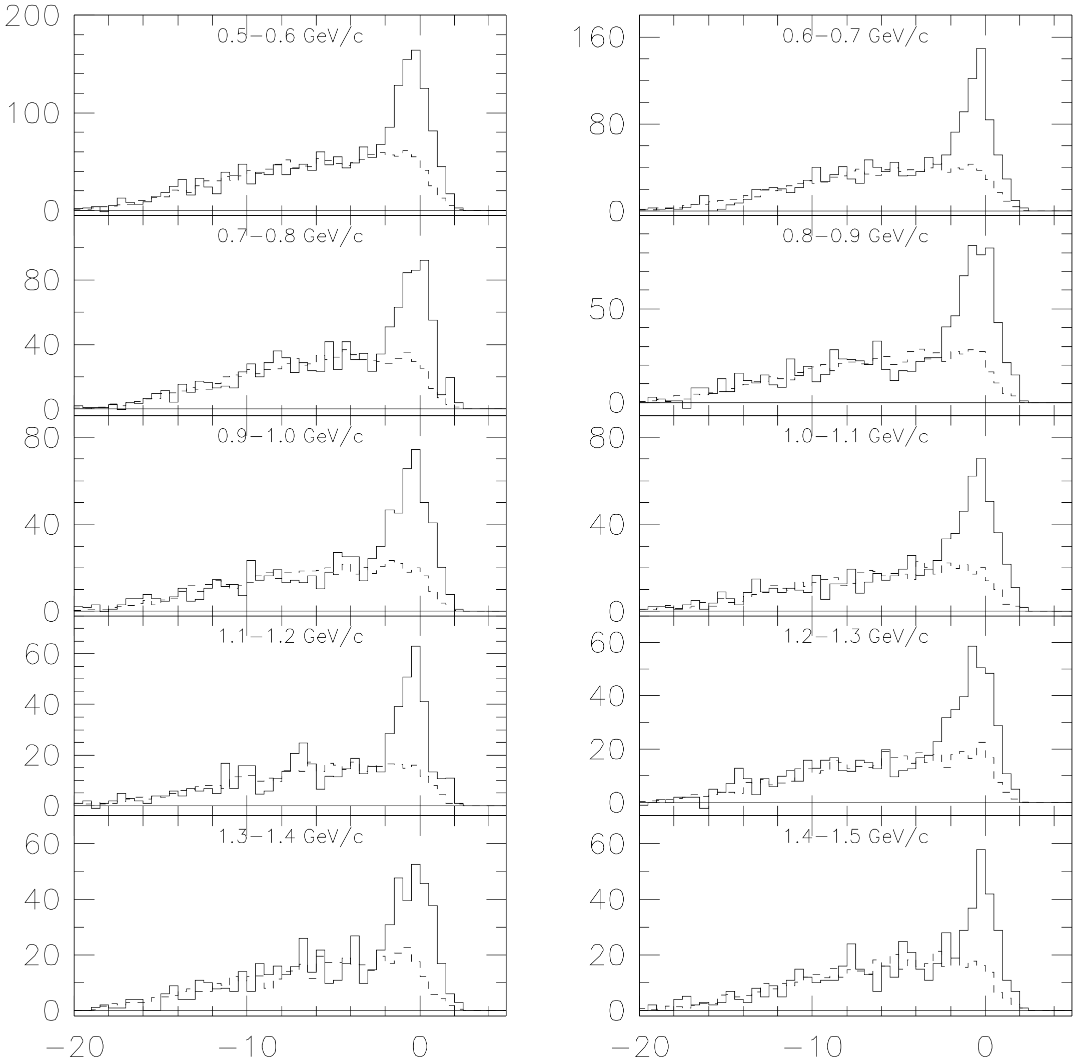

Figure 4.10: $\tilde{M}_\nu^2$ bin-by-bin for second lepton (electron) momentum between 0.5-1.5 GeV/c

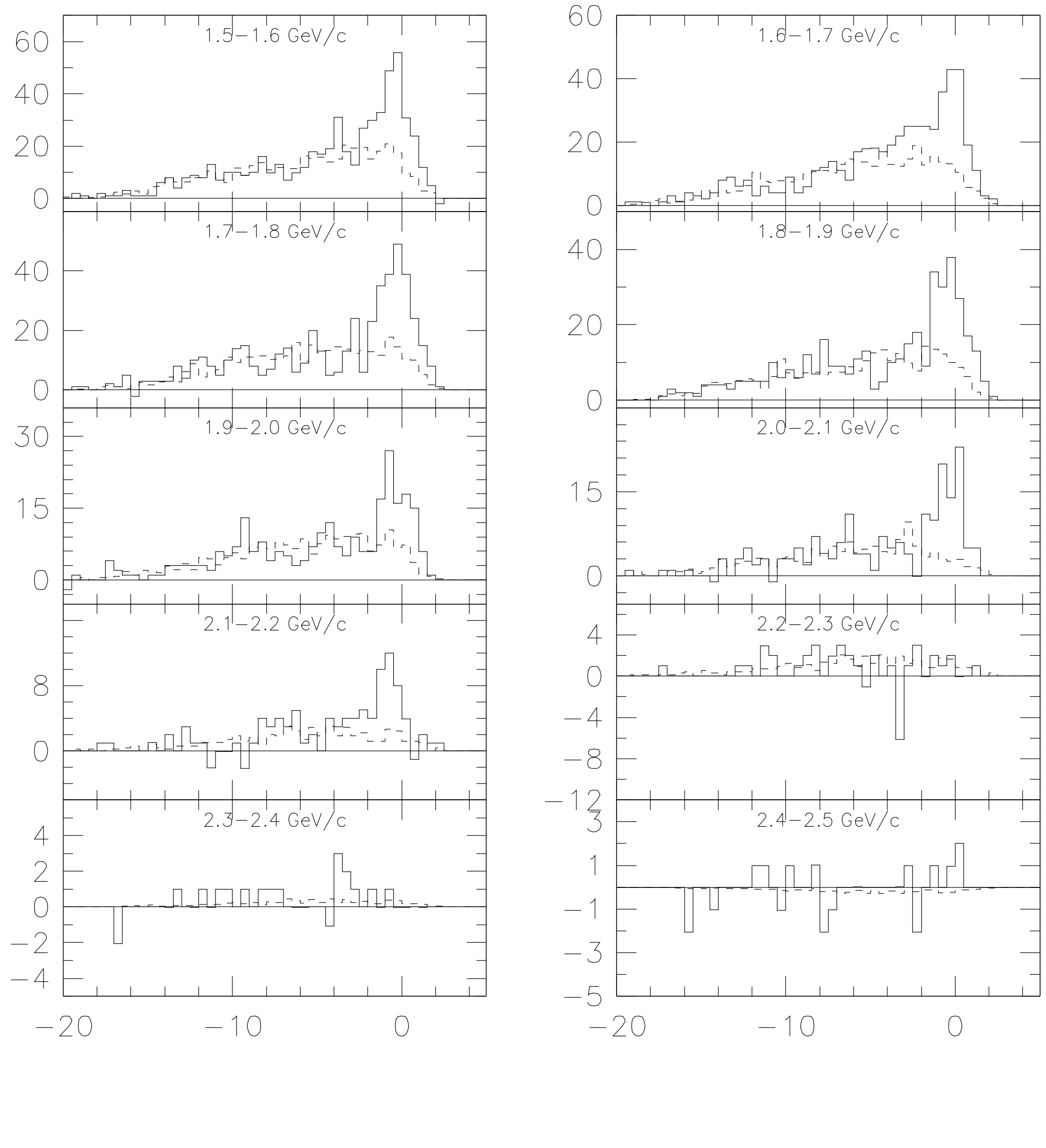

Figure 4.11: $\tilde{M}_{\nu}^{2}$ bin-by-bin for second lepton (electron) momentum between 1.5-2.5 GeV/c

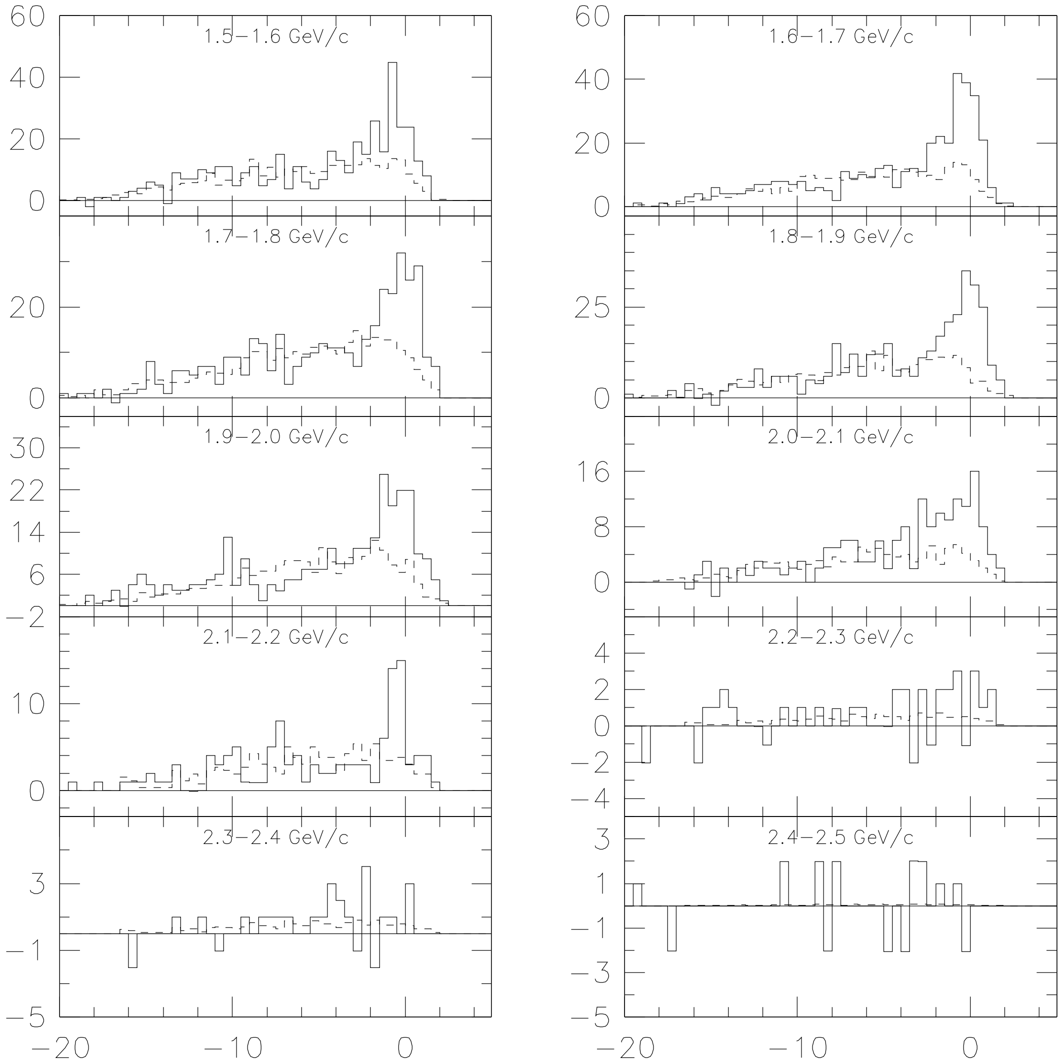

Figure 4.12: $\tilde{M}_\nu^2$ bin-by-bin for second lepton (muon) momentum between 1.5-2.5 GeV/c

Table 4.2: second lepton spectrum

(GeV/c) electrons	Data	MC	Data-MC	ϵ_{ID}	net event
0.5-0.6	861.0 ± 33.5	340.2 ± 16.7	520.8 ± 37.5	0.548	950.7 ± 68.4
0.6-0.7	636.8 ± 29.1	228.8 ± 13.1	408.0 ± 31.9	0.582	700.9 ± 54.9
0.7-0.8	472.9 ± 23.6	176.0 ± 11.3	296.8 ± 26.2	0.585	507.1 ± 44.8
0.8-0.9	445.9 ± 23.3	146.1 ± 10.5	299.8 ± 25.6	0.593	505.2 ± 43.1
0.9-1.0	357.4 ± 20.1	119.3 ± 9.4	238.0 ± 22.1	0.598	398.0 ± 37.0
1.0-1.1	339.1 ± 20.3	110.6 ± 9.0	228.5 ± 22.2	0.615	371.4 ± 36.2
1.1-1.2	260.8 ± 17.2	90.7 ± 8.7	170.1 ± 19.3	0.621	274.0 ± 31.0
1.2-1.3	277.7 ± 17.3	105.7 ± 9.5	172.0 ± 19.7	0.622	276.5 ± 31.7
1.3-1.4	280.7 ± 17.4	102.7 ± 9.2	178.1 ± 19.6	0.618	288.0 ± 31.7
1.4-1.5	232.0 ± 16.3	95.6 ± 8.5	136.4 ± 18.4	0.625	218.2 ± 29.4
1.5-1.6	237.3 ± 16.2	94.8 ± 9.0	142.5 ± 18.5	0.635	224.4 ± 29.2
1.6-1.7	205.5 ± 15.0	77.8 ± 7.9	127.7 ± 16.9	0.635	200.9 ± 26.7
1.7-1.8	232.8 ± 15.3	84.2 ± 8.4	148.6 ± 17.4	0.636	233.8 ± 27.4
1.8-1.9	173.8 ± 13.4	68.8 ± 7.6	105.0 ± 15.4	0.638	164.6 ± 24.2
1.9-2.0	105.7 ± 10.9	43.8 ± 6.0	61.9 ± 12.4	0.635	97.5 ± 19.6
2.0-2.1	87.8 ± 10.0	20.2 ± 3.7	67.6 ± 10.7	0.637	106.1 ± 16.8
2.1-2.2	40.8 ± 7.3	8.4 ± 2.3	32.4 ± 7.7	0.648	50.1 ± 11.9
2.2-2.3	5.8 ± 4.3	1.6 ± 0.6	4.2 ± 4.4	0.630	6.7 ± 6.9
2.3-2.4	2.0 ± 1.4	0.2 ± 0.1	1.8 ± 1.4	0.619	2.9 ± 2.3
2.4-2.5	3.9 ± 3.2	0.0 ± 0.1	3.9 ± 3.2	0.615	6.3 ± 5.2
muons					
1.5-1.6	152.7 ± 13.7	65.5 ± 7.5	87.1 ± 15.6	0.409	212.9 ± 38.2
1.6-1.7	184.0 ± 14.8	63.5 ± 7.1	120.5 ± 16.4	0.463	259.9 ± 35.4
1.7-1.8	163.6 ± 14.1	69.3 ± 7.6	94.4 ± 16.0	0.483	195.5 ± 33.2
1.8-1.9	163.3 ± 13.6	54.2 ± 6.7	109.1 ± 15.2	0.503	217.0 ± 30.2
1.9-2.0	124.5 ± 11.8	53.1 ± 7.1	71.4 ± 13.8	0.513	139.1 ± 26.8
2.0-2.1	71.1 ± 8.9	22.8 ± 4.5	48.3 ± 9.9	0.528	91.5 ± 18.8
2.1-2.2	47.3 ± 7.4	17.9 ± 3.5	29.4 ± 8.2	0.540	54.3 ± 15.1
2.2-2.3	11.5 ± 5.0	0.6 ± 0.7	10.9 ± 5.0	0.529	20.6 ± 9.5
2.3-2.4	2.6 ± 3.1	0.3 ± 0.2	2.3 ± 3.1	0.540	4.2 ± 5.7
2.4-2.5	-0.2 ± 2.5	0.0 ± 0.0	-0.2 ± 2.5	0.536	-0.4 ± 4.7

4.8.2 Second Lepton Momentum Spectrum Correction

Lepton Efficiency Correction

This inclusive lepton momentum spectrum needs to be corrected for the detection efficiency. There are three factors affecting the lepton detection: (1) general charged tracks finding, (2) lepton identification and (3) our geometrical cut in accepting the leptons.

The charged tracks finding is the charged track reconstruction efficiency. The lepton identification efficiency comes from the cut we made on lepton identification: $R2ELEC > 3$ for electrons, $MUQUAL = 0$ and $DPTHMU > 5$ for muon candidates. The geometrical acceptance was due to the fact that we accept electron within region $cos\theta \leq 0.71$ and muon within $cos\theta \leq 0.61$ in our search for additional leptons within the tagged event. Except this geometrical acceptance cut, the tracking and lepton identification cuts are a function of the momentum of the charged track.

The lepton identification and tracking reconstruction efficiency has been examined in detail by previous CLEO analysis [46] as mentioned earlier. Since we use essentially the same lepton cut as that analysis, we adopt that efficiency number and corrected for our geometrical acceptance cut. Our raw additional lepton momentum spectrum is then corrected by this efficiency bin-by-bin.

$B \to XJ/\Psi \to \ell^+\ell^-$ Subtraction

To estimate the number of leptons from J/Ψ decay, we use the generator level Monte Carlo to simulate the momentum spectrum of leptons from J/Ψ and normalize to data. The normalization is found by pairing an identified muon with any opposite charged track in the event to form the J/Ψ invariant mass distribution for both data and Monte Carlo. This invariant mass distribution was fit with Gaussian and a smooth background curve. The ratio of data entries in the Gaussian to Monte Carlo is our scaling factor, which will multiply the Monte Carlo J/Ψ lepton momentum spectrum to obtain the J/Ψ lepton distribution in data.

It is estimated that we have $15.3 \pm 3.2(22.7 \pm 4.4)$ for J/Ψ electron (muon) in our reconstructed additional lepton momentum spectrum.

4.9 Extracting Primary Leptons

We use a phenomenological model to fit this corrected lepton spectrum to estimate the contributions from primary and secondary leptons. The result of the fit needs to be corrected for the tagging efficiency difference for events with additional leptons and events with tag alone.

4.9.1 Fitting

The resulting additional lepton spectrum is the combination of primary leptons, $b \to X\ell\bar{\nu}$, and secondary leptons, $b \to c \to X\ell\bar{\nu}$, from B meson decay. We have introduced several theoretical functions in chapter 2 for extracting the primary leptons. In this analysis, the central value was read out from the fit result of ACCMM function because this function gives the best fit to previous CLEO inclusive lepton spectrum analysis [46].

For fitting purposes, we put electrons and muons in a single plot by placing electrons at momentum 0-4 GeV/c and add 4 GeV/c to muons to place it at momentum 4-8 GeV/c. The purpose is to fit the electron and muon spectrum simultaneously, assuming the lepton universality. This procedure has been employed by previous CLEO analysis [46]. The result of the fit can be seen in Fig 4.13.

4.9.2 Tagging Efficiency Correction

The number of primary leptons from the fit will further be corrected for the di-lepton opening angle cut $|cos\theta| < 0.99$, the cut on accepting events due to its charged multiplicity, and the different tagging efficiency between the tag and its additional lepton subsample.

The cut on the di-lepton opening angle is to prevent over-counting one lepton as two tracks. The correction for this di-lepton opening angle cut is purely geometrical in nature.

Since we accept event with at least five charged tracks, the difference in charge multiplicity for generic $B\bar{B}$ event and the subset of the semileptonic event needs to be corrected. Previous CLEO analysis has found that the mean value of charge multiplicity for tag with additional leptons is slightly lower than the tag[48] due to the fact that charge multiplicity of a semileptonic B decay is lower than for a generic B decay. This finding caused 0.5% under-efficiency for accepting semileptonic event than accepting the generic $B\bar{B}$ event.

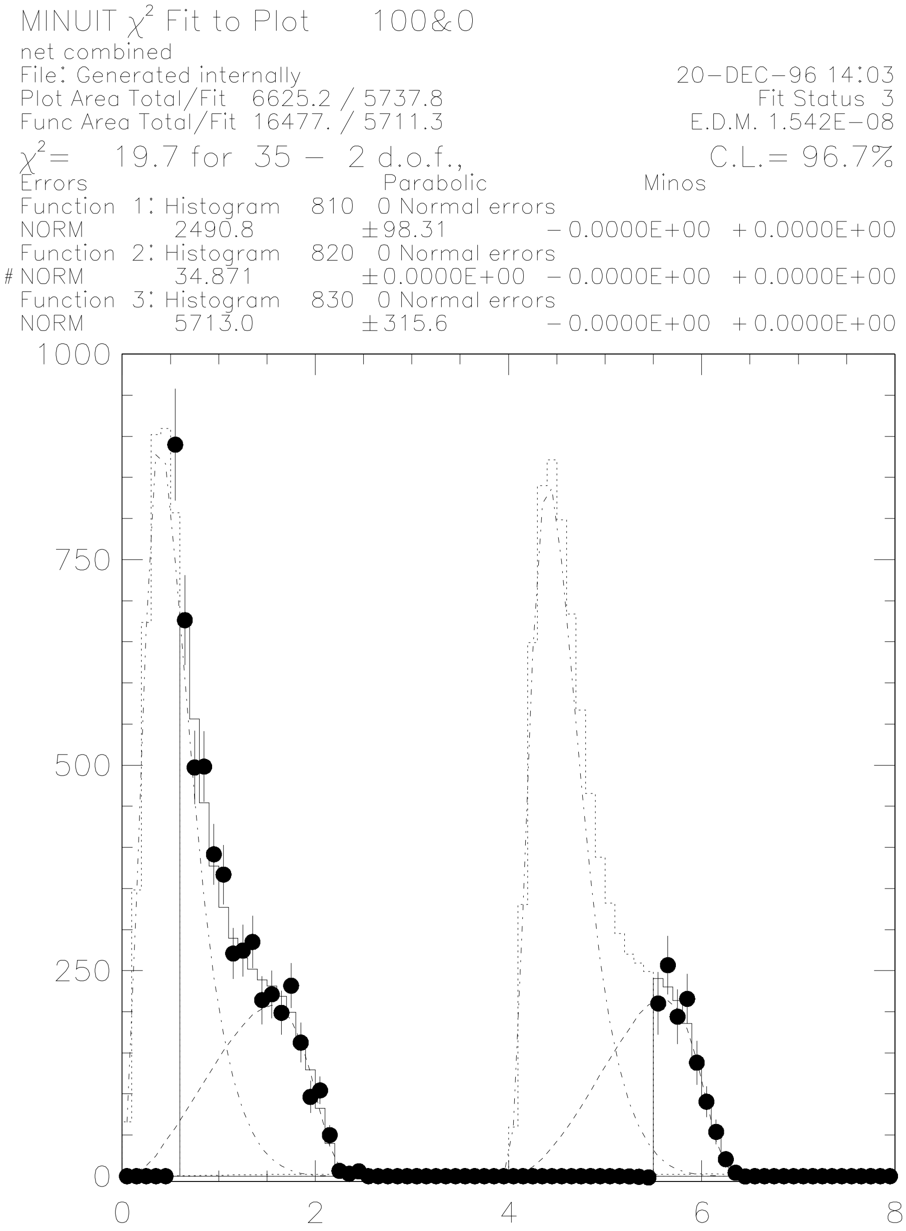

Figure 4.13: B decay lepton spectrum for simultaneous fit using ACCMM model. The electron is located from 0-4 GeV/c and muon is at 4-8 GeV/c.

The correction of the combination of these two cuts is found to be $(+1.1 \pm 1.1)\%$[48].

The third correction we have to make is the difference for tagging efficiency of tag and its additional leptons subsample, as results from the fact that it is easier to reconstruct a tag in a semileptonic decay event than a generic hadronic event when the number of charged tracks of the latter environment are higher.

We use Monte Carlo to study the tagging efficiency difference between the generic B decay and the B semileptonic decay. We first construct the tagging efficiency as a function of charge multiplicity in a generic $B\bar{B}$ event. Next, we obtain the charge multiplicity distribution for the semileptonic event. The charge multiplicity function for this semileptonic event subsample was sorted acording to the lepton momentum in 100 MeV/c bin each. We then multiplied the tagging efficiency function with the charge multiplicity distribution of semileptonic event bin-by-bin to find out the tagging efficiency of the B semileptonic event subsample. We found out the tagging efficiency for semileptonic event is independent of its leptonic momentum, and the number is about 1.029 ± 0.013 over-efficient then generic $B\bar{B}$ event.

The net correction of the all sources in our $N_{tag,\ell}$ is $(-1.8 \pm 1.7)\%$.

From the fit, We obtain 2529 ± 102 primary leptons. We have 2484 ± 100 after the tagging efficiency correction and di-lepton opening angle correction. We denote the ratio of the number of the additional primary lepton to the number of the tag as $b_{tag} = N(tag, \ell_{add})/N(tag)$. We have:

$$\boxed{b_{tag} = \frac{2484.0 \pm 100.0}{22880.0 \pm 283.0} = 10.86 \pm 0.46}$$

4.10 Comparison of Two Inclusive Lepton Spectra

The tagged spectra of electrons and muons, Fig 4.13, are then divided by the corresponding inclusive spectra from previous CLEO single lepton analysis, Fig 4.1, [46], bin-by-bin in momentum between 1.5-2.4 GeV/c. If the two primary spectra have the same shape, then the resulting distribution in this momentum range after subtracting the secondary leptons should be flat. The ratio of the two spectra is denoted as R. If the spectra have the same shape, R is constant and $R = b_{tag}/b_{incl}$, where b_{tag} and b_{incl} are the semileptonic branching fractions measured in the tagged and total events samples, respectively. The distributions appear indeed to be flat. They are thus fitted to a constant function. The spectrum comparison plots of electron and muon are shown in Fig 4.14 and Fig 4.15 respectively. The result of a flat straight line fit gives $R = 1.013 \pm 0.061$ with $\chi^2/DOF = 7.5/8$ for electrons and $R = 1.036 \pm 0.071$ with $\chi^2/DOF = 3.1/8$ for muons. The weighted error average is:

$$\boxed{R = 1.023 \pm 0.046}$$

We also obtain R by taking the ratio of the primary contributions to the spectra from the fits described above, and find excellent agreement.

The flat distribution of R indicates that the lepton spectrum for $\bar{B}^0$ and B^- semileptonic decay are very similar. And this value, along with the measurement from single lepton method, can lead us to obtain the semileptonic branching fraction for $\bar{B}^0$ and B^- respectively.

4.11 Systematic Error on R

Since the procedures for obtaining tagged and inclusive spectra have been made nearly identical, many of the systematic errors are highly correlated and cancel approximately in the ratio R. Among these are errors from lepton tracking and identification efficiencies,

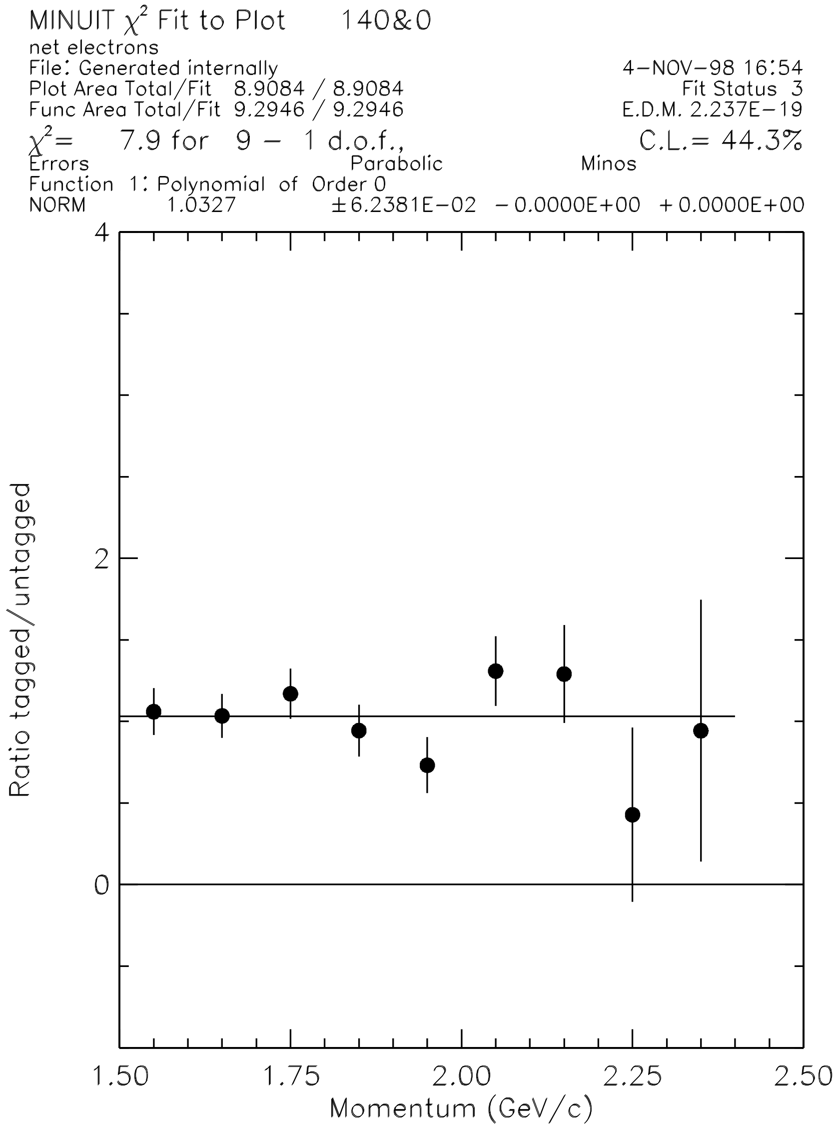

Figure 4.14: The lepton spectrum bin-by-bin comparison for single lepton inclusive measurement and this partial reconstruction method for electron momentum between 1.5-2.5 GeV/c

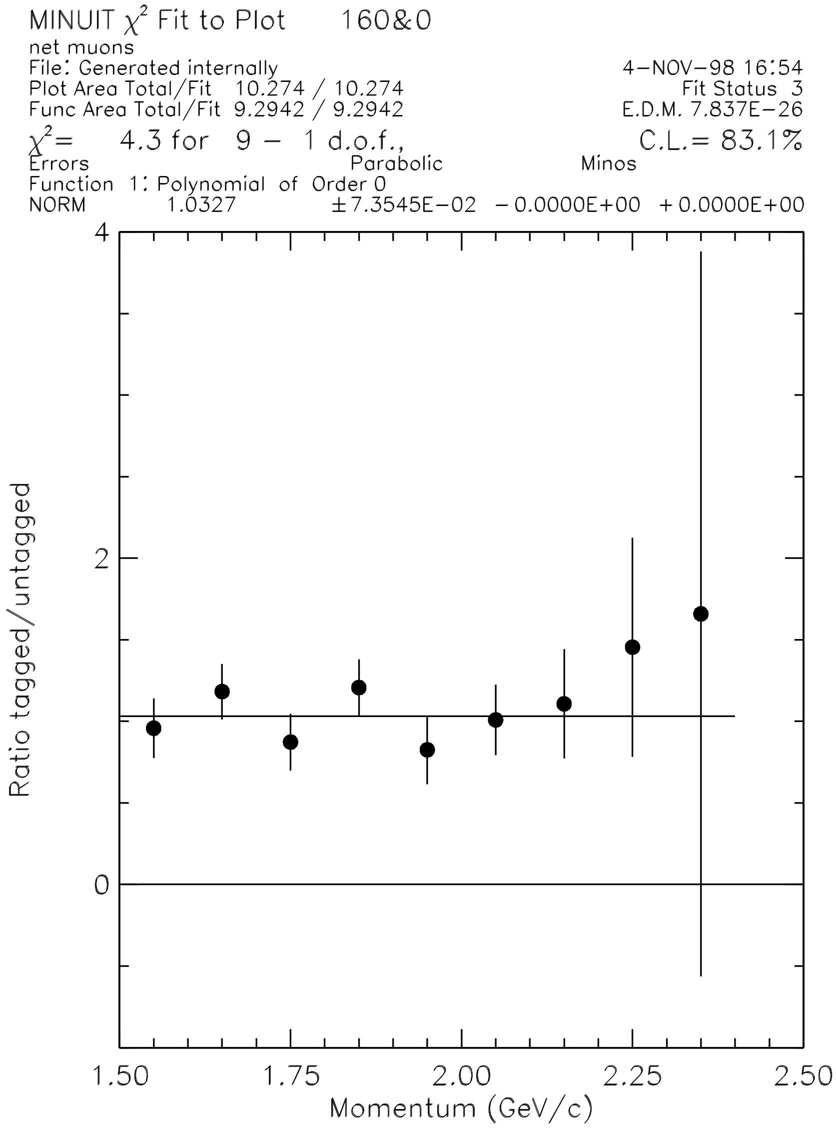

Figure 4.15: The lepton spectrum bin-by-bin comparison for single lepton inclusive measurement and this partial reconstruction method for muon momentum between 1.5-2.5 GeV/c

Table 4.3: Systematic Errors on R

Source	$\sigma_{sys}/value(\%)$	$\delta R/R$ (%)
Fake electron	50	0.1
Fake muon	25	0.2
Ψ contribution	30	0.3
primary spectrum	isgw**[18]	0.3
secondary spectrum		2.3
Event/tag selection	1.7	1.7
Background estimate	1.0	1.0
$(b \to u)/(b \to c)$	21	–
other leptons	see text	1.7
Total		3.5%

subtraction of the Ψ contributions, fake rates, and spectral shapes for fitting to find the secondary contribution.

All the systematic errors are tabulated in Table 4.3. The overall systematic error on R is found to be 3.5%.

4.11.1 Primary Leptons

The principal source for primary lepton shape is the product of ACCMM model [17]. We use primary lepton shape from ISGW** , a sum of exclusive modes using function derived from ISGW model[18], fixing D^*/D ratio at 2.3 and adjusting the D^{**} portion to 21% to fit our tagged inclusive lepton spectrum, as shown in Fig 4.16. The choice of 21% D^{**}, as opposed to model prediction 11%, is based on the best fit result of previous CLEO analysis [48], [46]. We also shifted the primary lepton function up and down 50 MeV/c to check the result. To be conservative, we take the biggest deviation from the central value as our systematic error. It was found that the model uncertainty on primary lepton introduced 0.3% deviation from central value of R.

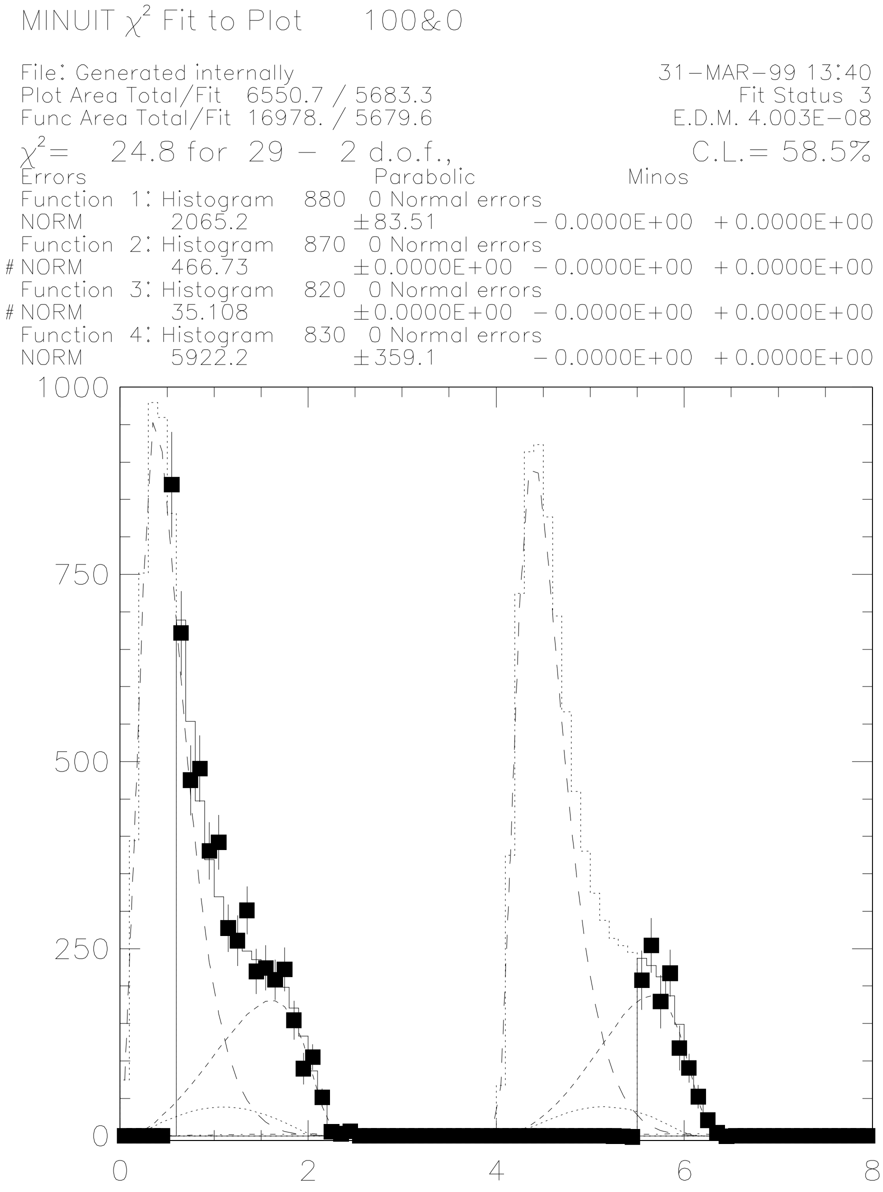

Figure 4.16: B decay lepton spectrum for simultaneous fit using ISGW** model. The electron is located from 0-4 GeV/c and muon is at 4-8 GeV/c.

4.11.2 Secondary Lepton

We used the secondary lepton spectrum generated by the following procedure, as done by previous CLEO analysis [78]. The lepton spectrum from the DELCO measurement[54] was boosted into B meson lab frame to give the secondary lepton shape different from models to estimate the uncertainty of the secondary lepton spectrum in our fit. An analytic function was used by CLEO to refit the DELCO measured $D \to X\ell\nu$ leptonic spectrum[54]. The boost factor is obtained from the inclusive D momentum spectrum measured by CLEO-I.5[77]. CLEO used a skewing function to multiply the D^0 and D^+ momentum spectrum to make the boosting harder or softer. Third change is CLEO also varied up and down the ratio of D^+ and D^0 according to the CLEO measured D^+ and D^0 production ratio in B decay[77]. We vary the uncertainties from the three sources up and down individually to get a series of secondaty lepton spectra. We fit using those secondary spectrua to evaluate the systematic error. We found the uncertainty of the secondary lepton spectrum introduces 2.3% systematic error in our value R.

4.11.3 Lepton from $B \to X\psi$ Decay

$B \to XJ/\Psi, J/\Psi \to \ell^+\ell^-$ introduces leptons from J/Ψ in our additional lepton spectrum. Though this comprises a tiny portion of our additional lepton spectrum, we still need to study its efficiency carefully because it has different spectrum shape from both the primary and the secondary leptons.

The J/Ψ lepton spectrum lies in the range $1.2 - 1.7$ GeV/c, where the primary leptons are dominating. To understand the impact of this contribution, we varied the portion of leptons from J/Ψ decay to see the result in our primary lepton spectrum. To be conservative, we moved it up and down by 30%, similarly with previous CLEO inclusive lepton

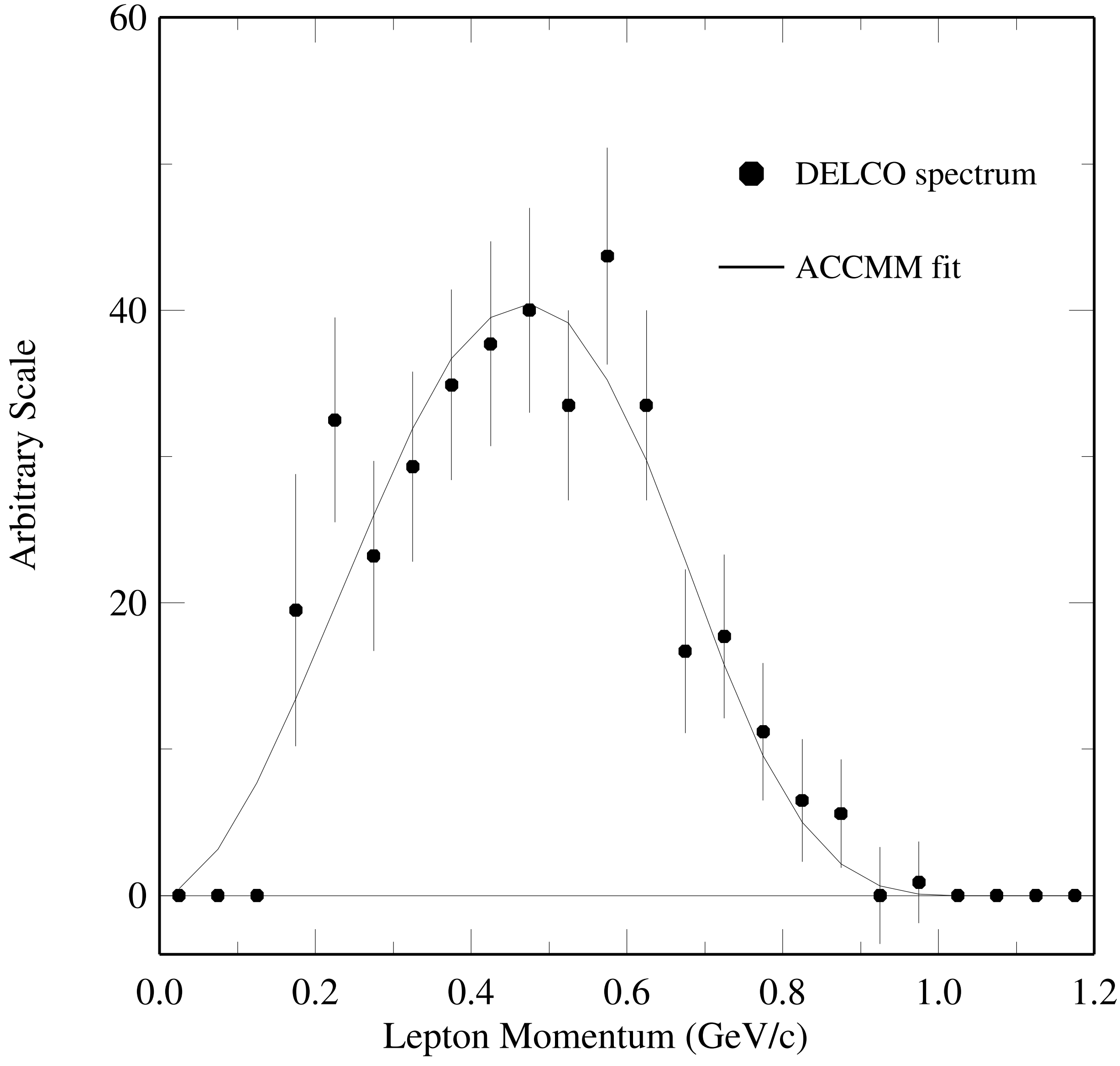

Figure 4.17: The ACCMM fit to DELCO Charm lepton spectrum

analysis[46]. This uncertainty contains the uncertainties of international radiation of Ψ and the contributions from Ψ'. The result is found to be insensitive to J/Ψ lepton spectrum. We found the uncertainity on R to be 0.3%.

4.11.4 Fake Second Lepton

The effect of the fake lepton subtraction from our reconstructed inclusive lepton spectrum can be influential in our lepton spectrum fit. This subtraction can alter our additional lepton spectrum shape thus changing the normalization for both primary and secondary leptons in the fit. We varied electron and muon fake rate bin by bin up and down for 50% and 25% respectively to study the sensitivity. The uncertainty on fake rate comes from the difference between the fake rate study of $\Upsilon(4S)$ and $\Upsilon(1S)$[46]

We found the fit to our lepton spectra is insensitive to the uncertainties of the fake rate, which introduces a tiny 0.1% and 0.2% shift for fake electrons and muons respectively. This is not too surprising since the distribution of fake leptons above lepton momentum 1.5 GeV/c is very tiny, where the lepton from primary decay saturates the spectra and ultimately determines the normalization of the fit through our simultaneous fitting procedure.

4.11.5 Leptons from Other Sources

There are small numbers of leptons coming from sources other than primary, secondary and J/Ψ decay. Leptons could be from D_s, τ, Λ_c, π^0 dalitz decay and from the process of converted photons. Our fit has approximated the spectra of all secondary leptons in the tagged spectra by those from D decay only. To estimate the uncertainty from this sources and from the fact that there may be small differences in shape between tagged and inclusive sample due to tag selection itself, we repeat the analysis after subtracting an estimated contributions of secondaries from sources other than D decay. We generate the spectrum shape of secondary leptons from sources other than D. We then combine this "other lepton" shape along with our primary and secondary lepton shape to fit our data. The portion corresponds to "other lepton" as the result of the fit will then be subtracted from our lepton spectrum at range 1.5-2.5 GeV/c. We vary it up and down according to the statistical fluctuation of the fit to estimate its systematic error on R. We found the shift to be 1.7% of R.

4.11.6 Systematic for Tag Only Events

There are uncertainties which apply only to the tagged but not to the inclusive measurement, including effects due to event selection, angular cuts and tagging efficiency difference. As was discussed in previous section, these contribute a total of 1.7%.

4.12 Spectrum Comparison Calculation

4.12.1 Estimation of Charged B Contamination

The N_{tag} has contributions not only from $\bar{B}^0 \to D^{*+}\ell^-\bar{\nu}_\ell$, but also from $B \to D^{**}(D^*\pi)\ell\bar{\nu}$. Since D^{**} can decay to $D^*\pi$, the $\pi^\pm$ from D^* and the lepton can form a right sign tag pair with missing mass square value near our signal region. Since both neutral and charged B can decay into $D^{**}/(D^*\pi)\ell\bar{\nu}$, we have $B^\pm$ contamination in our tag sample.

The charged B meson experiences D^{**} resonance decay:

$$B^- \to D^{**0}\ell^-\bar{\nu}_\ell, D^{**0} \to D^{*+}\pi^- \tag{4.9}$$

$$B^- \to D^{**0}\ell^-\bar{\nu}_\ell, D^{**0} \to D^{*0}\pi^0 \tag{4.10}$$

If we look at neutral B meson experiencing similar D^{**} resonance decay, we have:

$$\bar{B}^0 \to D^{**+}\ell^-\bar{\nu}_\ell, D^{**+} \to D^{*+}\pi^0 \tag{4.11}$$

$$\bar{B}^0 \to D^{**+}\ell^-\bar{\nu}_\ell, D^{**+} \to D^{*0}\pi^+ \tag{4.12}$$

We can see the $B \to D^{**}\ell\bar{\nu}$ components in our tag have sources from both charged and neutral B meson. The composition of $B \to D^{**}\ell\bar{\nu}$ from charged to neutral B meson is estimated by comparing the two decay width, (1.9) and (1.11). Using isospin symmetry, the ratio of the two decay width becomes the production ratio of π^- to π^0 in $D^{**} \to D^*\pi$ decay. We obtain the ratio of charged to neutral B decay width in $B \to D^{**}\ell\bar{\nu}$ to be 2:1 correspondingly. A similar argument can be held for non-resonance decay, $B \to D^*\pi\ell\bar{\nu}_\ell$

There was an exclusive analysis of $B \to D^{*+}\ell^-\bar{\nu}$ done with CLEO-I data [51]. That analysis calculated the M_ν^2 of the decay $B \to D^{*+}\ell^-\bar{\nu}$ where they reconstruct the D^0 and find the $D^* \to D^0\pi$ signal through the mass difference between D^* and D^0. They have estimated the contribution of $B \to D^{**+}/D^{*+}\pi\ell^-\bar{\nu}$ in the signal by combining the shape the shape of $B \to D^{**}/D^*\pi\ell\bar{\nu}$ with a Gaussian signal shape to fit their yield in $\widetilde{M_\nu^2}$ signal region. They found the overall contributions from the resonance as well as the non-resonance in $B \to D^*\ell\bar{\nu}_\ell$ to comprise about 0.17 ± 0.10 times the contribution from $\bar{B}^0 \to D^{*+}\ell^-\bar{\nu}_\ell$. This makes our peak tag have fraction about 0.14 ± 0.08 coming from resonance or non-resonance decay:[48]

$$\boxed{f^{**} = 0.14 \pm 0.08}$$

We also use a measurement from ALEPH, $Br(B \to D^{*-}\pi^+\ell^+\nu X) = (1.25\pm0.16\pm0.12)\%$ [68], and Monte Carlo simulation to obtain an independent value, $f^{**} = 0.10 \pm 0.02$, which is in agreement with the value measured by CLEO-I above Here we use the CLEO-I value because it is more directly obtained, and our evaluation of b_0, b_+ and f_{00} are insensitive to it.

With $f^{**} = 0.14 \pm 0.08$, the charged B content in our tag peak area is then calculated as: $2\alpha f^{**}/(1+2\alpha) = 9.6 \pm 5.6\%$ using isospin symmetry we mentioned earlier. The α in the formula is defined as:

$$\alpha \equiv f_{+-}b_+/f_{00}b_0 \tag{4.13}$$

where f_{+-} and f_{00} corresponds to the production fraction of charged and neutral B in $\Upsilon(4S)$ decay. b_+ and b_0 refers to the semileptonic branching fraction of charged and neutral B meson respectively.

4.13 Calculation and Result

$$\begin{aligned}
b_{incl} &= f_{00}b_0 + f_{-+}b_+ = f_{00}b_0 \times (1 + \frac{f_{+-}b_+}{f_{00}b_0}) \\
&= f_{00}b_0(1+\alpha) \\
b_{tag} &= f_{0,tag}b_0 + f_{+,tag}b_+ \\
&= b_0(1 - f_{+,tag}) + f_{+,tag}\frac{b_+}{b_0} = b_0(1 + f_{+,tag}[\frac{b_+}{b_0} - 1]) = b_0(1 + f_{+,tag}[\beta - 1]) \\
&= b_0(1 + f_{+,tag}\delta\beta)
\end{aligned}$$

where $\alpha \equiv f_{+-}b_+/f_{00}b_0$, $\beta \equiv \frac{b_+}{b_0}$, $\delta\beta \equiv \beta - 1$, $f_{0,tag}$ and $f_{+,tag}$ corresponds to the fraction of neutral and charged B candidates in our tag sample.

The calculation of b_0 and b_+ follows:

$$\begin{aligned} b_0 &= \frac{b_{tag}}{1+f_{+,tag}\delta\beta} = \frac{R \times b_{incl}}{1+f_{+,tag}\delta\beta} \\ b_+ &= \beta b_0 = (\frac{R \times b_{incl}}{1+f_{+,tag}\delta\beta})(1+\delta\beta) \end{aligned}$$

where $R \equiv b_{tag}/b_{incl}$

From the definition of R, we can obtain f_{00} as follows:

$$\begin{aligned} R &\equiv \frac{b_{tag}}{b_{incl}} = \frac{b_0(1+f_{+,tag}\delta\beta)}{f_{00}b_0(1+\alpha)} \\ \rightarrow f_{00} &= \frac{1+f_{+,tag}\delta\beta}{R(1+\alpha)} \end{aligned}$$

From the definition of α and β, we can also get f_{00}:

$$f_{00} = \frac{f_{+-}b_+}{\alpha b_0} = \frac{1+\delta\beta}{\alpha+1+\delta\beta} \tag{4.14}$$

Thus we can obtain:

$$(1+\delta R)(1+\alpha)(1+\delta\beta) = (1+f_{+,tag}\delta\beta)(1+\alpha+\delta\beta) \tag{4.15}$$

Because $f_{+,tag}$, $\delta\beta$ and $\delta R \equiv R-1$ are expected to be small, < 0.1, we can discard the term proportional to second order of $\delta\beta$, $f_{+,tag}(\delta\beta)^2$, to obtain a linear equation in $\delta\beta$:

$$\delta\beta = \frac{\delta R(1+\alpha)}{(1+\alpha)(f_{+,tag}-\delta R)-\alpha} \tag{4.16}$$

where $\delta\beta \equiv \beta - 1$,

There are two CLEO measurements for α value using isospin symmetry in B^- and B^0 decay: ($\alpha \equiv f_{+-}b_+/f_{00}b_0$)

$$\alpha = \frac{Br(\Upsilon(4S) \to B^+B^-, B^- \to \bar{D^{*0}}\ell^+\bar{\nu_\ell})}{Br(\Upsilon(4S) \to B^0\bar{B^0}, B^0 \to \bar{D^{*-}}\ell^+\bar{\nu_\ell})} = 1.14 \pm 0.14 \pm 0.13 \tag{4.17}$$

see [52]

$$\alpha = \frac{Br(\Upsilon(4S) \to B^+B^-, B^+ \to \psi K^{(*)+})}{Br(\Upsilon(4S) \to B^0\bar{B^0}, B^0 \to \psi K^{(*)+})} = 1.15 \pm 0.17 \pm 0.06 \tag{4.18}$$

see [53]

The weighted error average of the two α is 1.15 ± 0.13. The $f_{+,tag}$ has been evaluated in previous section. Combining altogether, we can calculate $\beta \equiv b_+/b_0$, and through α, we can calculate f_{+-}/f_{00}.

We can obtain $\beta = b_+/b_0$ through our measurement $R = 1.023 \pm 0.046 \pm 0.036$, $f^{**} = 0.14 \pm 0.08$ and $\alpha = 1.15 \pm 0.13$:

$$\beta = 0.950^{+0.117+0.091}_{-0.080-0.068} \tag{4.19}$$

Since $\bar{B}^0$ and B^- form an isospin doublet, their semileptonic decay width should be equal. The β is the lifetime ratio of charged to neutral B meson.

$$\begin{aligned}\frac{\tau_+}{\tau_0} &= \frac{\Gamma_{B^0}}{\Gamma_{B^-}} = \frac{\Gamma_{B^0}}{\Gamma_{B^0 \to X\ell\nu}} \times \frac{\Gamma_{B^- \to X\ell\nu}}{\Gamma_{B^-}} \\ &= \frac{b_+}{b_0}\end{aligned}$$

We can also calculate the fractional production of neutral to charged B meson in $\Upsilon(4S)$ decay: f_{+-}/f_{00}. Based on CLEO analysis on α and our measured b_+/b_0, we can calculate f_{+-}/f_{00} as follows:

$$\frac{f_{+-}}{f_{00}} = \frac{\alpha}{(\frac{b_+}{b_0})} \tag{4.20}$$

We obtain:

$$f_{+-}/f_{00} = 1.21 \pm 0.12 \pm 0.17 \tag{4.21}$$

We could also obtain the semileptonic branching fraction for neutral and charged B meson decay, b_0, b_+ respectively from our measured value R, and previous CLEO measurement on averaged inclusive B semileptonic branching fraction, b_{incl}. By taking $b_{incl} = (10.49 \pm 0.46)\%$ [46], R and β as we measured and calculated above, we obtain:

$$b_0 = (10.78 \pm 0.60 \pm 0.69)\% \tag{4.22}$$

$$b_+ = (10.25 \pm 0.57 \pm 0.65)\% \tag{4.23}$$

Chapter 5

Measurement of $B^0 - \bar{B}^0$ Mixing

5.1 Introduction

In this chapter, we measure the $B - \bar{B}$ mixing parameter χ_d, the probability that a B^0 meson decays as its anti-particle, $\bar{B}^0$, or vice versa:

$$\chi_d = \frac{N(B^0 \to \bar{B}^0)}{N(B^0 \to B^0) + N(B^0 \to \bar{B}^0)} \tag{5.1}$$

The measurement of mixing parameter χ_d is an important input to calculate the mass difference between the two CP eigenstate neutral B meson. The relation of χ_d with respect to mass difference between the two neutral B mesons, ΔM, and their averaged lifetime, Γ, is shown as follows:

$$\chi_d = \frac{(\Delta M/\Gamma)^2}{2((\Delta M/\Gamma)^2 + 1)} \tag{5.2}$$

ARGUS [55] and CLEO-II [49] independently measured mixing parameter χ_d by using di-lepton event. One hard lepton with momentum greater than 1.4 GeV/c is used to tag the flavor of a B meson. The charge of the second lepton, if it is a primary lepton from the other B meson, should carry opposite sign with respect to the tag lepton, or carry the same sign if the other B mixes. Lepton pairs of same sign divided by all pairs gives χ_d, as follows:

$$\chi_d = \frac{1}{(1-\Lambda)} \frac{N(\ell^\pm \ell^\pm)}{N(\ell^\pm \ell^\pm) + N(\ell^\pm \ell^\mp)} \tag{5.3}$$

The Λ accounts for the component of charged B in the data:

$$\Lambda = \frac{f_{+-} b_+^2}{f_{+-} b_+^2 + f_{00} b_0^2} \tag{5.4}$$

where the f_{+-} and f_{00} refer to the fraction of charged and neutral B meson in $\Upsilon(4S)$ events. The b_+ and b_0 correspond to the semileptonic branching fraction of B^- and $\bar{B}^0$ respectively.

The method does not distinguish B^+ from B^0, making the uncertainty on composition of B^- the biggest systematic error. The systematic error on Λ dominates the measurement.

Later CLEO[48] published another measurement based on method similar to our analysis. A hard lepton and a soft pion were used to obtain *partial reconstruction* of $\bar{B}^0 \to D^{*+} \ell^- \nu$, $D^{*+} \to D^0 \pi^+$ to identify B^0 meson. Then a search is made for additional leptons in the tagged event. With the charge correlation of this additional lepton and the tag, they are able to obtain the mixed signal when additional lepton has the same charge as the tag, or unmixed event when additional lepton and tag lepton has opposite charges.

5.2 Motivation

Previous CLEO measurement on χ_d using partial reconstruction method relies on a very complicated method to extract the mixing parameter. With the amount of B meson events we have, we can implement this measurement in a way that is less complicated and still reduce the systematic error. Besides, it is already five years after the most recent measurement of χ_d has been reported and much progress in B physics has been made since then, we felt to revisit this measurement is worth while.

5.3 Analysis Overview

This analysis is the extension of B^0 semileptonic branching ratio measurement in previous chapter. We use **partial reconstruction** to tag $\bar{B}^0$ and search for any additional leptons in the same event, then to construct the additional lepton momentum spectrum accordingly. The method of *partial reconstruction* and additional lepton momentum spectrum reconstruction has been described in detail in chapter 4.

One major modification needs to be made here. To measure χ_d, we need to separate the additional lepton according to the sign of its charge with respect to the charge of the tag lepton. We construct four additional lepton momentum spectra in our χ_d measurement; for each species of additional lepton (electron or muon), we also separate if the additional leptons carry the same charge as tagged lepton, *like sign lepton spectra*, and from the additional leptons carrying opposite charges; *unlike sign lepton spectra*. After reconstructing the four additional lepton spectra, theoretical function was used to estimate the primary portions to obtain the *like sign pair* entries $N(\ell^{\pm}_{add}, \ell^{\pm}_{tag})$, and the *unlike sign pair* entries $N(\ell^{\pm}_{add}, \ell^{\mp}_{tag})$. After the necessary correction for $N(\ell^{\pm}_{add}, \ell^{\pm}_{tag})$ and $N(\ell^{\pm}_{add}, \ell^{\mp}_{tag})$, we can obtain the mixing parameter χ_d.

5.4 Data and Event Cut

We use $3.1 fb^{-1}$ on-resonance and $1.6 fb^{-1}$ off-resonance for data, as well as 19 million generic $B\bar{B}$ Monte Carlo events.

The event cuts are the same as for semileptonic analysis except we adopt an improved ghost track killer TRKMNG[35], TRKMAN New Generation, in place of the older ghost track eliminator, TRKMAN.

5.5 Second Lepton Spectra Recreation

The procedure to construct the second lepton spectrum is very similar to that employed in the B^0 semileptonic branching fraction analysis. In addition to separating the additional lepton according to the charge relative to the tag lepton, we also subtract the leptons from π^0 dalitz decay and photon conversion before the correction of lepton detection efficiency was made on the raw additional lepton spectra. Unlike in our semileptonic branching fraction analysis, we do not subtract the $B \to J/\Psi \to \ell^+\ell^-$ in our spectrum, but use its lepton shape from generic $B\bar{B}$ Monte Carlo along with lepton shape from primary, secondary decay and other sources to fit the spectrum.

The collections of $\tilde{M}_\nu^2$ plots for like sign lepton pair can be found in Figure 5.1, Figure 5.2 and Figure 5.3. The unlike sign lepton pair can be found in Figure 5.4, Figure 5.5 and Figure 5.6. The table of like sign and unlike sign lepton spectrum before we subtract the π^0 dalitz decay and photon conversion leptons are tabulated in Table 5.1 for like sign pair, and in Table 5.2 for unlike sign pair.

After we reconstruct our additional lepton spectra, we fit the spectra with lepton shapes from primary, secondary, J/Ψ, D_s, Λ_c, τ and $b \to \bar{c} \to \ell^-$ altogether to estimate the primary

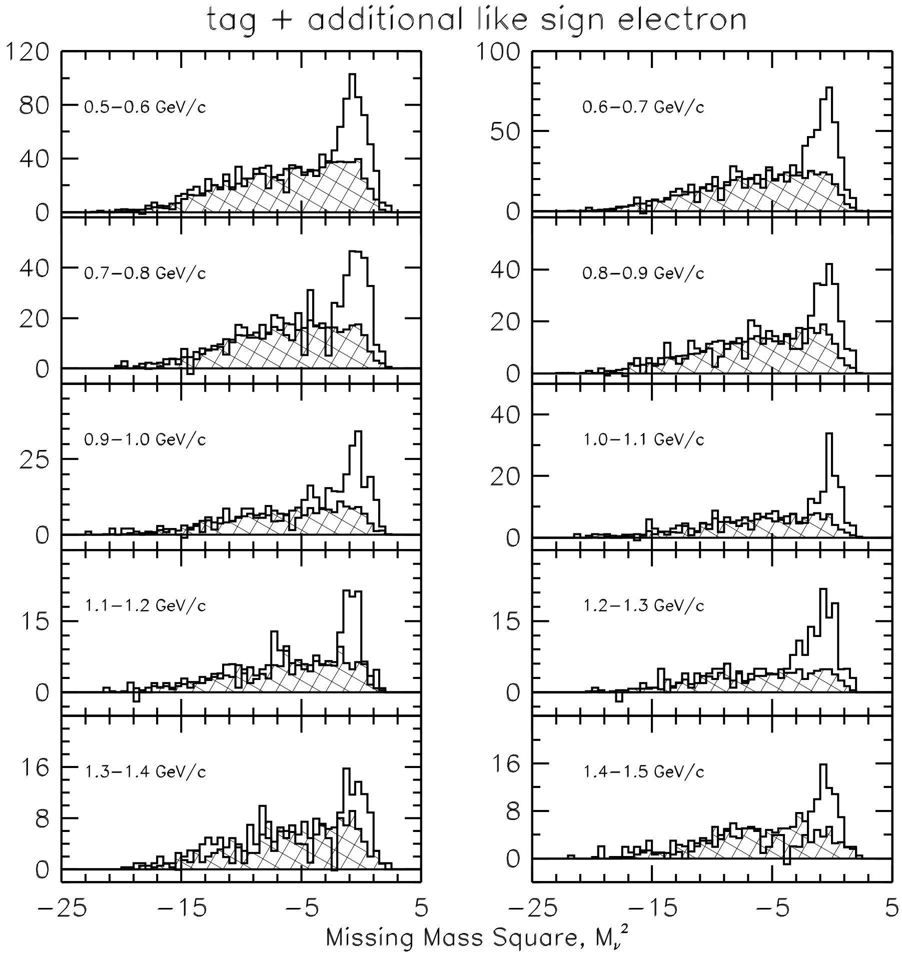

Figure 5.1: The bin-by-bin $\tilde{M}^2$ distribution of additional "like sign" electron 0.5-1.5 GeV/c, continuum and fake candidates have been subtracted, dotted line is the combinatoric background simulated by Monte Carlo

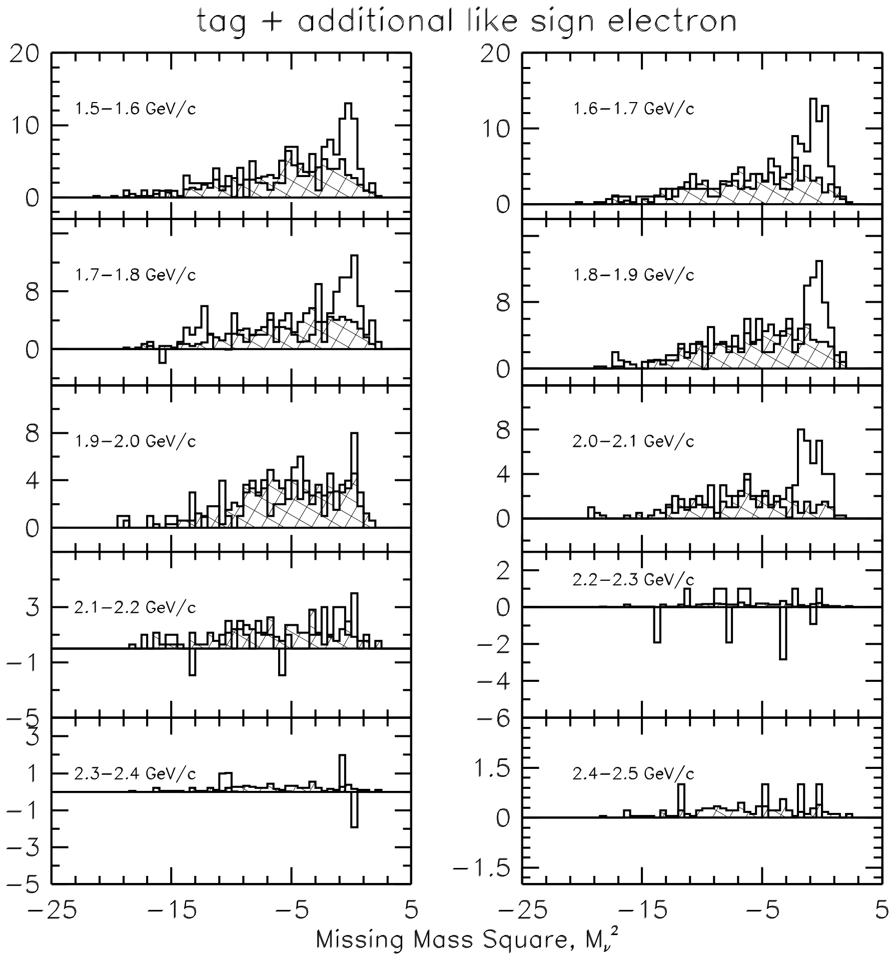

Figure 5.2: The bin-by-bin $\tilde{M}^2$ distribution of second "like sign" electron from 1.5-2.5 GeV/c,continuum and fake candidates have been subtracted, dotted line is the combinatoric background simulated by Monte Carlo

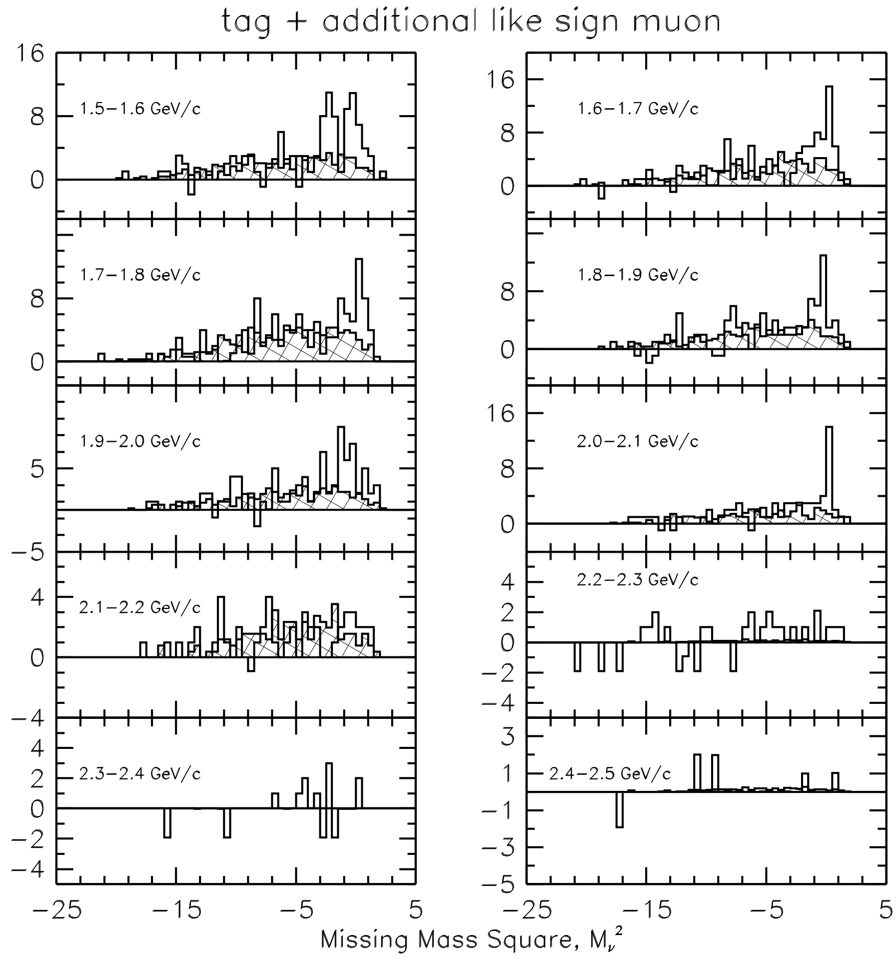

Figure 5.3: The bin-by-bin $\tilde{M}^2$ of second "like sign" μ from 1.5-2.5 GeV/c,continuum and fake candidates have been subtracted, dotted line is the combinatoric background simulated by Monte Carlo

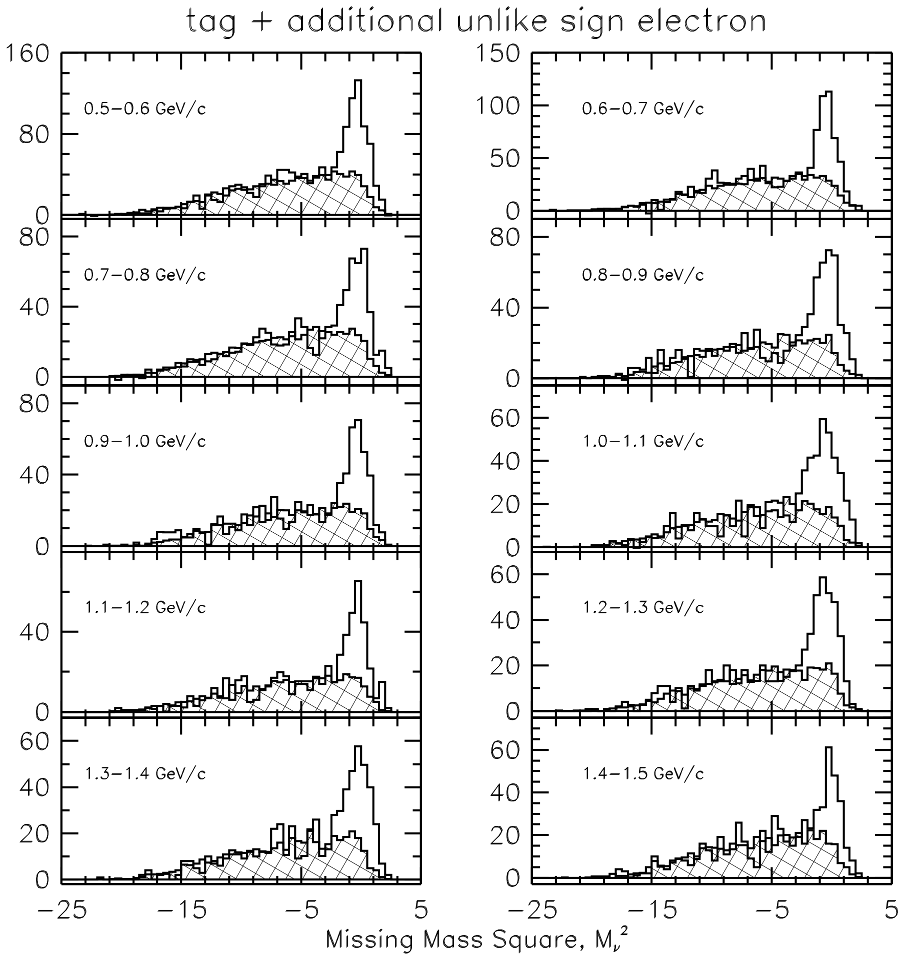

Figure 5.4: The bin-by-bin $\tilde{M}^2$ distribution of second "unlike sign" electron from 0.5-1.5 GeV/c,continuum and fake candidates have been subtracted, dotted line is the combinatoric background simulated by Monte Carlo

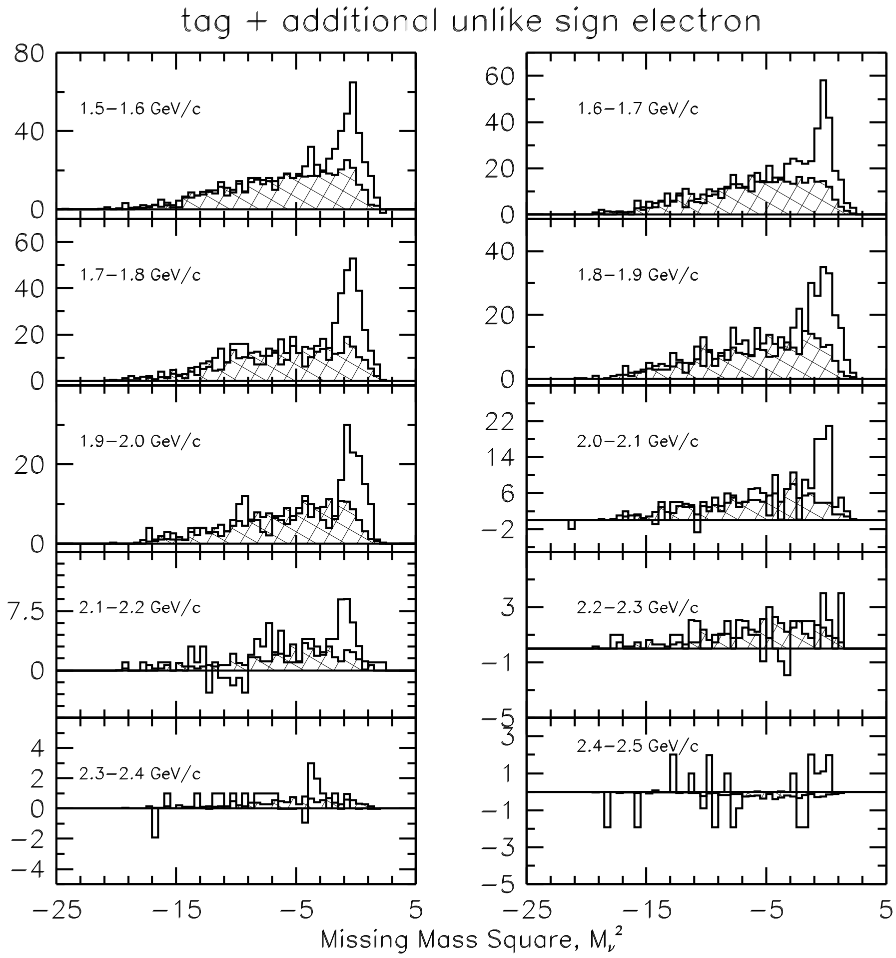

Figure 5.5: The bin-by-bin $\tilde{M}^2$ distribution of second "unlike sign" electron from 1.5-2.5 GeV/c,continuum and fake candidates have been subtracted, dotted line is the combinatoric background simulated by Monte Carlo

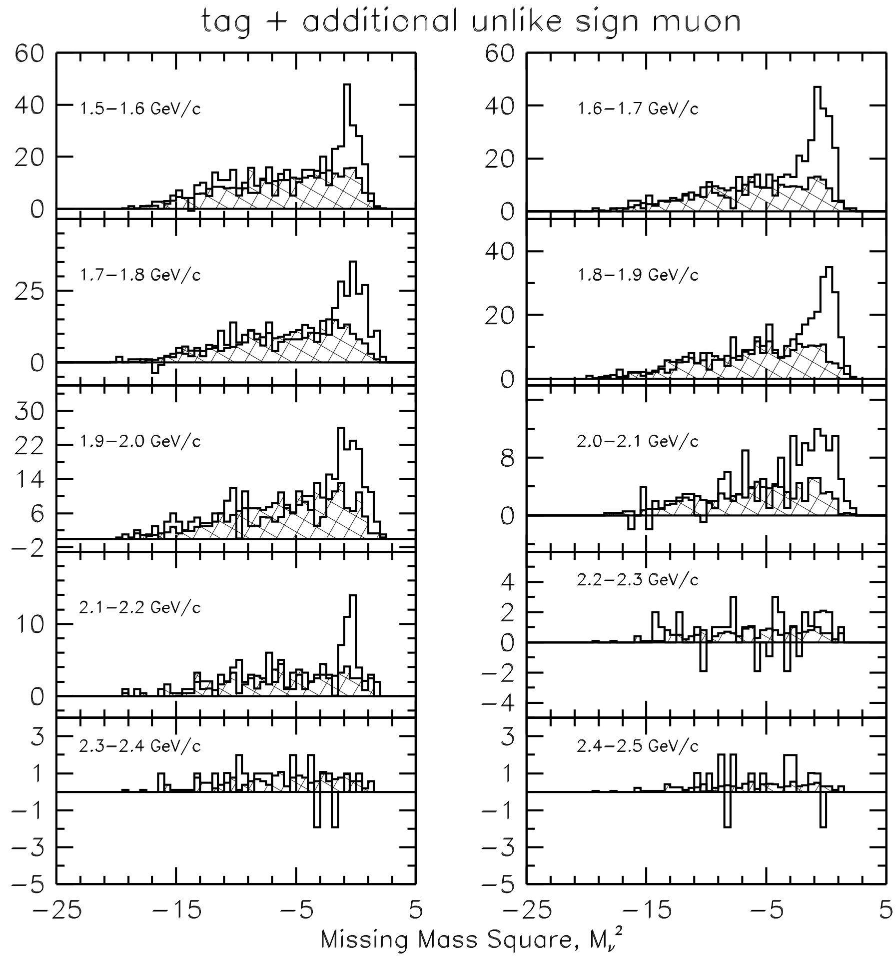

Figure 5.6: The bin-by-bin $\tilde{M}^2$ distribution of second "unlike sign" μ from 1.5-2.5 GeV/c,continuum and fake candidates have been subtracted, dotted line is the combinatoric background simulated by Monte Carlo

entries. The primary and secondary lepton normalization are allowed to float freely, with J/Ψ, D_s, Λ_c, τ and $b \to \bar{c} \to \ell^-$ lepton absolutely normalized to the primary portions. The normalization factor of leptons from J/Ψ, D_s, Λ_c, τ and $b \to \bar{c} \to \ell^-$ was derived from the 98 PDG value. Their shape was taken with the most updated generic CLEO $B\bar{B}$ Monte Carlo.

The fit to our additional lepton spectrum was shown in Figure 5.7 and Figure 5.8 for like sign and unlike sign lepton momentum distribution respectively. We have like sign pair = 562.37 ± 55.68, unlike sign pair = 2763.96 ± 105.30.

5.6 Calculation of χ_d

The ratio of like sign to all sign lepton pair, denoted as χ_{tag}, needs to be adjusted to obtain χ_d. As we noted in previous chapter, the charged B meson pair B^+B^- could enter our signal tag through $B \to (D^{**}/D^*\pi)X\ell\bar{\nu}_\ell$ decay to contaminate our mixing measurement. We need to estimate the portion of B^+B^- contribution in the tag with care.

The χ_{tag} can be written as follows:

$$\chi_{tag} = \frac{N(\ell^\pm_{add}, \ell^\pm_{tag})}{N(\ell^\pm_{add}, \ell^\pm_{tag}) + N(\ell^\pm_{add}, \ell^\mp_{tag})} = \frac{N(\ell^\pm_{add}, \ell^\pm_{tag})/N(tag)}{N(\ell^\pm\ell^\pm + \ell^\pm\ell^\mp)/N(tag)} \tag{5.5}$$

Since the $N(\ell^\pm_{add}, \ell^\pm_{tag})$ is the like sign pair where the addiitonal leptons are from primary decay, it can only come from the mixed B^0. The ratio of $N(\ell^\pm_{add}, \ell^\pm_{tag})/N(tag)$ thus can be written as:

$$N(\ell^\pm_{add}, \ell^\pm_{tag})/N(tag) = \chi_d b_0 f_{0,tag} \tag{5.6}$$

Where $f_{0,tag}$ is the fraction of tag that are from B^0 decay. The b_0 corresponds to the B^0

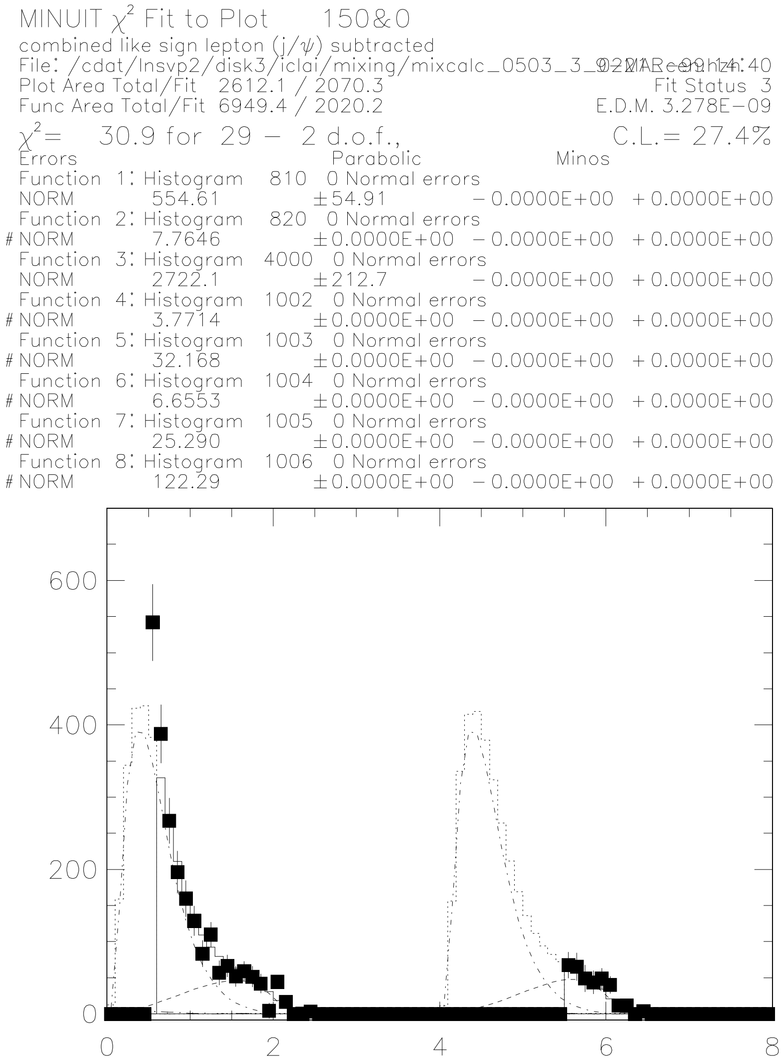

Figure 5.7: The second lepton spectrum for second lepton has the same charge sign as the tag lepton. The ACCMM model is used for the simultaneous fit of electron (0-4 GeV/c) and muon (4-8 GeV/c)

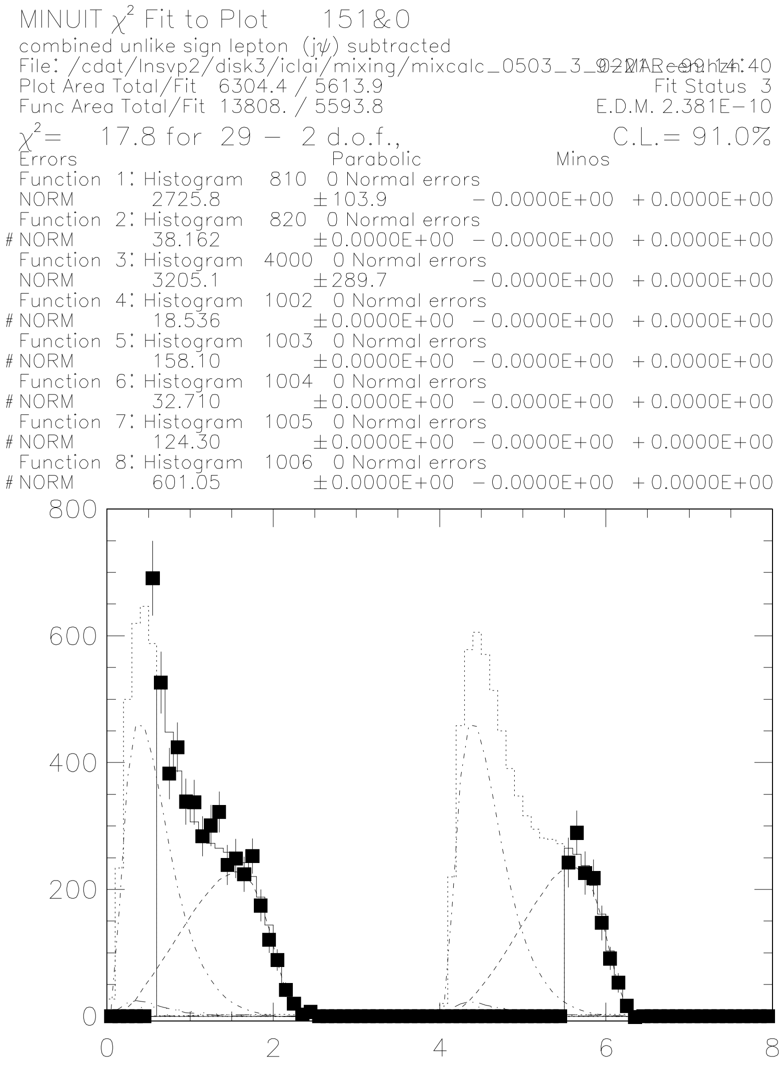

Figure 5.8: The second lepton spectrum for second lepton has the opposite charge sign as the tag lepton. The ACCMM model is used for the simultaneous fit of electron (0-4 GeV/c) and muon (4-8 GeV/c)

semileptonic branching fraction.

The denominator, $N(\ell^\pm\ell^\pm + \ell^\pm\ell^\mp)/N(tag)$, can be written as:

$$N(\ell^\pm\ell^\pm + \ell^\pm\ell^\mp)/N(tag) = f_{0,tag}b_0 + f_{+,tag}b_+ \tag{5.7}$$

The denominator is essentially the semileptonic branching fraction of our tagged event, b_{tag}, the quantity we measured in previous chapter. The $f_{0,tag}$ and $f_{+,tag}$ are the fraction of neutral and charged B in our tag. The b_+ and b_0 are the charged and neutral B semileptonic branching ratio respectively.

From the two information, we can write χ_{tag} as follows:

$$\chi_{tag} = \frac{\chi_d b_0 f_{0,tag}}{f_{0,tag}b_0 + f_{+,tag}b_+} \tag{5.8}$$

We define $\alpha \equiv \frac{f_{+-}b_+}{f_{00}b_0}$, where f_{+-} and f_{00} corresponds to the production fraction of B^+B^- and $B^0\bar{B}^0$ in $\Upsilon(4S)$. As from discussion in chapter 4 on $f_{+,tag}$, we can write $f_{+,tag} = 2\alpha f^{**}/(1+2\alpha)$ and $f_{0,tag} = 1 - f_{+,tag}$. We thus obtain χ_d in terms of α, f^{**} and b_+/b_0:

$$\chi_d = \chi_{d,tag}(1 + (\frac{f^{**}(\frac{2\alpha}{1+2\alpha})}{1 - f^{**}(\frac{2\alpha}{1+2\alpha})})(\frac{\tau_+}{\tau_0})) \tag{5.9}$$

where f^{**} is the fraction of $B \to (D^{**}/D^*\pi)\ell\nu$ in our tagged $\tilde{M}_\nu^2$ signal region, and $\tau_+/\tau_0 = b_+/b_0$ through the isospin symmetry of B semileptonic decay.

We estimate f^{**} as follows. From Monte Carlo we found out the ratio of the entries of $(B^-, B^0) \to (D^{**}/D^*\pi)\ell\nu$ to $B^0 \to D^*\ell\nu$ in our tag signal region is about 15.9%. We scale this number by taking the ratio of Br$(B \to D^{**}\ell\nu)$ [66] vs. its respective number at Monte Carlo, and divided by the ratio of Br$(B \to D^*\ell\nu)$ (from PDG) with its respective number in Monte Carlo:

$$
\begin{aligned}
N(D^{**}/D^*)_{new} &= N(D^{**}/D^*)_{old} * (\frac{Br(B \to D^{**})}{Br(B \to D^*)})_{new}/(\frac{Br(B \to D^{**})}{Br(B \to D^*)})_{old} \\
f^{**}_{new} &= N(D^{**}/D^*)_{new}/[1 + N(D^{**}/D^*)_{new}]
\end{aligned}
$$

The inputs to rescale the f^{**} are:

- $(Br(B \to D^{**}\ell\nu) * Br(D^{**} \to D^{*\pm}))_{old} = 2.357\%$. This is estimated from Prelib Monte Carlo.
- $Br(B \to D^*\ell\nu)_{old} = 5.44\%$ obtained from prelib Monte Carlo
- $(Br(B \to D^{**}\ell\nu) * Br(D^{**} \to D^{*\pm}))_{new} = (1.88 \pm 0.30 \pm 0.23)\%$. Obtained from 1997 LEP measurement[66]
- $Br(B \to D^*\ell\nu)_{new} = (4.60 \pm 0.27)\%$. obtained from 98 PDG
- $(D^{**}/D^*)_{old} = 0.159$ obtained from analyzing the $\widetilde{M_\nu^2}$ in prelib Monta Carlo sample

We found the value of $f^{**} = 0.150 \pm 0.025$, This number is consistent with $f^{**} = 0.14 \pm 0.08$ [48] which was derived by a CLEO-I.5 direct measurement[51].The small number of f^{**} has constrained the dependence on α and τ_+/τ_0 in this analysis, as can be seen from the above equation.

The dependence on α and τ_+/τ_0 at previous $\Upsilon(4S)$ $B - \bar{B}$ mixing analysis is expressed through the quantity Λ, which is the biggest systematic error on previous CLEO dilepton analysis on mixing as seen in equation 5.4:

$$
\begin{aligned}
\Lambda &= \frac{f_{+-}b_+^2}{f_{+-}b_+^2 + f_{00}b_0^2} \\
&= \frac{\alpha\tau_+/\tau_0}{1 + \alpha\tau_+/\tau_0}
\end{aligned}
$$

Comparing with previous CLEO measurement, this analysis has a weaker dependence on those two quantities for a small f^{**}. We will discuss about it more.

5.7 Result

Our fit with primary lepton shape extracted by ACCMM model gives us 562.37 ± 55.68 for like sign entries and 2763.96 ± 105.30 for unlike sign pair sample. The χ_{tag}, ratio of like sign pair divided by like sign plus unlike sign pair is 0.169 ± 0.017

We take $\alpha = 1.15 \pm 0.13$, cited from the weighted error average of the two CLEO measurements on α as we did in previous chapter. The $\tau_+/\tau_0 = 1.04 \pm 0.04$, is the value taken from the most recent PDG-98. $f^{**} istakentobe 0.150 \pm 0.025$, which was not available in previous analysis for B^0 and B^+ semileptonic branching fraction then. We then calculate the χ_d using Equation 5.9. We obtain:

$$\boxed{\chi_d = 0.189 \pm 0.019}$$

where the error is the statistical error only.

5.8 Systematic Error

The χ_d systematic error associated with the lepton detection efficiency canceled when we take the ratio of entries of like sign to all sign leptons. The sources of systematic error comes from the uncertainties on primary and secondary lepton shape in our fit, the uncertainties of leptons from π^0 dalitz decay and the photon conversions, the fake leptons and leptons from other sources like J/Ψ, D_s, Λ_c, τ, upper vertex charm $b \to \bar{c} \to \ell^-$. We also have dependence on f^{**}, α and $\tau(+)/\tau(0)$.

5.8.1 Primary Lepton Spectrum

Because different model predicts different primary lepton shape, the result of the fit will be different. We use the primary lepton shape derived from ISGW** model to estimate the differences. We replace the primary lepton shape predicted by ACCMM model in our fit by using shape predicted by ISGW** model. We found the deviation on χ_d due to this model difference to be 2.2%

5.8.2 Secondary Lepton Spectrum

We take the charm semileptonic lepton spectrum from the 1985 MARK-III analysis [65] and boosted it with the most recent CLEO measured inclusive D meson momentum distribution [74] as the function for our secondary lepton spectrum in our fit. The uncertainties of the secondary spectrum comes from the uncertainty of this D inclusive momentum spectrum. The systematic error on χ_d from the uncertainties of this secondary spectrum, as taken from the biggest variation in our fit, is evaluated as 1.3%.

5.8.3 Fake Lepton

Fake "additional leptons" in the like sign and unlike sign pair must be subtracted. Like in previous semileptonic branching fraction analysis, we varied the fake rate for electron and muon up and down 50% and 25% up and down respectively to evaluate the difference caused from the uncertainty of fake rate. We found out the effect from the fake leptons has been as small as 0.4%(0.1%) for fake electrons (muons).

5.8.4 Leptons from $\pi^0 \to e^+e^-\gamma$ and Photon Conversion

Only electrons are created from π^0 dalitz decay and photon conversion, when photons generated in B decay chain interact with detector material to produce leptons. Electrons generated from conversion are soft, mostly below 500 Mev/c. The electron- positron pair created from π^0 dalitz decay travel almost parallel to each other. The combination of di-lepton opening angle cut and the momentum requirement throw out 99.8% of electrons from $\pi^0 \to e^+e^-\gamma$ process.

We use Monte Carlo to estimate the portion of π^0 dalitz decay and photon conversion electrons and the momentum spectrum. We normalize their contribution to the primary leptons portions, then subtract it from our raw lepton spectrum. Since our cut for additional lepton is identical to the previous CLEO study on the inclusive lepton analysis [46], the normalization factor of π^0 dalitz and photon conversion was directly taken from that analysis. We vary their contributions according to the uncertainty of the normalization and found our fit is not sensitive to this uncertainty. This is not too surprising because we fit our electron and muon simultaneously, with the presence of high momentum muon (from 1.5-2.5 GeV/c), it has severely constrained the impact of the variation of leptons below 800 Mev/c. The χ_d systematic error due to the uncertainty of electrons from $\pi^0 \to e^+e^-\gamma$ is about 0.1%, and 0.1% for electrons from photon conversion.

5.8.5 Other Leptons

The "other leptons" are leptons from other sources like J/Ψ, D_s, Λ_c, τ decays and from upper vertex charm mesons, $b \to \bar{c} \to \ell$. Except the J/Ψ and τ lepton, leptons from D_s, Λ_c and upper vextex charm ($b \to \bar{c} \to \ell^-$, W boson decayed to charm in external spectator decay) all have momentum spectrum similar to the secondary leptons. We use generic Monte Carlo to obtain the respective lepton momentum shape for each source and fix their normalization to the primary lepton portion in our fit to get the central χ_d value. The systematic error for the "other leptons" comes from the uncertainty of their normalization scale. We vary it up and down according to the statistical error of this normalization to see how our χ_d has changed. The biggest deviation is taken to be our systematic error.

In Figure 5.9(Figure 5.10) are the momentum spectrum of electron(muon) from: J/Ψ, D_s, Λ_c, τ and upper vertex charm, $b \to \bar{c} \to \ell^-$, in comparison with the leptons from secondary decay, $b \to c \to \ell^+$.

J/Ψ leptons

Leptons from $B \to J/\Psi \to \ell^+\ell^-$ need to be subtracted. The product branching fraction $\mathrm{Br}(B \to J/\Psi X) * \mathrm{Br}(J/\Psi \to \ell^+\ell^-)$ is $(0.068 \pm 0.004)\%$, about $(0.68 \pm 0.04)\%$ with respect to the primary lepton aboundance.

The lepton spectrum of J/Ψ was taken from a newly updated generator level $B\bar{B}$ Monte Carlo. The uncertainty on the absolute branching fraction, $\mathrm{Br}(B \to XJ/\Psi)$* $\mathrm{Br}(J/\Psi \to \ell^+\ell^-)$ is the source of the systematic error. We normalize the contribution of J/Ψ leptons to the primary leptons in our fit, and varied the portion of this absolute normalization up and down accordingly. The biggest deviation from our central value is about 0.1%.

τ Leptons

Leptons from $B \to X\tau\bar{\nu_\tau}, \tau \to \nu_\tau \ell \bar{\nu_\ell}$ have a slightly different momentum spectrum from D_s and Λ_c leptons. Its relative abundance is also very small. From PDG we found $\mathrm{Br}(\bar{B} \to X\tau\bar{\nu_\tau}) = (2.75 \pm 0.3 \pm 0.37)\%$ and $\mathrm{Br}(\tau \to \nu_\tau \ell \bar{\nu_\ell}) = (17.37 \pm 0.09)\%$. The product branching fraction: $\mathrm{Br}(\bar{B} \to X\tau\bar{\nu_\tau}) * \mathrm{Br}(\tau \to \nu_\tau \ell \bar{\nu_\ell}) = (0.48 \pm 0.05)\%$. We estimate its effect on mixing

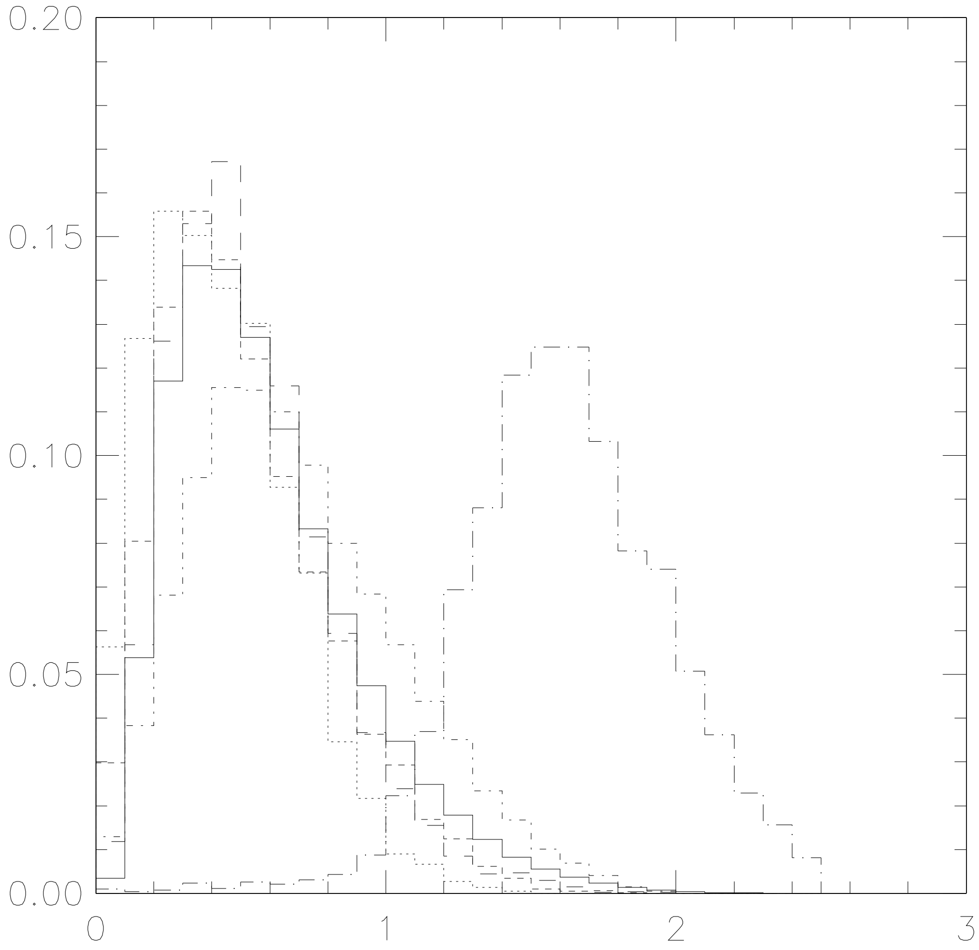

Figure 5.9: The electron spectrum shape from J/Ψ (long-dash dot), D_s(short dash), Λ_c(dot), τ(short-dash dot), and $b \to \bar{c} \to \ell^-$ (long-dash) in comparison with the secondary shape (hisotgram).

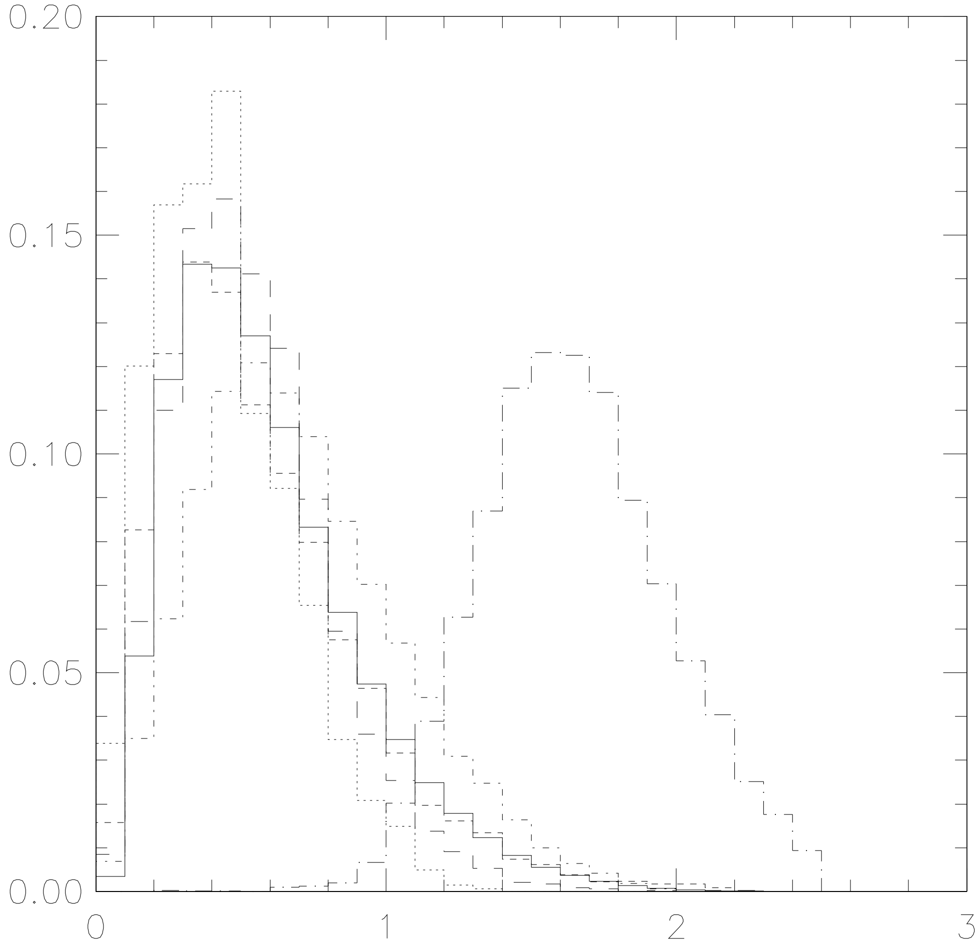

Figure 5.10: The muon shape from J/Ψ (long-dash dot), D_s(short dash), Λ_c(dot), τ(short-dash dot), and $b \rightarrow \bar{c} \rightarrow \ell^-$ (long-dash) in comparison with the secondary shape (hisotgram).

by employing the same procedure as above and found its impact is also small, about 0.1% deviation from central χ_d value.

Leptons from D_s Decay

The leptons from D_s decay have a spectrum that is similar to that of our secondary leptons. Because D_s can be produced from upper or lower vertex, its decaying lepton will contaminate our lepton charge sign correlation since upper and lower vertex leptons have opposite charge sign but a similar momentum spectrum. We have to estimate it with care.

We calculate the product branching fraction of $\mathrm{Br}(\bar{B} \to \bar{D}_s \to \ell^-)$ to be $(0.63 \pm 0.13)\%$ from PDG, about 5.8% of primary leptons. Our lepton momentum threshold cut suppresses 88.5% and 99.6% of electrons and muons from D_s decay respectively. We estimate the effect of the remainder on mixing by taking the lepton spectrum shape from Monte Carlo and varying it according to the uncertainty in its absolute normalization to our primary leptons in the fit. It is found that its effect is mostly absorbed by our secondary function and its impact has no sensitivity to our fit. We found its deviation is as small as 0.002%. For being conservative, we assign it to be 0.1% here.

Λ_c Leptons

Leptons from Λ_c decay also has a similar spectrum to that of secondary leptons. Its contribution is also far less than D_s leptons in the additional lepton population. From PDG, we compute the product branching fraction of $\mathrm{Br}(\bar{B} \to \Lambda_c \to X\ell\nu)$ to be $(0.13 \pm 0.04)\%$. Using identical method with D_s leptons contribution, we found it generated small effect, about 0.1% deviation on our χ_d measurement.

$b \to \bar{c} \to \ell^-$

Leptons from $B \to \bar{D} \to \ell^-$ has the same charge as the primary leptons, but with much smaller momentum because the small phase space for upper vertex charm production does not boost its daughter lepton as much. The branching fraction for the upper vertex charm production in B decay, $B \to \bar{D}^0 + D^- X$, is found to be 0.079 ± 0.022 [72]. This number is combined with the semileptonic branching fraction of D^0 and D^+ respectively to arrive the branching fraction of $B \to \bar{D} \to \ell$. We take the equal mixture of D^0 to D^- in upper vertex charm production.

Since there is no measurement of $B \to \bar{D}^* X$, we use Br($B \to \bar{D}^*$) from Monte Carlo and Br($D^* \to D\pi$ from 1998 PDG value to arrive the value of Br($B \to \bar{D}^* \to \bar{D}$. We multiply the $D^0(D^+)$ semileptonic branching fraction with this number to obtain the branching fraction of $B \to \bar{D} \to \ell$ when $\bar{D}$ meson comes from the decay of upper vertex vector D^*.

We combine the two results to obtain the branching fraction of lepton from upper vertex charm in B decay to obtain $(2.39 \pm 0.40)\%$. We use the identical procedure as we did for leptons from D_s mentioned earlier and found our χ_d value is insensitive to the uncertainty associated with upper vertex charm leptons. The systematic associated with this uncertainty is found to be about 0.1%. This is not surprising because the lepton spectrum of upper vertex charm has similar shape with our secondary leptons'. Our simutaneous fit procedure also has constrained the impact of the uncertainty of upper vertex charm.

5.8.6 Uncertainty on f^{**}

We have estimated f^{**} to be 0.150 ± 0.025. We varied f^{**} up and down 1 σ to estimate the systematic error on χ_d, and found it to be about 2.0%.

5.8.7 Systematic Error from α and τ_+/τ_0

The error on α and τ_+/τ_0 was used to vary the value of α and τ_+/τ_0 up and down respectively to estimate the associated systematic error on χ_d. We found the systematic error due to α is about 0.5% and on τ_+/τ_0 is about 0.4%. As explained earlier, the small χ_d dependence on α and τ_+/τ_0 can be traced to the small value of f^{**} in our conversion from $\chi_{d,tag}$ to χ_d in Equation 5.9

5.8.8 Summary of Systematic Error

We summarize the systematic error in Table 5.3

5.9 Summary

We measure the $\bar{B}^0 - B^0$ mixing parameter χ_d through partial reconstruction of $\bar{B}^0 \to D^{*+}\ell^-\bar{\nu}$ and the inclusive lepton momentum spectrum which is enriched in $\bar{B}^0$. This measurement makes no assumption of the fraction of B^+B^- pair in $\Upsilon(4S)$ decays. We measure χ_d:

$$\chi_d = 0.189 \pm 0.019(stat) \pm 0.005(sys) \pm 0.001(\alpha, \frac{\tau_+}{\tau_0})$$

The last error is the error on α and τ_+/τ_0.

In our previous analysis, we have obtained the ratio of charged vs. neutral B meson semileptonic branching fraction, shown in equation 4.19:

$$\frac{b_+}{b_0} = 0.952^{+0.117+0.060}_{-0.081-0.051}$$

if we replace the $\tau_+/\tau_0 = 1.04 \pm 0.04$ with the b_+/b_0 value shown above, the χ_d value is $0.187 \pm 0.019 \pm 0.005^{+0.003}_{-0.002}$. The last error is from the uncertainity of the b_+/b_0 where we take the squared root of the sum of squared statistical and systematic error.

We listed the measured χ_d between two CLEO analysis with similar method *partial reconstruction* on the same dataset in Table 5.4. We found the two agree well with each other.

We also compare this result with previous CLEO measurement and scale the difference of α and τ_+/τ_0. we our result has the lowest dependence on the different value of α and τ_+/τ_0, as shown in Table 5.5.

From averaged LEP measurement of $x_d = 0.734 \pm 0.035$ [67], the χ_d can be calculated as follows:

$$\begin{aligned} \chi_d &= \frac{(\frac{\Delta M}{\Gamma})^2}{(2 * (1 + (\frac{\Delta M}{\Gamma})^2))} = \frac{x_d^2}{2 * (1 + x_d^2)} \\ &= 0.175 \pm 0.011(\sigma(x_d)) \end{aligned}$$

Our result has weak dependence on α and τ_+/τ_0 , the biggest systematic error in dilepton analysis. The method of second lepton spectrum construction also reduces much systematic error associated with previous CLEO analysis based on similar method of partial reconstruction[48].

Table 5.1: like sign lepton spectrum

(GeV/c) electrons	Data	MC	Data-MC	ϵ_{ID}	net event
0.5-0.6	502.5 ± 26.1	205.3 ± 13.0	297.2 ± 29.1	0.548	542.4 ± 53.2
0.6-0.7	354.7 ± 21.5	128.8 ± 9.7	225.9 ± 23.6	0.582	388.1 ± 40.5
0.7-0.8	247.4 ± 17.0	90.7 ± 7.4	156.6 ± 18.5	0.585	267.6 ± 31.7
0.8-0.9	205.6 ± 15.2	89.1 ± 8.2	116.5 ± 17.3	0.593	196.3 ± 29.1
0.9-1.0	147.2 ± 13.5	51.7 ± 6.5	95.5 ± 15.0	0.598	159.7 ± 25.1
1.0-1.1	117.5 ± 11.6	38.2 ± 5.0	79.3 ± 12.6	0.615	128.9 ± 20.5
1.1-1.2	89.3 ± 10.2	37.5 ± 5.3	51.8 ± 11.5	0.621	83.4 ± 18.5
1.2-1.3	94.5 ± 9.8	26.3 ± 4.4	68.2 ± 10.7	0.622	109.7 ± 17.2
1.3-1.4	75.5 ± 8.8	40.3 ± 6.0	35.2 ± 10.6	0.618	57.0 ± 17.2
1.4-1.5	67.3 ± 8.6	25.8 ± 4.4	41.5 ± 9.7	0.625	66.4 ± 15.4
1.5-1.6	55.6 ± 7.9	22.5 ± 4.6	33.1 ± 9.1	0.635	52.1 ± 14.3
1.6-1.7	59.7 ± 7.7	22.0 ± 4.1	37.7 ± 8.8	0.635	59.3 ± 13.8
1.7-1.8	58.8 ± 7.7	26.1 ± 5.0	32.7 ± 9.2	0.636	51.5 ± 14.5
1.8-1.9	51.8 ± 7.2	25.1 ± 4.6	26.7 ± 8.5	0.638	41.9 ± 13.4
1.9-2.0	24.0 ± 5.4	21.3 ± 4.4	2.7 ± 7.0	0.635	4.3 ± 11.1
2.0-2.1	34.9 ± 5.9	6.7 ± 1.9	28.2 ± 6.2	0.637	44.3 ± 9.7
2.1-2.2	13.0 ± 3.6	2.1 ± 1.1	10.8 ± 3.8	0.648	16.7 ± 5.8
2.2-2.3	0.1 ± 2.4	0.1 ± 0.4	0.0 ± 2.4	0.630	-0.1 ± 3.8
2.3-2.4	0.1 ± 2.4	0.0 ± 0.0	0.0 ± 2.4	0.619	0.0 ± 3.8
2.4-2.5	2.0 ± 1.4	0.0 ± 0.0	2.0 ± 1.4	0.615	3.2 ± 2.3
muons					
1.5-1.6	41.9 ± 6.6	14.2 ± 3.5	27.7 ± 7.5	0.409	67.6 ± 18.4
1.6-1.7	49.2 ± 7.9	18.9 ± 4.4	30.3 ± 9.0	0.463	65.4 ± 19.5
1.7-1.8	45.9 ± 8.0	22.1 ± 4.4	23.7 ± 9.1	0.483	49.2 ± 18.9
1.8-1.9	37.6 ± 7.1	15.7 ± 4.0	21.9 ± 8.1	0.503	43.5 ± 16.2
1.9-2.0	38.4 ± 6.7	13.4 ± 3.5	25.1 ± 7.5	0.513	48.8 ± 14.7
2.0-2.1	30.6 ± 5.6	9.4 ± 3.2	21.2 ± 6.4	0.528	40.2 ± 12.1
2.1-2.2	14.7 ± 3.9	8.4 ± 2.5	6.3 ± 4.6	0.540	11.7 ± 8.6
2.2-2.3	6.1 ± 4.2	0.1 ± 0.4	6.0 ± 4.2	0.529	11.3 ± 7.9
2.3-2.4	-0.1 ± 2.4	0.0 ± 0.1	-0.1 ± 2.4	0.540	-0.2 ± 4.4
2.4-2.5	1.8 ± 1.4	0.0 ± 0.0	1.8 ± 1.4	0.536	3.4 ± 2.6

Table 5.2: unlike sign lepton spectrum

(GeV/c) electrons	Data	MC	Data-MC	ϵ_{ID}	net event
0.5-0.6	598.9 ± 29.3	220.2 ± 13.7	378.7 ± 32.4	0.548	691.2 ± 59.1
0.6-0.7	483.6 ± 25.8	177.1 ± 11.7	306.5 ± 28.3	0.582	526.6 ± 48.6
0.7-0.8	364.7 ± 21.2	140.6 ± 10.6	224.2 ± 23.7	0.585	383.0 ± 40.5
0.8-0.9	368.8 ± 21.4	117.1 ± 9.3	251.7 ± 23.3	0.593	424.1 ± 39.3
0.9-1.0	325.7 ± 19.6	123.3 ± 9.8	202.4 ± 21.9	0.598	338.4 ± 36.6
1.0-1.1	309.0 ± 19.9	101.5 ± 8.7	207.5 ± 21.8	0.615	337.3 ± 35.4
1.1-1.2	271.7 ± 17.4	95.5 ± 8.9	176.3 ± 19.5	0.621	283.9 ± 31.5
1.2-1.3	292.9 ± 17.8	105.8 ± 9.2	187.1 ± 20.1	0.622	300.8 ± 32.2
1.3-1.4	295.9 ± 18.0	96.7 ± 8.5	199.2 ± 20.0	0.618	322.2 ± 32.3
1.4-1.5	256.9 ± 17.5	107.8 ± 9.1	149.2 ± 19.7	0.625	238.6 ± 31.6
1.5-1.6	268.9 ± 17.1	110.9 ± 9.4	158.0 ± 19.5	0.635	248.8 ± 30.7
1.6-1.7	224.2 ± 16.1	81.9 ± 7.7	142.2 ± 17.8	0.635	223.8 ± 28.0
1.7-1.8	244.8 ± 15.7	84.3 ± 8.0	160.5 ± 17.6	0.636	252.5 ± 27.7
1.8-1.9	183.0 ± 14.1	71.8 ± 7.7	111.3 ± 16.1	0.638	174.5 ± 25.2
1.9-2.0	124.0 ± 11.6	47.5 ± 6.1	76.5 ± 13.2	0.635	120.6 ± 20.7
2.0-2.1	83.1 ± 9.7	26.7 ± 4.8	56.4 ± 10.8	0.637	88.5 ± 17.0
2.1-2.2	34.2 ± 7.1	7.3 ± 2.3	26.9 ± 7.5	0.648	41.6 ± 11.6
2.2-2.3	14.0 ± 4.4	1.7 ± 0.6	12.3 ± 4.5	0.630	19.6 ± 7.1
2.3-2.4	1.9 ± 1.4	0.3 ± 0.2	1.7 ± 1.4	0.619	2.7 ± 2.3
2.4-2.5	4.2 ± 3.9	0.0 ± 0.0	4.1 ± 3.9	0.615	6.7 ± 6.4
muons					
1.5-1.6	177.3 ± 14.0	78.1 ± 7.9	99.2 ± 16.1	0.409	242.4 ± 39.3
1.6-1.7	196.5 ± 14.9	62.4 ± 6.9	134.1 ± 16.4	0.463	289.2 ± 35.4
1.7-1.8	177.1 ± 14.6	68.2 ± 7.5	108.9 ± 16.4	0.483	225.6 ± 34.0
1.8-1.9	166.4 ± 13.4	56.9 ± 6.4	109.6 ± 14.9	0.503	217.9 ± 29.6
1.9-2.0	131.9 ± 12.0	56.3 ± 7.3	75.5 ± 14.1	0.513	147.2 ± 27.4
2.0-2.1	69.3 ± 8.7	21.3 ± 4.0	48.0 ± 9.6	0.528	90.9 ± 18.2
2.1-2.2	42.8 ± 7.7	14.3 ± 3.0	28.5 ± 8.3	0.540	52.7 ± 15.4
2.2-2.3	9.8 ± 4.6	1.2 ± 0.6	8.6 ± 4.7	0.529	16.2 ± 8.8
2.3-2.4	-0.4 ± 2.4	0.4 ± 0.2	-0.7 ± 2.4	0.540	-1.4 ± 4.4
2.4-2.5	0.0 ± 2.4	0.0 ± 0.0	0.0 ± 2.4	0.536	0.0 ± 4.4

Table 5.3: Systematic error on χ_d

Source	$\sigma_{sys}/value(\%)$	$\delta(x_d)/x_d(\%)$
Fake electron	50%	0.4%
Fake muon	25%	0.1%
primary spectrum	isgw**	2.2%
secondary spectrum (andy's spectrum)		1.3%
γ conversion		0.1%
$\pi^0 \rightarrow e^+e^-$		0.1%
D_s		0.1%
Λ_c		0.1%
τ		0.1%
Ψ contribution		0.1%
$\bar{B} \rightarrow \bar{D} \rightarrow \ell^-$		0.1%
f^{**}	17%	2.0%
α	12.2%	0.5%
$\tau(+)/\tau(0)$	4%	0.4%
Net systematic error		3.3%

Table 5.4: comparison with previous CLEO χ_d measurement using partial reconstruction technique in the same dataset

Method	$f^{+-}/f^{00} = 1$ $\tau_+/\tau_0 = 1.00 \pm 0.14$	$f^{+-}/f^{00} = 1.13 \pm 0.14$ $\tau_+/\tau_0 = 1.04 \pm 0.04$
previous analysis	0.149 ± 0.023	0.155 ± 0.024
this analysis	0.151 ± 0.034	0.152 ± 0.034

Table 5.5: comparison with previous CLEO χ_d value

Method	$\alpha = 1.0 \pm 0.15$ $\tau(+)/\tau(0) = 1.0 \pm 0.14$	$\alpha = 1.15 \pm 0.13$ $\tau_+/\tau_0 = 1.04 \pm 0.04$
CLEO-93 d-lepton	$0.157 \pm 0.016 \pm 0.018^{+0.028}_{-0.021}$	$0.172 \pm 0.018 \pm 0.018^{+0.010}_{-0.011}$
CLEO-93	$0.149 \pm 0.023 \pm 0.019 \pm 0.010$	$0.155 \pm 0.024 \pm 0.019 \pm 0.004$
This analysis	$0.188 \pm 0.019 \pm 0.005 \pm 0.003$	$0.189 \pm 0.019 \pm 0.005 \pm 0.001$

Chapter 6

Conclusion

This thesis presents the measurements of $B^0 - \bar{B}^0$ mixing parameter χ_d and the semileptonic branching fraction of B^0 and B^+. The latter measurement was made possible by combining this measurement with the result of averaged B meson semileptonic branching fraction in other CLEO measurement.[46]. Assuming the isospin symmetry of neutral to charged B meson in semileptonic decay, the ratio of charged to neutral B semileptonic branching fraction can give us the result of charged to neutral B lifetime ratio.

6.1 Summary of $B^0\bar{B}^0$ mixing parameter χ_d

We measured χ_d through a B^0 enriched sample which has weak dependence on α, $f_{+-}b_+/(f_{+-}b_+ + f_{00}b_0)$, and b_+/b_0. Our result of χ_d is $0.189 \pm 0.018 \pm 0.006$. This result is consistent with the χ_d derived from LEP experiment, 0.175 ± 0.011.

We listed the χ_d measurements for comparison in Tab 6.1. As can be seen from the table, this result is consistent with other χ_d measurements. In comparison, this result presents the smallest systematic error.

Table 6.1: comparison with other measured χ_d value

	χ_d
This result	$0.189 \pm 0.019 \pm 0.006$
ARGUS(94)	$0.16 \pm 0.04 \pm 0.04$[80]
CLEO (93)	$0.149 \pm 0.023 \pm 0.022$[49]
ARGUS(92)	0.171 ± 0.048[55]
CLEO (89)	$0.158^{+0.052}_{-0.059}$ [81]

We can convert our χ_d into x_d through $\chi_d = \frac{x_d^2}{2(1+x_d^2)}$ and the x_d value is found to be $0.774 \pm 0.109 \pm 0.035$. This value is consistent with the averaged result of LEP, 0.734 ± 0.035.[67].

6.1.1 calculation of V_{td} vs. f_B

Taking the world averaged B^0 lifetime as 1.56 ± 0.04 ps from 98-PDG[76], we can calculate the mass difference of the two neutral B meson CP eigenstate, Δm_{B^0}, through our newly computed x_d. We obtain $\Delta m_{B^0} = 0.496 \pm 0.073$. The Equation 2.41 relates χ_d with $|V_{td}|^2$. The V_{td} value converted from χ_d has its biggest uncertainty from B meson decay constant f_B which ranges from 130 Mev to 230 Mev[92]. We obtained the the diagram of V_{td} vs. f_B at Fig 6.1. Value in that diagram uses the bag parameter $B_d = 1.4 \pm 0.1$, $\eta_{QCD} = 0.55$[90]. The top quark mass takes the value $m_{top} = 173.8 \pm 5.2$ GeV[91] and the lifetime of B^0 is $\tau_{B^0} = 1.56 \pm 0.04$ ps[76]. As shown at Fig 6.1, the uncertaint of V_{td} clearly reflects its sensitivity to the uncerttainty of f_B. The V_{td} value from the diagram is between 0.007-0.017, consistent with T. Browder and K. Honscheid's estimate $V_{td} = 0.0092 \pm 0.0003 \pm 0.0009$, where the first error is statistical error, the second error is due to top quark mass and the third error is due to $B_B^{1/2} f_B$ [92].

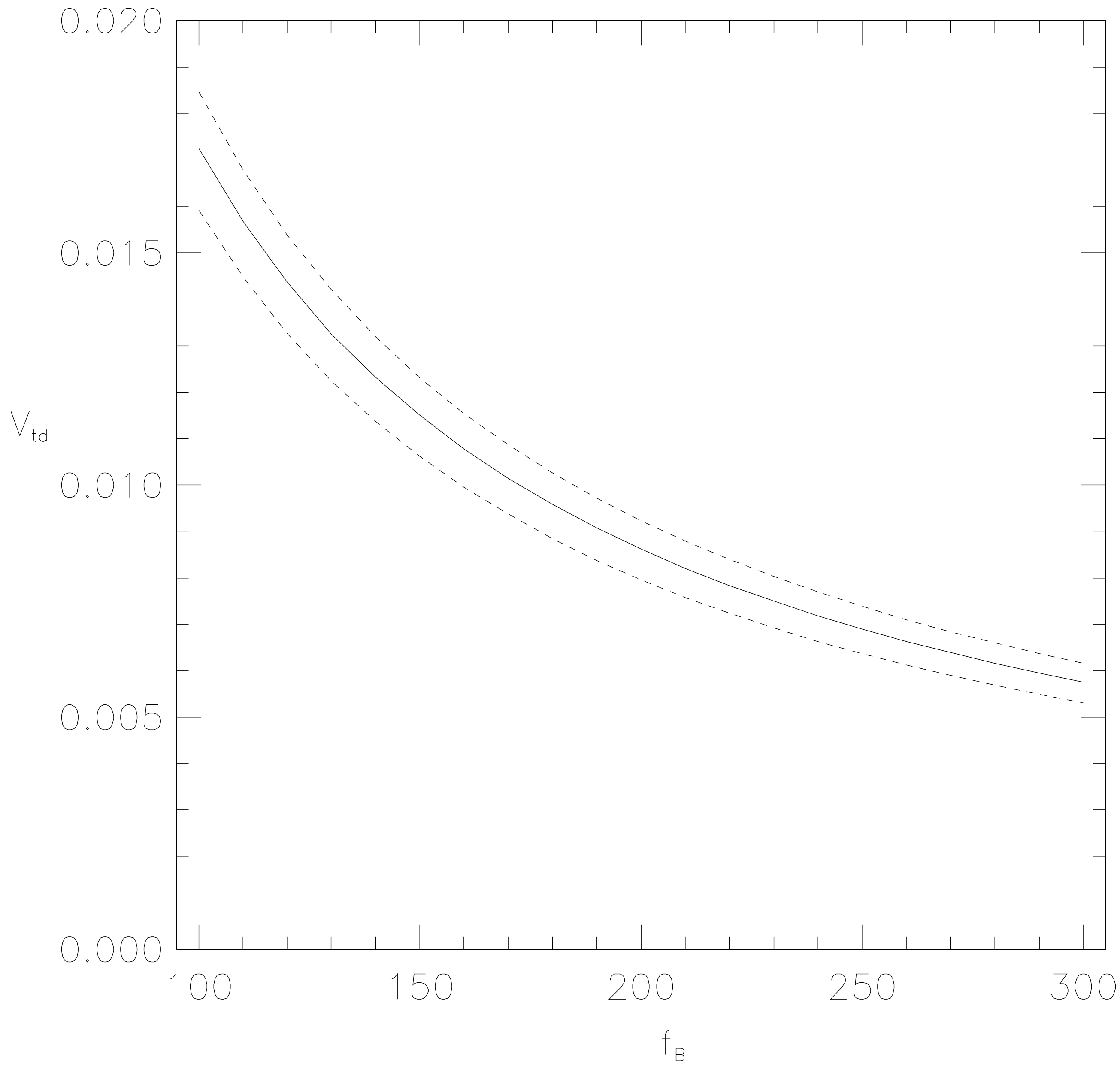

Figure 6.1: V_{td} as a function of f_B. We take top quark mass, $M_{top} = 173.8$ GeV, $\tau_{B^0} = 1.56$ ps and $\eta_{QCD} = 0.55$. The $\pm 1\sigma$ error bands are due to uncertainty on χ_d only.

Table 6.2: comparison with other $B \to X\ell\nu$ value

	$B^0 \to X\ell^-\bar{\nu}$
Our result	$(10.78 \pm 0.60 \pm 0.69)\%$
CLEO(94)	$(10.9 \pm 0.7 \pm 1.1)\%$[75]
ARGUS(94)	$(9.3 \pm 1.1 \pm 1.5)\%$[80]
	$B^- \to X\ell^-\bar{\nu}$
Our result	$(10.25 \pm 0.57 \pm 0.65)\%$
CLEO(94)	$(10.1 \pm 1.8 \pm 1.5)\%$[75]

6.2 Summary of B Meson Semileptonic branching Fraction

Our measurement of semileptonic branching fraction gives:

1. $b_0 = (10.78 \pm 0.60 \pm 0.69)\%$
2. $b_+ = (10.25 \pm 0.57 \pm 0.65)\%$
3. $\frac{b_+}{b_0} = 0.952^{+0.117+0.060}_{-0.081-0.051}$

Our value of $\mathrm{Br}(B^0 \to X\ell^-\bar{\nu})$ is consistent with previous CLEO published result, $(10.9 \pm 0.7 \pm 1.1)\%$ [75]. Our result of charged B semileptonic branching fraction is consistent with previous CLEO measurement, $(10.1 \pm 1.8 \pm 1.5)\%$[75], which was published in the same CLEO paper as the result of semileptonic branching fraction of neutral B meson. We listed different measurements on $B \to X\ell\nu$ for comparison in Tab 6.2.

Our measurement on the inclusive semileptonic branching fraction for neutral and charged B meson adds to the growing body of evidence that the discrepancy between experiment and theoretical prediction , which expects the minimum value should be no less than 12.5%, is

Table 6.3: Table of V_{cb}

Model	γ_c, ps^{-1}	V_{cb} from $B^0 \to X\ell\nu$	V_{cb} from $B^+ \to X\ell\nu$
ACCMM	40 ± 8	$0.039 \pm 0.002 \pm 0.005$	$0.039 \pm 0.002 \pm 0.006$
ISGW**	42 ± 8	$0.041 \pm 0.001 \pm 0.004$	$0.038 \pm 0.002 \pm 0.004$
Shifman	41.3 ± 4	$0.041 \pm 0.002 \pm 0.002$	$0.039 \pm 0.001 \pm 0.001$
Ball	43.2 ± 4.2	$0.040 \pm 0.002 \pm 0.002$	$0.038 \pm 0.002 \pm 0.002$

real. There are yet no consensus in physical community as the source of discrepancy and the issue remains a controversial one.

We can calculate the CKM matrix element V_{cb} from the value of B semileptonic branching ratio:

$$Br(b \to c\ell\nu) = \tau_B \gamma_c |V_{cb}|^2$$

The γ_c is the prediction from model. The value of V_{cb} from different model with our measured branching fraction is tabulated at Tab 6.3. For the calculation, we take $\tau_{B^0} = 1.56 \pm 0.04$ and $\tau_{B^+} = 1.65 \pm 0.04$ [76] and evaluate V_{cb} from four different model predictions: ACCMM[17], ISGW[18], Shifman*et.al*[87] and Ball *et.al*[88]. The first error is the experimental error and the second error comes from the theoretical uncertainty associated with each model. Our V_{cb} result is consistent with PDG-98 averaged value $V_{cb} = 0.0395 \pm 0.0017$.[89].

6.3 Summary of τ_+/τ_0

We tabulated the recent measurements on lifetime ratio of neutral to charged B meson in higher energy experiments as a comparison with our result in Tab 6.4.

Our result of $\frac{b_\pm}{b_0}$ also is compatible with previous CLEO result, $(0.93 \pm 0.18 \pm 0.12)$[75].

Table 6.4: τ_+/τ_0 measurement comparison

	τ_+/τ_0
Our result	$0.950^{+0.117+0.091}_{-0.080-0.068}$
CDF(98)	$1.06 \pm 0.07 \pm 0.02$[82]
SLD(97)	$1.01 \pm 0.07 \pm 0.06$[83]
CDF(96)	$1.01 \pm 0.11 \pm 0.02$[84]
ALEPH(96)	$0.98 \pm 0.08 \pm 0.03$[85]

We also compare our result with the world average of the direct measurement on $\tau_+/\tau_0 = 1.04 \pm 0.04$[76] and found no discrepancy.

Appendix A

Electroweak Radiation Correction

All our theoretical functions has been corrected for electroweak radiation before fitting to our lepton spectrum. It was described by Marciano and Atwood in [59]. The correction is made by multiplying the theoretical lepton spectrum with the electroweak radiation correction factor, $f_{EW}(E_\ell)$, as follows:

$$f_{EW}(E_\ell) = (\frac{E_{max} - E_\ell}{CE_\ell})^r \tag{A.1}$$

where, $r = \frac{2\alpha}{\pi}[ln(\frac{2E_\ell}{m_\ell}) - 1]$, and the m_ℓ and E_ℓ are the lepton mass and energy. C is related to the averaged and maximum energies of the lepton through:

$$C = (E_{max} - \bar{E}_\ell)/\bar{E}_\ell \tag{A.2}$$

Bibliography

[1] M. Kobayashi and T. Maskawa, Prog. Theor. Phys. **49**, 652 (1973)

[2] L. Wolfenstein, Phys. Rev. Lett. **51**,1945 (1983)

[3] Particle Data Group, C. Caso *et. al*, Review of Particle Properties, Euro. Phys. Journal. **C**, Vol. 3

[4] Schaad*et.al.* Phys. Lett. **B 160**, 188 (1985) (Mark II)

[5] D. Andrews *et.al* Phys. Rev. Lett. **44**, 1108 (1980) (CUSB)

[6] S. W. Herb *et.al*, Phys. Rev. Lett. **39**, 252 (1977)

[7] W. R. Innes *et.al.*, Phys. Rev. Lett. **39**, 1240 (1977)

[8] D. Andrew *et.al.* Phys. Rev. Lett. **45**, 219 (1980) (CLEO)

[9] G. Finocchiaro *et.al.* Phys. Rev. Lett. **45**, 222 (1980) (CUSB)

[10] M. L. Perl *et.al.*, Phys. Rev. Lett. **35**, 1489 (1975) (Mark)

[11] J. Burmester *et.al.*, Phys. Lett. **B 68**, 297, 301 (1977) (Pluto)

[12] N. Cabibbo abd N. Maiani, Phys. Lett **79B**, 109 (1978)

[13] M. Suzuki, Nucl. Phys. **145 B**, 420 (1978)

[14] C. Quigg and J. Rosner, Phys. Rev. **D 19**, 1532 (1979)

[15] G. Altarelli and L. Maiani, Phys. Lett. **52 B**, 351 (1974)

[16] M. K. Gaillard and B. W. Lee, Phys. Lett **33**, 108 (1974)

[17] G. Altarelli, N. Cabibbo, G. Corbo, L. Maiani and G. Martinelli, Nucl Phys **208 B**, 365 (1982)

[18] N. Isgur, D. Scora, B. Grinstein and M. Wise, Phys. Rev. **D 39**, 799, 1989

[19] A. Ali, Zeit. Phys. **C1**, 25 (1979)

[20] N. Cabibbo *et.al* Nucl. Phys. **B 155**, 93 (1979)

[21] N. Isgur and M. Wise, Phys. Lett. **B 232**,113 (1989); N. Isgur and M. Wise, Phys. Lett. **B 237**,527 (1990); E. Eichten and B. Hill, Phys. Lett. **B 234**,511 (1990); H. Georgi Phys. Lett **B 240**, 447 (1990)

[22] Cortes, J.L., X.Y.Pham, and A. Tounsi, Phys. Rev. **D. 25**, 188 (1982)

[23] Altarelli,G. and L. Mainai., Phys Lett **B. 52**, 351 (1974)

[24] M. Wirbel, B.Stech, M. Bauer, Z. Phys. **C. 29**, 637 (1985)

[25] J. G. Korner and G. A. Schuler, Z. Phys. **C. 38**, 511 (1989)

[26] M.Gell-Mann and A.Pais, *Phys. Rev.* **97**, 1387 (1955).

[27] E.E.Lande et al. *Phys. Rev.* **103**, 1901 (1956).

[28] H.Albrecht et al. (ARGUS) *Phys Lett.* **B192**, 245 (1987).

[29] H-Y, Cheng. *Phys. Rev.* **D. 26**, 143 (1982)

[30] A.J. Buras, W. Slominski, H. Steger, *Nucl. Phys.* **B. 245**, 369 (1984)

[31] J.S. Hagelin, *Nucl. Phys.* **B. 193**, 123 (1981)

[32] Y. Kubota *et al.* (CLEO), *Nucl. Instrum. Methods* **A 320**, 66 (1992).

[33] Jonathan L. Rosner in *B Decays*, 2nd edition, S. Stone, ed. (World Scientific 1994).

[34] I.I.Bigi, in *The Fermilab Meeting* **DPF. 92** C. Albright, P. Kasper, R. Raja, J. Yoh. eds. (World Scientific, Singapore, 1992), P.610

[35] S. Roberts *et.al.* CLEO internal notes. CBX 96-103

[36] V.L. Fitch, J.W. Cronin, J.H. Christensen, R. Turlay: Phys. Rev. Lett **13,138** (1964)

[37] H. Albrecht, *et.al.* Phys. Lett. **B, 249**, 359 (1990)

[38] K. Wachs, *et.al.* Z. Phys. **C, 42**, 33 (1989)

[39] C. Yanagisawa *et.al* Phys. Rev. Lett. **66**, 2436 (1989)

[40] S. Henderson *et.al.* Phys. Rev. **D, 45**, 2212 (1992)

[41] D. Buskulic *et.al.* Z. Phys. **C, 62**, 179 (1994)

[42] CERN Preprint PPE/95-08

[43] R. Akers. *et.al* Z. Phys. **C,60**, 199 (1993)

[44] H. Albrencht *et.al.* Phys. Lett. **B, 318**, 397 (1993)

[45] B. Barish *et.al* Phys. Rev. Lett. **76**, 1570 (1996)

[46] Roy Wang, Ph.D Thesis. University of Minnesota. (1994)

[47] H. Albrecht *et.al* DESY-92-029

[48] Mike. S. Sauliner, Ph.D thesis. Harvard University. (1995)

[49] J. Bartelt *et.al.* Phys. Rev. Lett. **71**, 1680 (1993)

[50] M. Athanas *et.al* Phys. Rev. Lett **73**, 3503 (1994)

[51] D. Bortoletto, *"Exclusive and Inclusive Semileptonic Decay of the B meson"*, Ph.D thesis, Syracuse University (1989)

[52] B. Barish *et.al.* (CLEO) Phys. Rev. **D, 51**, 1014 (1995)

[53] C.P. Jessop *et.al.* preprint CLEO 96-24, submitted to Phys. Rev. Lett

[54] W. Bacino *et.al.* (DELCO) Phys. Rev. Lett. **43**, 1073 (1979)

[55] H. Albrecht. *et.al,* (ARGUS) Z. Phys. **C.55,** 357 (1992)

[56] M. Artuso. *et.al.* (CLEO) Phys. Lett. **B 399**, 321 (1997)

[57] I. Bigi *et. al* Phys. Lett. **B 323**, 408 (1994)

[58] F. Abe *et. al* Phys. Rev. **D.50**, 2966 (1994)

[59] D. Atwood and W. Marciano, Phys. Rev. **D.41**, 1736 (1990)

[60] Neubert, M ., Phys Reports **245**, 259 (1994)

[61] D. Scora and N. Isgur, Phys. Rev. **D 52**, 2783 (1995)

[62] S. Henderson *et.al*, (CLEO) Phys, REv. **D 45**, 2212 (1992)
M.A. Worris, Ph.D Thesis, Cornell University (1991)

[63] M. Garcia-Sciveres, Ph.D. thesis, Cornell University, 1994 (unpublished).

[64] H. Schroder, $B\bar{B}$ Mixing, in **B Decays** S. Stone, 2nd ed. (World Scientific, 1994)

[65] R. M. Baltrusaitis *et.al.* Phys. Rev. Lett. **54**, 1976 (1985) MARK-III collaboration

[66] Buskulic *et. al* (ALEPH) Z. Phys. **C73**, 601 (1997)

[67] Particle Data Group, C. Caso *et. al*, Review of Particle Properties, Euro. Phys. Journal. **C**, Vol. 3, 557

[68] J. Richman, in: Proc. XXVIII Int'l Conf. on High Physics (Warsaw, Poland 1996) in press.

[69] M.S. Witherell, *The Physics of B and D Mesons* in St. Croix lectures see http://charm.physics.uscb.edu/papers/StCroix.ps

[70] M. Neubert, Int. J. Mod. Phys. **A 11**, 4173 (1996)

[71] T. Skwarnicki, CLEO internal notes. CSN 90-301 (1990)

[72] T. E. Coan *et.al,* (CLEO) Phys. Rev. Lett **80**, 1150 (1998)

[73] S.E.Schrenk, Ph.D Thesis, University of Minnesota (1994)

[74] L. Gibbons, *et.al* (CLEO) Phys. Rev. **D 56**, 3183 (1997)

[75] M. Athanas, *et.al* (CLEO) Phys. Rev. Lett, **73** 3503 (1994)

[76] Particle Data Group, C. Caso *et. al*, Review of Particle Properties, Euro. Phys. Journal. **C**, 544

[77] Bortoletto *et.al* (CLEO) Phys. Rev. **D 45**, 21 (1992)

[78] Wang Chung-Hsiang, Ph.D Thesis, University of Rochestor (1993)

[79] Albrecht *et.al* (ARGUS) Phys. Lett. **B 374**, 256 (1996)

[80] Albrecht *et.al* (ARGUS) Phys. Lett. **B 324**. 249 (1994)

[81] Artuso *et.al* (CLEO) Phys. Rev. Lett **62**, 2233 (1989)

[82] Abe *et.al* (CDF) Phys. Rev. **D 57**, 5382 (1998)

[83] Abe *et.al* (SLD) Phys. Rev. Lett **79**, 590 (1997)

[84] Abe *et.al* (CDF) Phys. Rev. Lett **76**, 4462 (1996)

[85] Buskulic *et.al* (ALEPH) Z Phys. **C 71**, 31 (1996)

[86] G. Fox and S. Wolfram, Phys. Rev. Lett. **41** 1581 (1978)

[87] Shifman, M., N.G. Uraltsev, and A. Vainshetin, Phys. Rev. **D 51**, 2217 (1995)

[88] Ball. P, M. Beneke, and V.M. Braun, hep-ph/9503492

[89] Particle Data Group, C. Caso *et. al*, Review of Particle Properties, Euro. Phys. Journal. **C**, 104

[90] J.M. Flynn Hep-Lat/9611016

[91] Particle Data Group, C. Caso *et. al*, Review of Particle Properties, Euro. Phys. Journal. **C**, 345

[92] T. Browder and K. Honscheid, Prog. of Nuclear and Particle Physics **Vol. 35**, Preprint UH 511-816-95